International PhD Program in Biomolecular Sciences

Department of Cellular, Computational and Integrative Biology – CIBIO

34th Cycle

"Development of a gene targeting strategy for liver metabolic diseases using the Crispr/Cas9 platform"

Tutor

Dr. Serena ZACCHIGNA

ICGEB, Italy

Advisor

Dr. Andrés F. MURO

ICGEB, Italy

Ph.D. Thesis of

Michela LISJAK

ICGEB, Italy

Academic Year 2021-2022

Original Authorship Declaration

I, Michela Lisjak, confirm that this is my own work and the use of all material from other sources have been properly and fully acknowledged.

Acknowledgments

It was a challenging journey and many people contributed in different ways to make all this possible.

First, I would like to thank my supervisor, Dr. Andrés F. Muro, for guiding me through my PhD, for his constant support, all the scientific knowledge he shared with me, for his patience, trust and for being always available to clear any doubts I may have.

My gratitude goes to all Mouse Molecular Genetics laboratory members. Dr. Giulia Bortolussi and Alessandra Iaconcig their advice and help from day one to now greatly contributed to this work. All the present and previous colleges: Alessia De Caneva, Fabiola Porro, Giulia De Sabbata, Vipin Singh Rawat, Joseph Olajide Olayemi, Filippo Ferrucci, Claudia Galletta, Luca Camparini, Himanshi Saxena, Bhaswati Banerjee, Antonio Vicidomini and Laura Moretti. Thank you for the science shared, all the help, support and nice time together.

Thanks to all the participants who took part in this PhD work, the collaborators in Paris, for the hemophilia B project and to Dr. Corrado Guarnaccia for mass spectrometry analysis. This work wouldn't be possible without them.

I would like to thank Alessia who was there for me at the beginning of this journey, teaching me patiently all the lab techniques and how to work with mice. Most importantly I want to thank her for being an amazing friend and always there for me in all these years.

Thanks to Himanshi and Antonio for always helping me, making experiments a little easier and a lot funnier. I couldn't have wished for better lab partners and friends. I will never forget the dinners, time spent talking about cats and construction works together with Laura.

Thanks to my friends I met in ICGEB, Urša, Živa, Nina, Claudio, Roman, Elena, for all the fun time shared at coffees, aperitives, dinners and birthday parties.

I want to thank Mari for sharing every step of this journey with me, for being someone I can always count on, for all the laughs and tears, but above all, for being like family to me.

I am grateful for David, all my friends, my grandparents, my aunt and all my family. Your love, help and constant support mean everything to me.

I want to thank my roommate Viktor, for filling my days with happiness.

Last, but not least, I would like to thank my dear parents, who always trusted and supported all my life decisions and for raising me to live fearlessly and to not be afraid of having big dreams.

Abstract

Many inborn errors of metabolism require life-long treatments and, in severe conditions, organ transplantation remains the only curative treatment. Non-integrative AAV-mediated gene therapy in the liver has shown to be efficient in different clinical trials of adult patients, but treatment in pediatric or juvenile settings may result in the rapid loss of episomal viral DNA associated with hepatocyte duplication during liver growth.

Gene targeting approaches have shown potential clinical applications in the treatment at pediatric stages, as the therapeutic transgene is permanently integrated into the genome, ensuring long-term therapeutic efficiency.

This PhD project focuses on two liver disorders: citrullinemia type I and hemophilia B. Citrullinemia type I (CTLN1) is a severe liver monogenic urea cycle disorder caused by deficient activity of the *ASS1* gene, leading to the accumulation of blood ammonia and citrulline.

Hemophilia B instead, is a bleeding disorder, caused by the non-functionality of the coagulation factor 9 (FIX), produced by hepatocytes, leading to a deficient clotting activity and frequent spontaneous bleeding episodes. Both disorders require life-long treatments and, in the case of CTLN1, liver transplantation remains the only permanent cure.

We previously developed a gene therapy strategy targeting a therapeutic cDNA into the albumin locus, using the Crispr/SaCas9 platform.

We applied this treatment to CTLN1 neonate mice ($ASS1^{fold/fold}$). A single injection completely rescued phenotype lethality, decreasing plasma citrulline levels, although without reaching *wild-type* values. We then treated juvenile (P30) $ASS1^{fold/fold}$ mice with an episomal hASS1 AAV8 vector (non-integrative) or with the gene targeting strategy applied previously to neonate mice. The animals treated with the non-integrative gene therapy vector showed a complete rescue of the diseased phenotype, with plasma ammonia and citrulline levels similar to *wild-type* values up to 3 months post-administration, while mice treated with the gene targeting strategy had an increase in their lifespan.

In the second part of this work, we targeted the human coagulation factor IX (FIX) cDNA into the genome of a mouse model of hemophilia B. In this case, a single

injection of the AAV vectors into neonate FIX KO mice led to long-term and stable expression of above-normal hFIX levels. Treated mutant mice were subjected to tail clip analysis in which their coagulation activity was comparable to *wild-type* animals, demonstrating the complete normalization of the phenotype. However, in adult FIX KO mice the targeting rate was less efficient and it did not lead to a correction of the coagulation activity.

Altogether, our data demonstrate that a gene-targeting strategy is very promising in the neonatal treatment of disorders where a smaller correction rate is enough to restore the phenotype or to considerably improve the phenotype in disorders where higher levels of correction are required to restore liver functionality. Non-integrative gene therapy may be applied to CTLN1 juvenile mice ensuring a stable therapeutic effect. Gene targeting strategies on adults are still worth further developing, as the non-integrative approach may lose its efficiency associated with the natural rate of hepatocyte duplication and to liver disease conditions resulting in hepatocyte duplication.

Table of Content

List of Figures

List of Tables

1. Introduction

1.1. Inborn Errors of Metabolism

Inborn errors of metabolism (IEM) are rare genetic disorders that are caused by a mutation in single genes causing an enzyme deficiency. The defects are singularly taken rare, but all IEM together are more than 1400 and their incidence is 1 in 800 to 2500 persons, which represent an important part of the population (Harthan, 2018). Almost all metabolic pathways can be involved: carbohydrates, phospholipids, and amino acids. The role of those enzymes is in the conversion of substrates into metabolites. Metabolic alterations can result in significant consequences, such as accumulation of toxic metabolites, reduction of essential downstream compounds, enzyme deficiency, feedback inhibition or activation of proximal metabolites, abnormal substrate metabolism (Brunetti-Pierri and Lee, 2005; Chakrapani, 2001; Harthan, 2018; Schneller et al., 2017). Many of the defects present in IEM occur in the liver and can be also named monogenic liver diseases. Monogenic liver diseases can be roughly classified according to the liver condition: 1) those characterized by liver parenchymal damage and hepatic injury with primary hepatic expression, 2) those characterized by a structurally normal liver where genes encoding enzymes or circulating proteins are expressed by the liver and 3) those in which liver involvement is just a clinical manifestation and the genetic defect is expressed in a systemic level (Table 1) (Fagiuoli et al., 2013). Most of those diseases show their first signs rapidly after birth when the neonate is no longer protected from the placenta dialysis system (Chakrapani, 2001). The presentation of symptoms is usually non-specific and can be acute or chronic including sepsis-like presentation, lethargy, vomiting, acidosis, and developmental delay. If not managed, acute symptoms may lead to neurological damage, metabolic crisis, or death (Harthan, 2018). For most of those conditions, the treatment involves the reduction of substrates, removal of toxic intermediates, the supplement of essential compounds, activation of alternative metabolic pathways with diet, drugs, vitamin cofactors, or injections of recombinant enzymes (Schneller et al., 2017). Liver transplantation remains the only curative strategy that permits life-long restoration. However, this procedure is limited by organ availability and severe side effects (Baganate et al., 2018). Many defects are caused by a loss of function mutations and, for this reason, gene therapy and genome editing are very promising therapeutic strategies, as in some IEMs only a minimal correction of the defect can lead to a

restoration of the metabolic pathway. Also, gene-based therapies can be an option to avoid complications after liver transplantation (Brunetti-Pierri and Lee, 2005; Schneller et al., 2017).

Monogenic diseases with primary hepatic expression and parenchymal damage
Genetic cholestasis (PFIC and Alagille syndrome)
Wilson's disease
Hereditary hemochromatosis
Tyrosinemia type 1
α-1-antitrypsin deficiency
Argininosuccinic aciduria (ASL)
Glycogen storage disease (GSD) type I (adenoma/hepatocellular carcinoma)
Monogenic diseases with primary hepatic expression without significant parenchymal damage
Urea cycle disorders (excepted ASL)
Crigler-Najjar syndrome
Familial amyloid polyneuropathy
Atypical haemolytic uremic syndrome-1
Primary hyperoxaluria type 1
Maple syrup urine disease (MSUD)
Acute intermittent porphyria
Coagulation defects
GSD type Ia (in metabolic control)
Homozygous familial hypercholesterolemia
Monogenic diseases with both hepatic and extrahepatic expression
Organic acidurias (excepted MSUD)
Cystic fibrosis
Erythropoietic protoporphyria
Gaucher disease

Table 1: Inherited liver monogenic disorders. They can be classified according to the pathogenic liver condition into 1) primary hepatic expression with parenchymal damage, 2) primary hepatic expression without parenchymal damage, 3) both hepatic and extrahepatic expression. Examples of the different categories are listed (Adapted from Fagiuoli et al., 2013).

1.2. Enzyme replacement therapy and liver transplantation

Many therapeutic approaches have been developed to increase the excretion of toxic metabolites and to ameliorate the symptoms, as dietary prescriptions, pharmacologic intervention, oral replacement of enzymatic cofactors, chelation to increase excretion. In the case of an enzyme deficiency or non-functionality, enzyme replacement therapy (ERT) may be performed (if available) and it consists of intravenous administration of a solution containing the recombinant enzyme (Fagiuoli et al., 2013). However, ERT is a very expensive life-long treatment with questionable efficiency. They are not suitable in the central nervous system treatment, as crossing the blood-brain barrier is very inefficient for recombinant enzymes. In addition, treated patients can develop anti-recombinant protein antibodies that can potentially reduce the efficacy or lead to an immune response (Concolino et al., 2018).

Liver transplantation remains the only curative approach to permit life-long liver restoration. In diseases with parenchymal damage, liver transplantation is restoring the defect and replaces a dysfunctional liver. In diseases expressed on a systemic level, liver transplantation cannot be considered, as the diseased phenotype will remain maintained by the defect in extra-hepatic tissues (Fagiuoli et al., 2013). Despite its curative potential, liver replacement is limited by the availability of organs. In general the risk of mortality is 10-15 % at 1 year after LT based on the report of the United Network for Organ Sharing (UNOS) in the United States (Baganate et al., 2018; Fayek et al., 2016). According to the European Liver Transplant Registry (ELTR), the 5-year survival rate for liver metabolic diseases is 79 % (Adam et al., 2012). The main causes of death after LT are graft failure, cardiovascular causes, pulmonary causes, and infections (Baganate et al., 2018). Besides, post-transplantation complications, life-long treatment with immunosuppressive therapy, that prevents graft rejection, is increasing the risk of skin and lymphoproliferative tumors, represent severe side effects.

1.3. Gene-based therapies

Gene therapy and genome editing approaches have shown to be promising treatments for diseases where there is a loss of function in a gene that is widely expressed in hepatocytes. The treatment is performed by adding an exogenous gene into the diseased cell or organ, to regulate, repair, replace, add, or delete a genetic sequence. The goal of the therapy is to achieve high levels of therapeutic transgene in diseased hepatocytes or extrahepatic tissues, reversing the diseased phenotype (Bryson et al., 2017; Chandler and Venditti, 2016; Fagiuoli et al., 2013; Schneller et al., 2017; Wirth et al., 2013). Gene-based therapies can be performed *ex vivo*, where the patient's cells are first removed, treated, and then re-infused into the body. Alternatively, it can be performed *in vivo*, where the vector carrying the corrected gene is directly administered into the patient's body correcting the diseased organ (Kay, 2011).

In many inborn errors of metabolism where the disease is a consequence of an enzyme deficiency or complete absence, the restoration of the enzyme activity up to 5 – 25 % is enough to ensure protection from the disease. That propriety makes them suitable for gene therapy treatment. An example is Hemophilia B where the severe phenotype is

present when FIX activity is below 1 % of normal values. FIX activity above 10 % is causing a moderate phenotype, which can result in no apparent clinical manifestation (Kay and Woo, 1994).

1.3.1. Clinical trials

The first clinical trial using gene therapy as a treatment was performed in 1990 on severe combined immunodeficiency patients. The disease is a severe immunodeficiency, caused by a deficiency in adenosine deaminase (ADA-SCID). The treatment was performed *ex-vivo*, where white blood cells were taken and transduced with a retroviral vector expressing adenosine deaminase (Blaese et al., 1995). Soon after, another clinical trial on ADA-SCID patients was carried out in Italy (Bordignon et al., 1995). Gene therapy then showed extraordinary promise when a tumor suppressor was successfully delivered into the brain tumors using retro- and adenoviral vectors (Puumalainen et al., 1998). After that gene therapy faced a difficult period. Five (5) out of 20 X-linked severe combined immunodeficiency (SCID-X1) patients that were treated *ex vivo* with a retrovirus-mediated gene transfer into hematopoietic progenitor cells, developed leukemia. The retroviral vector integrated into the LMO2 proto-oncogene promoter, which resulted in the clonal expansion of mature T lymphocytes (Herzog, 2010). Another clinical trial using an adenoviral vector, for ornithine transcarbamylase deficiency (OTC), lead to the death of a young adult by the vector-induced immune response (Raper et al., 2003). Researchers all around the world started to focus on developing safer and more effective gene therapies. The first gene therapy product for clinical use was approved in China. Gendicine™ is an adenoviral vector generated for the treatment of cancer patients. Despite its withdrawal from the market, in Europe, Glibera®, gene therapy for lipoprotein lipase deficiency, was the first gene therapy product to be released on the market was in 2013 (Baruteau et al., 2017; Wirth et al., 2013). After that, many companies started to develop gene therapies, and the number of clinical trials rapidly increased. Currently, there are 22 gene and cell therapy products approved by the U.S Food and Drug Administration (https://www.fda.gov/).

1.3.2. Viral delivery

The most common and efficient delivery systems are viral vectors, which can mediate the delivery of the gene therapy, leading to cell infection and transgene expression. Several viral vectors were developed and have shown a successful gene transfer. Many viruses have been engineered as recombinant viral vector tools (Table 2). The most used viral vectors are divided into two categories based on their capacity to integrate into the host genome. Viral vectors can integrate permanently into the genome (retroviruses and lentiviruses) or they can persist in an episomal form (adenoviruses and adeno-associated viruses) (Kay, 2011; Thomas et al., 2003). The viral vectors used are recombinant viruses that derive from natural ones but have the pathogenic genes removed and replaced with the therapeutic transgene cassette. The removal of the viral genome can increase safety as the vector is not able to replicate (Chandler and Venditti, 2016). Due to their efficiency and safety, AAV vectors became the most used vectors as *in vivo* gene therapy delivery platforms among viral and non-viral vectors.

Virus	Adenovirus	Adeno-associated virus	Retrovirus	Lentivirus
Family	Adenoviridae	Parvoviridae	Retroviridae	Retroviridae
Genome	dsDNA	ssDNA	ssRNA	ssRNA
Genome Size	26–40 kb	5 kb	7–12 kb	7–12kb
Coat	naked	naked	enveloped	enveloped
Viron Diameter	70–100 nm	18–26 nm	80–100 nm	80–100 nm
Pathogenic	yes	No	yes	yes
Infects	dividing and non-dividing	dividing and non-dividing	dividing	dividing and non-dividing
Interaction with Host Genome	non-integrating	non-integrating	integrating	integrating
Transgene Expression	transient	sustained	sustained	sustained
Packaging Capacity	7.5 kb	4.5 kb	8 kb	7 kb

Table 2: Characteristics of recombinant vectors. Comparison of characteristics between available viral vectors: adenovirus, adeno-associated virus, retrovirus, and lentivirus (Chandler and Venditti, 2016).

1.3.2.1. Adeno-associated virus (AAV)

Adeno-associated viruses (AAVs) are currently the most used viral vectors for *in vivo* gene therapy. AAVs are very small (25 nm) and non-pathogenic, with a single-stranded DNA genome (Table 2). They cannot replicate unless it is present as a helper virus (adenovirus or herpesvirus). In the absence of the helper virus, the *wild-type* AAV can repress its gene expression and integrate into chromosome 19q13.4 (AAVS1 locus) to establish latent infection. However, it is estimated that this event can occur in approximately 0,1 % of the transductions, while also in recombinant AAV vectors the integration events are occurring at lower frequencies (Chandler et al., 2017; Deyle and Russell, 2010). The gene therapy vectors were engineered to lack the Rep proteins and cis-active integration efficiency elements (IEE), which are involved in site-specific integration. The non-coding inverted terminal repeat (ITR) sequences are kept, as they have a role in packaging the genome into the capsid. When the recombinant AAV (rAAV) vector enters the cell nucleus, they synthesize the second strand and persist as extra-chromosomal genetic material (Chandler and Venditti, 2016; Daya and Berns, 2008; Ferrari et al., 1996). The rAAV cargo capacity is 4,7 kb, which represents an important limitation for large genes. In that case, different systems have been tested, such as the engineering of the therapeutic transgene into *trans*-splicing vectors. With this method, the transgene cassette is divided into two rAAV vectors, which have donor and acceptor splice sites. After transcription, the genes undergo *trans*-splicing, and they generate a functional mRNA product up to 9 kb long (Daya and Berns, 2008). Another method to deliver larger proteins is by a protein *trans*-splicing mechanism. This mechanism is mediated by the presence of split-inteins that are located in two separate polypeptides (on N- and C- term). When they interact, they can excide and ligate the protein, reconstructing it precisely (Tornabene and Trapani, 2020). The synthesis of the second strand is time-consuming and may also result in a reduction in therapeutic efficiency, although this concept is debated. Self-complementary AAVs (scAAV) vectors, which can immediately self-anneal and produce a transcriptionally active double-stranded DNA, have been extensively used. However, the use of scAAV faces a limitation in the cargo capacity, which is reduced and can encapsidate about 3,3 kb of genetic material (Daya and Berns, 2008).

AAV can be classified in different serotypes based on their capsid structure. Different serotypes have variable capsid features, which are involved in different receptor binding sites, transduction potential and different immunological profiles. This is a very important feature in gene therapy, as therapeutic vectors have different infectivity rates and tissue targeting specificity. AAV serotype 8 is well known to have a high liver tropism. Studies performed on non-human primates have demonstrated that their tropism to the liver is 10 – 100 fold higher compared with other serotypes (Gao et al., 2002). Also, in a clinical trial for hemophilia B, a recombinant AAV2/8 showed to have advantages over the previously used AAV2, as specific liver tropism enabled to deliver the gene therapy systemically, instead of intra-hepatically (Nathwani et al., 2011a).
One of the major challenges of AAV vectors remains the activated immune response against them. An example is a clinical trial for Hemophilia B, where there was a decrease of the therapeutic protein, as a consequence of the presence of neutralizing antibodies and elevated levels of transaminases (Manno et al., 2006). Also, 70 % of the human population has preexisting immunity to AAV2, which makes the delivery more challenging. To overcome this limitation some strategies may be adopted such as the selection of patients without NAbs, identification of new serotype variants with lower prevalence in the population, the generation of new artificial capsid variants, administration of higher vector doses, use of immune-suppressive drugs, plasmapheresis, isolated organ perfusion or increased dose (Mingozzi and High, 2013; Verdera et al., 2020).

1.4. Non-viral delivery

Non-viral gene delivery can overcome some viral-vectors limitations, such as immunogenicity, integration, they don’t have a limitation in transgene package size and the production is easier and cheaper (Nayerossadat et al., 2012). However, the majority of clinical trials for gene therapy of both genetic and acquired diseases are carried out with viral delivery because they still show higher efficiency, compared to the non-viral methods (Jayandharan, 2018; Yin et al., 2014). Non-viral vector systems can be divided into two subgroups: *via-physical* and *via-chemical* delivery.

1.4.2.1. Physical methods

With physical methods, the DNA, RNA (siRNA, dsRNA, shRNA, mRNA), or proteins can be introduced into the cell's membrane through a physical force. Those delivery systems include single DNA injection, high-pressure gene gun delivery, electroporation, sonoporation, photoporation, hydroporation, ultrasound, hydrodynamic injection, and magnetofection delivery (Nayerossadat et al., 2012; Ramamoorth, 2015). Physical methods have been mainly used for *ex vivo* delivery or embryos microinjections to generate transgenic models. When applied to a live organism, these techniques are limited by the number of cells that can be edited (Rui et al., 2019).

1.4.2.2. Chemical methods

Chemical delivery methods raised great interest as an alternative to viral-delivery systems. They are usually nanoparticles, engineered, and optimized to pass cellular barriers and escape degradation systems. Those delivery vectors are classified as lipids, liposomes, polymers, polymersomes, cell-penetrating peptides, and inorganic nanoparticles (Yin et al., 2014a). Chemical systems are small nanometric complexes containing positive charged polycationic particles that interact with negatively charged nucleic acids all packed into an envelope, for example, cationic liposome/micelle or cationic polymers (Nayerossadat et al., 2012). The nanoparticle carrier must escape cellular mechanisms, like immune detection and endosome degradation, premature cargo release, and protein aggregation. It has to ensure an efficient delivery into the nucleus, allowing the transcription of the transgene. To avoid recognition by the immune system and increase circulation, nanoparticles are coated by hydrophilic molecules like polyethylene glycol (PEG) (Rui et al., 2019). An important factor for an efficient transfection is cell status. It was seen that dividing cells that undergo the breakdown of the nuclear envelope are more suitable for the treatment (Yin et al., 2014a). An alternative to DNA delivery into the nucleus is a protein or mRNA delivery. mRNA once in the cytoplasm can be instantly translated, without the need to enter the nucleus. mRNA and protein delivery enables a faster, more efficient, and specific

operation also in quiescent cells, but the therapeutic effects are usually transient (Kay, 2011).

1.5. Genome editing

Treating pediatric patients can be challenging as the liver is growing and the episomal vector DNA is lost associated with hepatocyte duplication. Also, re-administration of the gene therapy can be ineffective as the humoral immunity system generates neutralizing antibodies against the recombinant AAV vector after the first AAV administration (Calcedo and Wilson, 2016; Nathwani et al., 2007; Wang et al., 2012). Therefore, obtaining a long-term correction in pediatric patients is one of the main challenges of the field, as hepatocytes are actively proliferating. Genome editing, correcting permanently the genome, can overcome this problem (Gonçalves and Paiva, 2017; Herzog et al., 2010; Kay, 2011). The endonucleases used in this approach are specifically designed to target a genomic region to perform a double-strand break (DSB). After the DSB is performed, the cell can repair the damaged DNA by different mechanisms, based on the stage of the cell (Carroll, 2014). DNA damage can be repaired by the error-prone non-homologous end joining (NHEJ) mechanism, which is active all along the cell cycle, with higher activity in the G1, S and G2 phases, or by the precise homology-direct repair (HDR), active in late S and G2 phases of the cell cycle, when a template with homology regions is present. The result of the editing can be gene knockout, gene deletion, gene correction, or gene addition (Heyer et al., 2010).

Engineered nucleases increase the efficiency of the homologous recombination rate, which is a key point in gene therapy (Rouet et al., 1994a, 1994b; Smih et al., 1995). The generation of a DSB can enhance homology recombination events from 100 to 1000 folds (Rouet et al., 1994a, 1994b). The four endonucleases families most commonly used are meganucleases, zinc finger nucleases (ZFNs), transcription activator-like effector nucleases (TALENs), and clustered regularly interspaced short palindromic repeats and CRISPR- associated protein (CRISPR/Cas) (Table 3). In particular, the clustered regularly interspaced short palindromic repeats and CRISPR- associated protein (Crispr/Cas9) platform due to its easy use, become the main used genome editing tool (Hsu et al., 2014).

Feature	Meganucleases	ZFNs	TALENs	CRISPR/Cas9
Source	Microbial mobile genetic elements	Eukaryotic gene expression regulators	Plant pathogenic bacteria *Xanthomonas*	Adaptive immune system of bacteria and *archaea*
Target specificity	Target recognition domain	Zinc Finger proteins	TALEs	sgRNAs
Work mode per target	Single/chimeric	Pair	Pair	Single
Cleavage module	Nuclease domain	FokI	FokI	Cas9
Recognition	Protein/DNA	Protein/DNA	Protein/DNA	RNA/DNA
Multiplexing	No	No	No	Yes
Size	Variable	1kbx2	3kbx2	4.2 kb + 0.1 sgRNA
Efficiency	High	Variable	High	High
Costs	High	High	Moderate	Low
Limitation	Very difficult to design and screen; Target site choice very limited	Very difficult to design; target site choice limited; off target effects	Difficult to construct; large protein size with repetitive sequences	High dimension; immunity to Cas9
Advantages	Very precise	Small protein size, able to be packaged into rAAV; in advanced phase clinical trials	Target choice almost unlimited; very precise; very efficient	Target choice unlimited; very easy to design and construct; easy to multiplexing; very efficient

ZFNs, zinc finger nucleases; TALENs, transcription activator-like effector nucleases; CRISPR/Cas9, clustered regularly interspaced short palindromic repeat/(CRISPR)-associated nucleases 9.

Table 3: Endonucleases used for genome editing. Comparison between available engineered nucleases for genome editing: characteristics, limitations, and advantages are listed for meganucleases, ZNFs, TALENs, and CRISPR/Cas9.

1.5.3. The double-strand break repair mechanisms

1.5.3.1. Non-homologous end-joining

The NHEJ mechanism repairs DSB in cells outside the S/G2 phases, where homology recombination is predominant because the two sister chromatids are adjacent. NHEJ is a flexible mechanism that can recognize and join together diverse DNA ends and can revision multiple times DNA ends independently. It can also join together different chromosomes, resulting in chromosomal translocations. The joining of two ends can lead to INDELs (INsertions-DELetions): nucleolytic restriction or nucleotide loss, and nucleotide addition when polymerase adds nucleotides in a template-independent manner (Lieber, 2010). The NHEJ DNA repair mechanism requires a series of enzymes to repair the DSB: a nuclease to resect damaged DNA, a polymerase, which serves to

insert new synthesized DNA and a ligase, that brings together the two DNA strands (Figure 1).

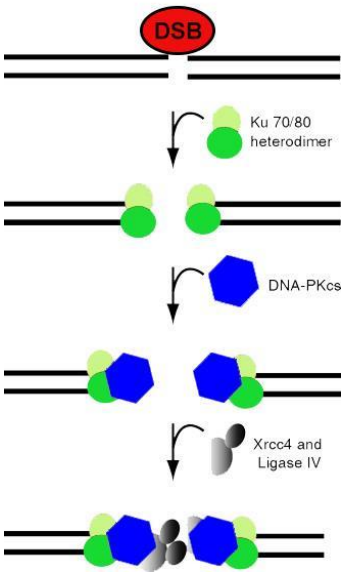

Figure 1: Non-homologous end-joining (NHEJ) pathway. After DSB, Ku heterodimer binds to DNA and recruits DNA-PK_{CS}. The ends are brought together and DNA-PK_{CS} phosphorylates each other. An intermediate step can occur when the two ends are further processed. The final result is the ligation of the two ends performed by DNA-ligase IV-XRCC4 activity (Modified from http://atlasgeneticsoncology.org/).

1.5.3.2. Homologous directed repair

Alternatively to NHEJ, the double-strand break can be repaired by three mechanisms: homologous recombination (HR), single-strand annealing (SSA) and alternative end-joining (altEJ) (Ceccaldi et al., 2016). The most predominant, homologous recombination, is an important cellular mechanism involved in maintaining genome integrity and stability of the organism karyotype. It repairs dangerous DSBs caused by exogenous agents, repairs incomplete telomers, DNA interstrand crosslinks, and damaged replication forks. In meiosis, it can mediate the exchange of information between maternal and parental alleles, resulting in diversity between precursor cells from the same parents. In meiosis after the crossover, HR is also involved in the accurate segregation of the two homologous chromosomes.

It is regulated and promoted during the S/G2 phase of the cell cycle and it can occur only if a template sequence is present (Figure 2) (San Filippo et al., 2008).

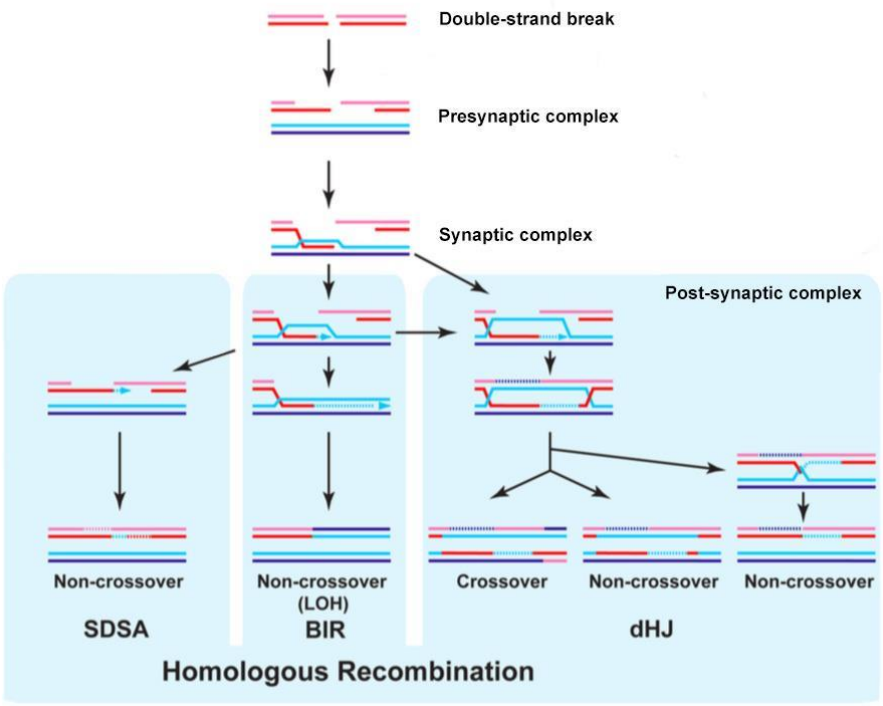

Figure 2: Homologous recombination (HR) pathway. After a DSB a 5' resection occurs to form a presynaptic complex, followed by a synaptic phase. In the post-synaptic phase, the HR can undergo three different sub-pathways: synthesis-dependent strand annealing (SDSA), break-induced repair (BIR), and double Holliday junctions (dHJ) (Modified from Heyer et al., 2010).

1.5.4. The CRISPR/Cas system

The CRISPR/Cas system is today one of the main genome editing tools. It was first discovered in 1987 in the adaptive immune system of *E. Coli*, and in 2013 started to be used as a biotechnology tool for genome editing (Hsu et al., 2014). Prokaryotes have evolved an RNA-based system called CRISPR/Cas that is involved in the recognition and degradation of genetic parasites. Foreign genetic material can be recorded in the host chromosome in a sequence of repetitive loci, also called Clustered Regularly Interspace Short Palindromic Repeats (CRISPR). Those sequences contain non-contiguous direct repeats separated by stretches of variable sequences called spacers,

which are flanked by *Cas* genes. Spacers that contain identical phage or plasmid sequences can provide resistance against them (Barrangou et al., 2007). CRISPR loci can be transcribed and processed into CRISPR-derived RNAs (crRNAs) and can identify foreign genetic material, defined as proto-spacers. For the immunity process, three stages are required: adaptation/acquisition, expression, and interference. In the adaptation/acquisition phase, sequences complementary to viruses or plasmids genetic material are first selected based on the specific Protospacer Adjacent Motif (PAM), then are processed into precursors and integrated into the CRISPR loci, conferring a spacer approximately 30 bp long. Subsequently, a flanking repeat is duplicated to maintain the structure of repeat-spacer-repeat. Two principal endonucleases are involved in spacer acquisition: Cas1 and Cas2 and are conserved between all CRISPR/Cas systems. In the second, expression phase, in type I and III systems, the pre-crRNA is generated and processed from the CRISPR locus. Cas-6 like nuclease is involved in the pre-crRNA cleavage, which results in a crRNA with an 8 nucleotides repeat fragment on the 5' end, forming a hairpin structure on the 3' end. In type II systems, a trans-encoded small RNA (tracrRNA) can guide the processing of pre-crRNA. TracrRNA contains a 25 bp sequence which is complementary to the crRNA transcript and it generates a double-strand region that is recognized and cleaved by the RNase III in the presence of Cas9 (van der Oost et al., 2014). Cas9 can perform a blunt end DNA cut with its two nuclease catalytic domains, also called RuvC and HNH, each of them cleaving one single strand (Hsu et al., 2014). After the cut, crRNA-tracrRNA hybrid remains associated with Cas9, as it is necessary for the last, interference phase. In this stage, the crRNA guides and the Cas proteins form a crRNP complex can travel to the complementary foreign sequence and can mediate its cleavage and elimination (van der Oost et al., 2014). The crRNP complexes need to interact with the 3 nucleotides PAM which enables base-pairing the spacer seed region with the protospacer (Deveau et al., 2008). In the type I system, the crRNP complex is called Cascade and it has similarities with the type III system (van der Oost et al., 2014). In the type II system instead, the interference mechanism differs. It consists of Cas9 protein and two RNAs (crRNA and tracrRNA) which need to be complementary and direct Cas9 to perform a double-strand break three nucleotides upstream the PAM in the target DNA (Jinek et al., 2012). PAM binding is essential, because it triggers the Cas9 nuclease catalytic activity, in particular by activating the two RuvC and HNH domains (Nishimasu et al., 2014).

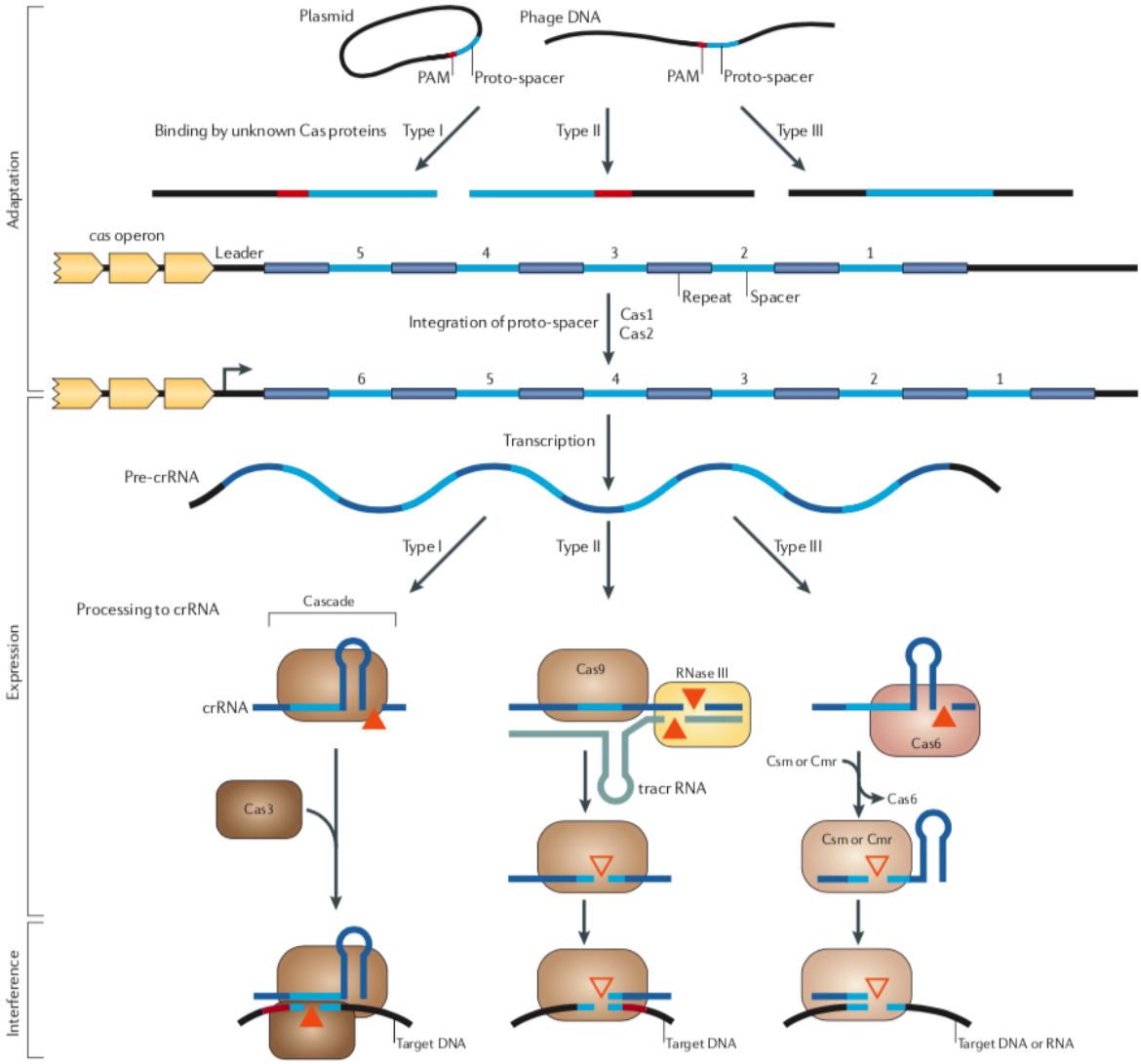

Figure 3: CRISPR/Cas system. The three phases of the CRISPR/Cas adaptive immune system: adaptation, expression, and interference. The mechanism differs between types I, II, and III (Modified from Makarova et al., 2011).

The CRISPR/Cas9 type II system is simpler compared to the other two. To perform a double-strand cut it needs only the activating tracrRNA and the targeting crRNA. This system was further modified to obtain a dual-RNA DNA interference mechanism with a single chimeric RNA. To achieve this, at the 5' end, which contains the target recognition sequence, was added a hairpin structure linker loop, followed by a complementary base-paired structure generating the single guide RNA (sgRNA), that mimics the dual structure crRNA:tracrRNA, essential to guide the Cas9 nuclease to perform a site-specific DNA cleavage (Figure 4) (Jinek et al., 2012).

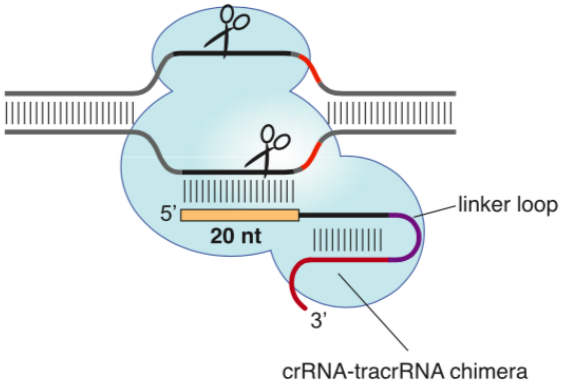

Figure 4: Programmed CRISPR/Cas9 system. The system can be re-engineered by fusing tracrRNA and crRNA into a single guide RNA (Modified from Jinek et al., 2012).

Further modifications were performed on the CRISPR/Cas9 system of *S. pyogenes* Cas9 and RNAse III to obtain a more efficient codon-optimized tool with nuclear localization signals (Cong et al., 2013). This system can also be projected towards different genes at the same time by co-expressing different sgRNAs, creating simultaneous editing at different genomic sites (Mali et al., 2013). The modified Cas9 system became an easy tool to perform gene-editing modifications where the only requirement is the presence of a PAM downstream of the target DNA. However, even this limit was overcome with the generation of Cas9 orthologous able to recognize different PAM interacting domains (Nishimasu et al., 2014). With this flexibility, the CRISPR/Cas9 system has been facilitating genome editing efficiently *in vitro*, on various cell types, and *in vivo*, on different species such as zebrafish, yeast, mouse, fruit fly, roundworm, rat, common crops, pig and monkey. One of the biggest advantages over the other two mega-nucleases, ZFNs and TALENs, is their easy production. While in the other two, the production is challenging, as it requires screenings of proteins with particular sequence specificity, with the CRISPR/Cas9 system targeting requires only the production of the guide RNA (Hsu et al., 2014).

However, the limit of all nucleases, CRISPR/Cas9 included, is the risk of binding and cleaving similar sites, denominated "off-target" cleavage. Many studies confirmed that SpCas9 can tolerate mismatches in a guide sequence, which leads to off-target activity (Fu et al., 2013; Hsu et al., 2013, 2014; Mali et al., 2013). Off-target studies demonstrate that SpCas9 can tolerate up to 5 nucleotides mismatches in the target sequence increasing the possibility of unwanted off-target mutagenesis (Fu et al., 2013;

Semenova et al., 2011). This is a serious disadvantage especially when this approach is used for the treatment of genetic disorders. Efforts to solve this issue and achieve an increased Cas9 specificity have been of great interest to many research groups in this field.

1.5.4.1. Improved CRISPR/Cas9 platform

The biggest limitations of using the CRISPR/Cas9 system *in vivo* are poor target specificity, the inability of entering the cells, activation of the immune response, and off-target events (Wilbie et al., 2019). Off-target prediction starts with computational analysis, predicting Cas9 nuclease possible off-target sites, based on the target seed sequence and PAM site. This can be performed using bioinformatic software packages that rank the guide RNAs according to their genomic specificity. Choosing the most unique target sequence is one option if there are present more than one possible guide RNAs with the same outcome.

Many biological engineers have worked to improve the CRISPR/Cas9 system, optimizing its specificity and safety by re-engineering *Sp*Cas9 protein and the guide RNA, and by modifying its delivery system (Tycko et al., 2016). To enhance specificity different approaches have been developed, such as a "double-nickase " strategy (Mali et al., 2013), "*Sp*Cas9 PAM Variant D1135E" (Kleinstiver et al., 2015), "High Fidelity *Sp*Cas9-HF" (Kleinstiver et al., 2016) and truncated gRNAs "tru-guides" (Fu et al., 2014).

Cas9 orthologous have been engineered to simplify its use as a genome-editing tool. *Staphylococcus aureus* Cas9 (*Sa*Cas9) has demonstrated a highly specific and efficient nuclease activity compared to the most commonly used Cas9 of *Staphylococcus pyogenes*. A longer target sequence (21-24 nt for *Sa*Cas9 and 17-20 nt for *Sp*Cas9) and a longer and more complex PAM preference (5'-NNGRRT for *Sa*Cas9 and 5'-NGG for *Sp*Cas9), results in a lower off-target activity (Ran et al., 2015; Tycko et al., 2016). *Sa*Cas9 is also 1kb smaller than *S. pyogenes* Cas9, which makes it also more suitable for packing the *Sa*Cas9 protein and the guide RNA into the same AVV vector (Ran et al., 2015).

As previously explained, the DSB induced by the Cas9 enzyme increases the rate of HDR. However, especially in non-proliferating cells, the DSB will be repaired by NHEJ. This limitation took scientists to generate an alternative editing approach that doesn't need the donor template. Therefore, a catalytically disabled Cas9 nuclease with a single guide RNA was firstly fused to cytidine deaminase. This Cas9 optimization, named Base Editor (BE), enables the conversion of cytidine into uridine, creating a substitution C −> T or G −> A (Komor et al., 2016). Later, adenine base editors (ABE) were generated to allow the editing of adenine or thymine into guanine or cytidine (Gaudelli et al., 2017). The base editing approach led to precise genome editing to perform point mutations in DNA or RNA without the use of DNA cleavage and the presence of the donor template. However, it has been seen in mouse embryos through a technique called GOTI (genome-wide off-target analysis by two-cell embryo injection), that cytosine base editors also introduce single nucleotide variants (SVN) in unspecific target sites, generating off-target activity. This made the use of the cytosine base editors unreliable, which makes the platform not safe for potential application in clinics. In contrast, editing performed by adenine base editors did not increase SVNs (Zuo et al., 2019).

Another fact that is related to off-target activity, is the nuclease concentration level. It has been demonstrated that higher nuclease levels can contribute to off-target cleavage sites (Hsu et al., 2013). For this reason, many strategies have been applied to inactivate Cas9 expression, once the cells have been edited (Chen et al., 2016; Petris et al., 2017; Ruan et al., 2017). One of the emerging Cas9 optimizations consists in the development of a Self-Limiting Cas9 Circuit for Enhance Safety and Specificity (SLiCES). This system enables the removal of the nuclease from edited cells, preventing off-target activity. This system, also denominated "hit and go" *Sp*Cas9 delivery system, consists of a co-expression of Cas9 protein (*Sp*Cas9), a single guide RNA targeting a specific genomic locus and another self-targeting sgRNA, driving the kill-switch (Figure 5). SLiCES successfully demonstrated genome editing modification avoiding the accumulation of off-target cleavages, which can greatly improve the safety aspect of this technology (Petris et al., 2017).

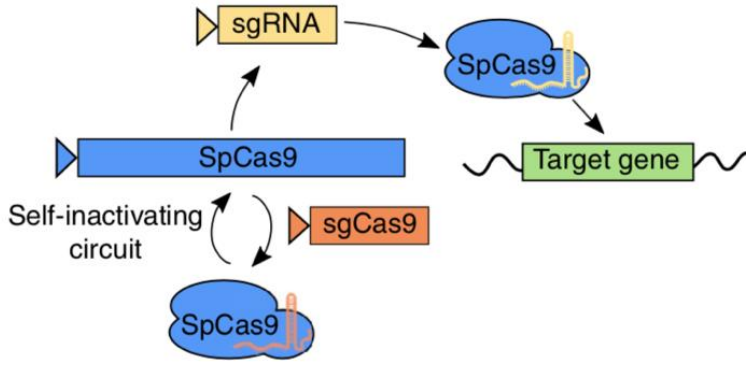

Figure 5: SLiCES system. The self-limiting circuit is formed of *Sp*Cas9 protein and two gRNA: one targeting a specific locus and the other targeting the *Sp*Cas9 gene (Petris et al., 2017).

Another important aspect that increases the safety of the mechanism is to deliver the Cas9 enzyme through alternative methods of administration. Viral systems limitations include the packaging capacity, immunogenicity, and the long-term expression of the endonuclease. Non-viral systems can overcome those problems. Synthesized Crispr/Cas9 enables faster, more efficient, and more specific operation compared with the introduction via a plasmid. The advantages are related to the reduction of the off-target effects by the short-term presence of the endonuclease in the target cell, and the absence of DNA encoding for the nuclease, avoiding the integration of plasmid/viral DNA in the host genome. The direct introduction of RNP Cas9 resulted in increased efficiency of HDR, compared to TALEN technology and with nucleic acid-based delivery (Kay, 2011).

1.5.5. Nuclease-free approach

Genome editing and genome targeting using reprogrammable nucleases are rapid methods to achieve desired DNA modifications. However, despite its precise and robust work, possible side-effects have to be considered, especially when it comes to clinical use. Besides off-target cleavage, also a humoral and cellular immune response against the Cas9 nuclease may occur (Charlesworth et al., 2019; Nelson et al., 2019). Despite the high editing levels that can be achieved with the use of nucleases, there have been reported several successful studies using nuclease-free approaches. One was developed

by Barzel and colleges, where an AAV8 donor DNA is inserted by homologous recombination, under the albumin promoter in mice liver, leading to a rescue of the phenotype in hemophilia B mice (Barzel et al., 2015). Another study used a nuclease-free strategy to correct the fumarylacetoacetate hydrolase (FAH) gene in Fah^{5981SB} mice, a mouse model for tyrosinemia type I. In this case, the repair frequency was low, but due to a positive clonal expansion of Fah-positive hepatocytes, the diseased phenotype could be rescued, achieving therapeutic efficacy (Paulk et al., 2010). A growth advantage for corrected hepatocytes was observed in a mouse model for alpha-1 antitrypsin deficiency (AATD), when a cDNA encoding for a PIZ variant, was targeted under the albumin locus. Corrected hepatocytes re-populated the liver, improving the diseased phenotype (Borel et al., 2017). However, a higher gene repair rate may be reached with the use of HDR enhancers. There are already many factors known that can enhance gene targeting rate, either by promoting HR or by suppressing the NHEJ pathway (Yang et al., 2020). A study from the University of Stanford tested different molecules for their recombination enhancing effect and showed that fludarabine increases the homologous recombination of a donor DNA *in vivo*. This FDA-approved drug is a ribonuclease reductase (RNR) inhibitor and works by inducing DNA damage that can significantly increase the targeting rate with limiting toxicity (Tsuji et al., 2020, under revision).

1.5.6. Liver-directed genome editing

Traditional gene therapy during the past decade became a safe and effective treatment for liver diseases. The viral delivery vehicles, especially the rAAV vectors are very effective to deliver their DNA to hepatocytes when injected intravenously to adult patients, resulting in long-lasting transgene expression. Many approaches have been developed for treating liver diseases with the use of genome-editing tools, enabling a permanent change into the genome. One of the most widely used is the CRISPR/Cas9 platform, which can introduce different types of changes in the genome to reverse a diseased phenotype. Many preclinical studies showed promising results in the treatment of different liver metabolic diseases and their translation towards the clinics. The permanent restoration of the mutation or gene introduction through HDR is a promising

approach for pediatric patients to restore an endogenous gene expression, where the liver is growing and the vector, if not integrated, can be lost (Aravalli and Steer, 2018; Ruiz de Galarreta and Lujambio, 2017; Schneller et al., 2017; Trevisan et al., 2020).

Hereditary tyrosinemia type I (HT-I) is an inborn error of metabolism caused by the deficiency of fumarylacetoacetate hydrolase (FAH) involved in the catalysis of fumarylacetoacetate. A genome editing strategy using the CRISPR/Cas9 platform was applied to a mouse model for HT-I. Mice were injected via hydrodynamic tail-vein injection with Cas9, sgRNA, and an ssDNA to correct the point mutation. The initial targeting frequency was 0,40 %, but later the positive clonal expansion led to an increase to 33,5 % of FAH-positive hepatocytes, due to the growth advantage of corrected hepatocytes over the mutated ones. This enabled the rescue of the phenotype from the diseased induced liver damage (Yin et al., 2014b). After, the same group treated the HT-I mouse model with an AAV8 delivery of the single guide RNA and HDR template together with a lipid nanoparticle delivery of the Cas9 nuclease. With this strategy, the initial targeted hepatocyte rate was 6 %, resulting in the rescue of the phenotype, demonstrating the high efficiency of AAV8 in hepatic transduction (Yin et al., 2016). Another strategy, as an alternative to HDR, used the Cas9 together with a donor vector containing a microhomologous sequence that triggers error-prone end-joining (MMEJ). In two separate studies, this strategy proved its efficiency on a hereditary tyrosinemia mouse model, leading to mice survival from liver failure (Shin et al., 2018; Yao et al., 2017).

Another genome editing preclinical study was performed in 2014 to treat hypercholesterolemia. The aim was to knock out the pro-protein convertase subtilisin/kexin type 9 (PCSK9). The LDL receptor is involved in the uptake of LDL particles from extracellular fluids, reducing LDL concentration. When PSK9 is present, the LDLR is directed to lysosomal degradation. When PCSK9 is blocked or inactivated, the LDL receptors can be efficiently recycled and more receptors can be present on the cell surface, increasing cholesterol uptake and decreasing its concentration in plasma. A pathologic gain of function of the PCSK9 gene leads to high levels of LDL cholesterol. Mice were injected with *Sp*Cas9 targeting the PCSK9 gene to reduce PCSK9 levels. The PCSK9 gene was inactivated by the NHEJ mechanism, which then resulted in a reduction of cholesterol (Ding et al., 2014). Later studies delivered different Cas9 systems (*Staphyloccocus aureus* and *Neisseria meningitides* Cas9) with rAAV vectors,

and both of them proved their efficiency in downregulating the PCSK9 serum protein and cholesterol (Ibraheim et al., 2018; Ran et al., 2015).

Treatment of neonatal mice by Cas9 HDR mediated technology was confirmed in a mouse model for ornithine transcarbamylase (OTC) deficiency. OTC is a urea cycle enzyme involved in ammonia metabolism. Its deficiency is causing hyperammonemia and may lead to death. This approach was performed on *spf*^{ash} mice, which are characterized by a partial activity of the OTC gene. An IV injection in the neonatal period of spf^{ash} mice with rAAV8 *Sa*Cas9 and rAAV8 sgRNA+donor showed the correction of 10 % of hepatocytes. In contrast, the same strategy on adult mice didn't lead to the same results. The treatment in adult mice resulted in the death of the animals due to the presence of large deletions, as a consequence of the NHEJ DNA repair mechanism. Concluding that in adult mice the promoted DSB repair mechanism is NHEJ instead of HDR, resulting in indels, and subsequently gene knockout with a reduction in OTC residual activity (Yang et al., 2016).

1.5.7. Gene targeting into the albumin locus

Modification of the human genome showed great success in the past decade in the treatment of genetic diseases. Despite all the progress that has been made to find an alternative vector delivery and ensure a safety profile, viral gene delivery is still one of the most used and effective delivery methods for treating monogenic diseases. As previously mentioned, AAV vectors are a safe delivery system that results in the long-term presence of the episomal vector DNA in quiescent cells, but there is vector DNA loss associated with cell proliferation. Retroviral vectors, consisting of γ-retroviruses or lentiviruses, are based on the permanent integration of the transgene. They integrate into the host genome in a semi-random manner, with a preference for transcribed regions (Sadelain et al., 2012). The main concern is the risk of integration in cancer-related genes. If the vector integrates into the proximity of proto-oncogenes, it can lead to an increased activation, causing oncogenesis (Aiuti et al., 2013; Herzog, 2010). Integration can also arise in a silent area preventing the expression of the transgene and, in this case, decreasing the therapeutic efficacy. One of the main objectives is to prevent variable transgene expression and insertional mutagenesis. One possible

approach is to permanently integrate genetic material into a defined genomic locus. Researchers have strived to find ideal genomic regions for targeting therapeutic transgenes. Those loci, also denominated “genomic safe harbors”, accept a transgene DNA ensuring its efficient and sufficient expression, without altering normal cell function and preventing malignant cell transformation (Sadelain et al., 2012). In genome editing, the use of engineered endonucleases has proved to be an appropriate method to perform precise site-specific genome modification. The double-strand break in the presence of a donor cDNA recalls the machinery of DNA repair which can facilitate gene targeting through homologous recombination enhancing the gene targeting rate.

For gene transfer to the liver, the serum albumin locus was selected as a genomic harbor. The albumin gene is transcriptionally highly active, due to its strong promoter, which functions only in the hepatocytes. There is a wide window in the plasma albumin levels in the population, thus minor changes in albumin production are not expected to affect the treated patients/animals. These proprieties make this locus suitable for promoterless gene targeting strategies. Sharma et al. (2015) targeted the plasma coagulation *FIX* into the first intron with the use of zinc-finger nucleases. The *albumin* exon 1 encodes a secretory peptide that is cut away from the final product, permitting transgene expression. This study was performed on a mouse model for hemophilia A and B and successfully proved that albumin locus can be used as a platform for liver-directed protein replacement (Sharma et al., 2015).

Another strategy for targeting *F9* in the hemophilia B mouse model was adopted by Barzel et al. (2015). They developed a method to target the albumin locus without the use of a promoter and nucleases. This strategy ensures a higher safety, as the lack of promoter disables the activation of other genes if inserted in another region. The absence of nucleases prevents the possibility of gene inactivation due to off-target cleavage, also avoiding any concern related to potential immunological responses. This strategy is based on targeting the transcriptional efficient *albumin* gene, right upstream of its stop codon. They used a 2A-peptide, which was derived from *porcine teschovirus* (P2A), and due to its glycyl-prolyl peptide bond, it causes ribosome skipping (Kim et al., 2011). In this strategy, the transgene is preceded by the peptide-2A to obtain two different proteins from a single mRNA: albumin and F9 (Figure 6) (Barzel et al., 2015).

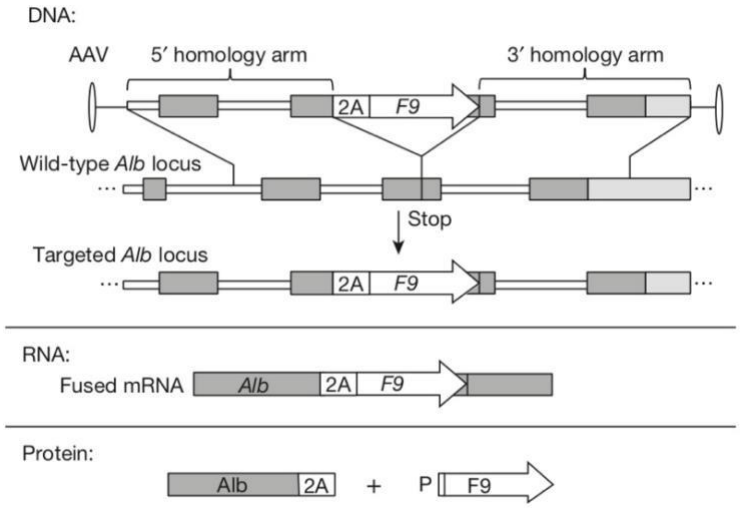

Figure 6: Experimental design. The rAAV8 vector with the human coagulation factor 9, preceded by the 2A-peptide. Flanking the two genes are albumin homology arms. After the homology recombination, the transgene is integrated after the stop codon signal. Albumin and F9 are transcribed in one mRNA molecule, but after translation two different proteins are produced (Barzel et al., 2015).

In the Mouse Molecular Genetics laboratory, Barzel's approach was used to treat the mouse model of Crigler-Najjar type I syndrome. CNI is an ultra-rare disease, caused by the deficiency of liver-specific UDP glucuronosyltransferase 1A1 (UGT1A1), resulting in the toxic accumulation of unconjugated bilirubin (UCB) in all body tissues, with brain damage and death, if not treated (Kadakol et al., 2000). This gene-targeting strategy resulted in the rescue of the diseased phenotype, due to the reduction of plasma bilirubin levels. The success of this strategy is given by both site-specific stable integrations that are maintained over time and by the efficiency of the albumin promoter, which increases gene expression (Porro et al., 2017). Even though all mice were rescued, their plasma bilirubin levels were still too high to use this strategy as a therapeutic approach to Crigler-Najjar patients. For this reason, in an attempt to enhance the recombination rate and therapeutic efficacy, the "GeneRide" approach was coupled with the Crispr/*Sa*Cas9 platform (Figure 7). A preliminary study was performed in which *wild-type* mice were injected with a reporter AAV8 donor vector containing the *EGFP* cDNA. The donor vector was delivered alone or together with an AAV8 expressing the *Sa*Cas9, to evaluate homologous recombination (HR, no nuclease) or homology-directed repair (HDR, with nuclease that generates a DSB) rate, respectively. The targeted hepatocytes were evaluated through immunofluorescence and, in the case of HDR, the level of recombination showed an overall 26-fold increase

compared to HR (Figure 8). After, the strategy was tested in the Crigler-Najjar mouse model. Targeted neonatal Ugt1A1 KO mice showed a complete rescue of the diseased phenotype. The level of plasma bilirubin decreased to the level of their *wild-type* littermates. The bilirubin values were stable up to 10 months, which proved therapeutic long-term efficacy. Also, the single guide RNA used for targeting the albumin locus showed to be specific, as there were no indels in the predicted off-target sites, as determined by next-generation sequencing analysis. Therefore, with these results, "GeneRide" coupled with the CRISPR/Cas9 platform showed to be a promising therapeutic strategy that can be potentially applied to pediatric patients (De Caneva et al., 2019).

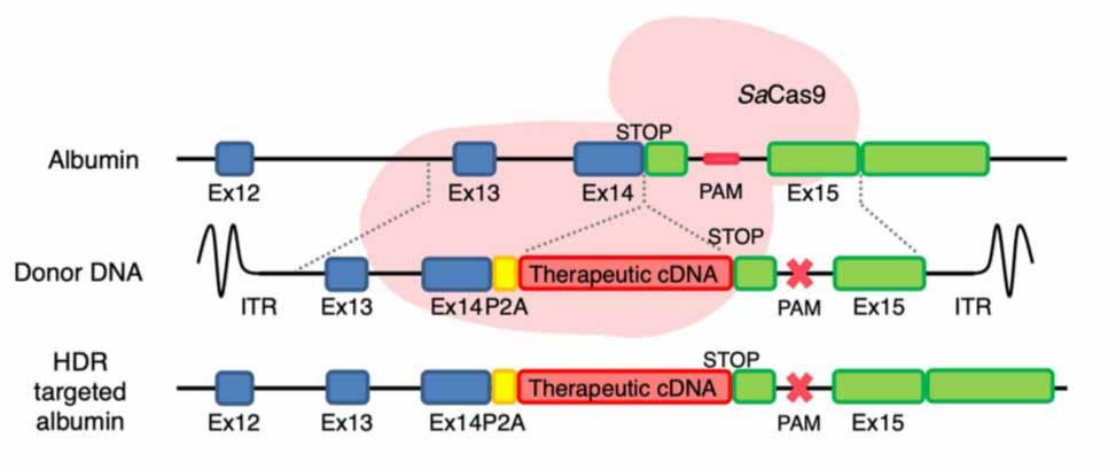

Figure 7: "**GeneRide" strategy coupled with CRISPR/*Sa*Cas9**. The CRISPR/*Sa*Cas9 performs a double-strand break to increase the homologous directed repair rate. In the donor DNA, the PAM site is mutated to avoid donor targeting and its degradation (Adapted from De Caneva et al., 2019).

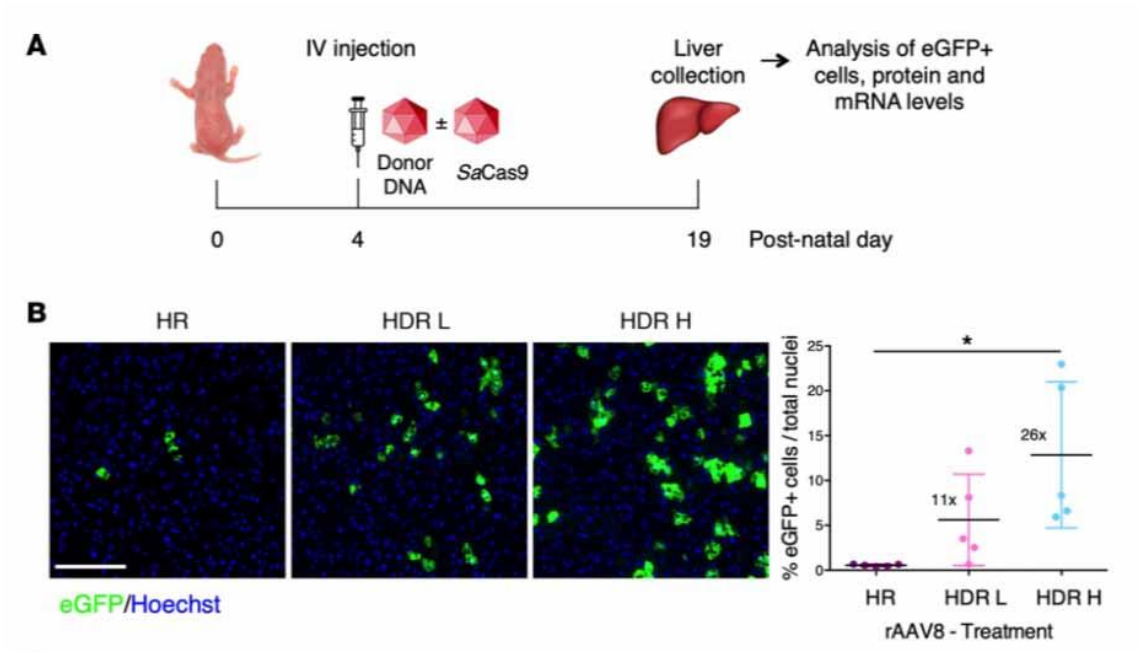

Figure 8: Validation of HDR and HR on *wild-type* mice. **A**) Mice treated at P2 were injected with a donor containing an *EGFP* cDNA with or without a *Sa*Cas9 AAV8. **B**) Targeted hepatocytes in the HDR – high dose group were 26-fold higher compared to the HR group. In the low-dose HDR group, the increase was 11-fold (Modified from De Caneva et al., 2019).

1.6. Citrullinemia type I

Citrullinemia type I (CTLNI) is an inborn error of metabolism and one of the urea cycle disorders. It is an autosomal recessive inherited defect, caused by a mutation in the argininosuccinate synthetase gene (*ASS1*), leading to a decrease or absence of the ASS1 protein. The urea cycle is essential in mammals and many amphibians to convert toxic ammonia, the byproduct of amino acid catabolism, into urea. In the urea cycle are engaged 5 enzymes: carbamyl phosphate synthetase-I (CPS-I), ornithine transcarbamylase (OTC), argininosuccinate synthetase (ASS), argininosuccinate lyase (ASL) and arginase (Fig. 9). ASS1 is the third enzyme of the urea cycle and is involved in the condensation of citrulline and aspartate into argininosuccinate (Dennis et al., 1989). CTLN1 is distinct in two clinical forms: a common acute neonatal form and a milder late-onset form, with symptoms only during pregnancy or post-partum. The estimation of prevalence in the population of the severe neonatal form is 1 in 44,300–

200,000 depending on population consanguinity (Karthikeyan et al., 2013; Woo et al., 2014). Infants appear normal after birth, but quickly after, they become lethargic, feed poorly and they can often vomit. If neonates are not treated immediately they develop hyperammonemia and accumulate toxic metabolites which lead to more severe symptoms. This results in increased inter-cranial pressure (ICP), increased neuromuscular tone, spasticity, ankle clonus, seizures, loss of consciousness, significant neurologic deficit, and death. The determination of the disease is done by the measurement of ammonia and citrulline plasma concentrations using mass spectrometry, measurement of ASS enzyme activity, and genetic testing. In CTLN1 patients citrulline levels are higher than 1000 µmol/L (normal < 70 µmol/L), while ammonia concentration is usually more than 100 µmol/L and it may increase up to 2000-3000 µmol/L. CTLN1 can be also confirmed by the absence or incompetent activity of the ASS1 enzyme in liver tissue or skin fibroblast (Karthikeyan et al., 2013; Quinonez and Thoene; Woo et al., 2014).

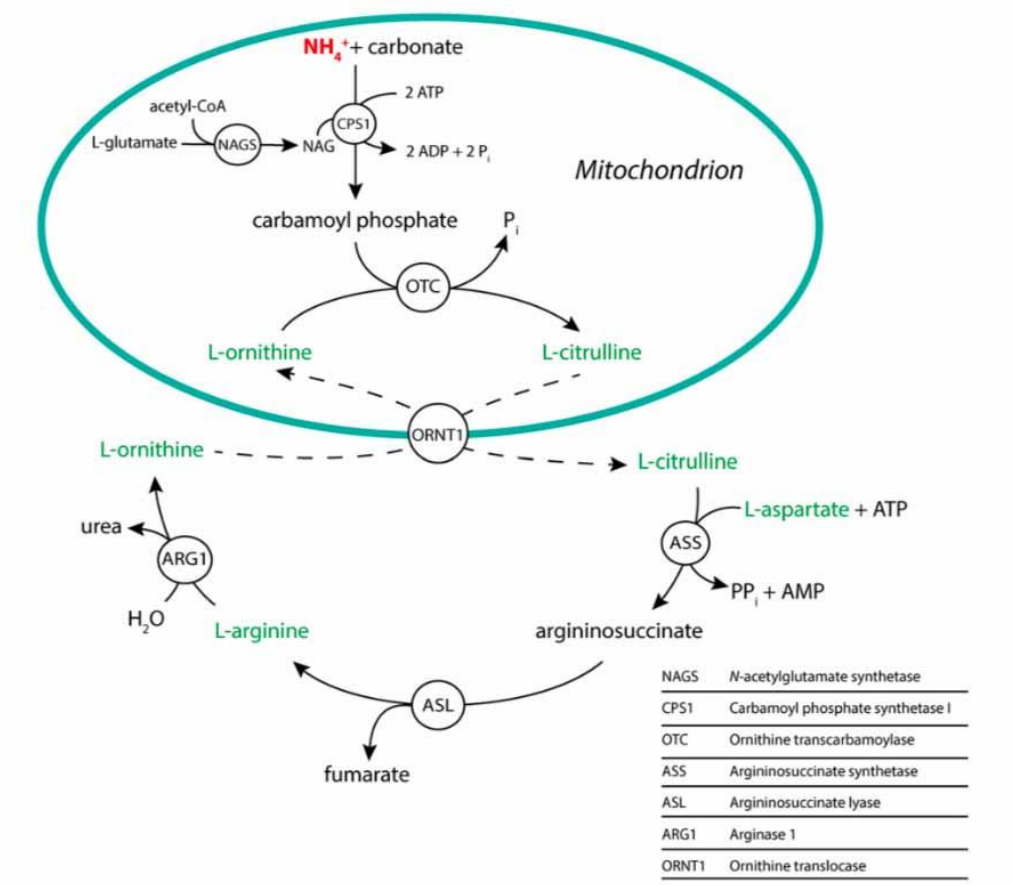

Figure 9: The urea cycle. In periportal hepatocytes, the urea cycle is used to convert toxic ammonia into a non-toxic form – urea. Five major enzymes are involved in this process: carbamyl phosphate synthetase-I (CPS-I), ornithine transcarbamylase (OTC), argininosuccinate synthetase (ASS), argininosuccinate lyase (ASL) and arginase (ARG1) (Adapted from Matoori and Leroux, 2015).

1.6.8. Treatments for citrullinemia type I

The first management of CTLN1 involves lowering ammonia levels by restricting protein intake through diet. The pharmacological treatments are nitrogen scavenger therapy (sodium benzoate, sodium phenylacetate) and L-arginine therapy. Phenylacetate is converting glutamine into phenylacetylglutamine that contains two moles of nitrogen. Benzoate instead is converting glycine into hippuric acid, which contains 1 mole of nitrogen. These molecules can be then excreted. When ammonia is still above normal levels, sodium phenylbutyrate can be administered, as a prodrug for phenylacetate. It is also important to avoid subsequent hyperammonemia crises. L-

arginine can also be administered, as it facilitates the removal of 1 or 2 moles of nitrogen (Harthan, 2018; Quinonez and Thoene). In case of severe hyperammonemia or a failure in the response to the treatment, patients have to go through hemodialysis. Similar to other inborn errors of metabolism, the only curative treatment remains liver transplantation (Quinonez and Thoene).

1.6.9. The *ASS1* gene

The *ASS1* gene is located on chromosome 9 (9q24.11-9q23.12), it is 63 kb long, with an open reading frame of 1239 bp. It includes 16 exons, starting with exon 3 (Diez-Fernandez et al., 2016, 2017). *ASS1* encodes for argininosuccinate synthetase, an enzyme that is involved in three metabolic pathways. *ASS1* is vital in the liver in the process of ammonia excretion through the urea cycle. It is the third enzyme of the cycle and it catalyzes the condensation of citrulline and aspartate into argininosuccinate. It is highly expressed in the periportal hepatocytes, while its expression is lower in other tissues (http://www.proteinatlas.org/ENSG00000130707-ASS1/tissue). It has also a role in the production of arginine from citrulline. Additionally, together with argininosuccinate lyase and nitric oxide synthetase, is involved in the citrulline-nitric oxide cycle (Diez-Fernandez et al., 2016, 2017; O'Brien, 1979). The enzyme is a cytosolic homotetrameric protein, where each monomer weighs 46 kDa and it includes a nucleotide-binding domain, a synthetase domain, and a C-terminal helix that is important for the oligomerization (Diez-Fernandez et al., 2016).

The majority of genetic alterations in CTLN1 patients are missense mutations, distributed from exon 3 to 16. Less frequent are nonsense mutations, mutations that alter the splicing, and deletions. The most common mutation is the change of p.Gly390Arg, located in the oligomerization helix, inactivating the enzyme. Other mutations have been found in portions that encode the substrate-binding residues. No mutations have been found in exon 1, 2 or 16 (Diez-Fernandez et al., 2017).

1.6.10. Citrullinemia type I mouse models

To study the disease several CTLN1 mouse models have been generated. The first mouse model available was the ASS1 knockout (KO) mouse, in which the exon 4 was disrupted. Homozygous mice have no detectable activity of the ASS1 enzyme, with high ammonia and citrulline levels. ASS1 KO mice die in 24-48 h, with ammonia levels reaching up to 2680 ± 970 µM (Patejunas et al., 1994). Later, another group described three milder CTLN1 mouse models obtained from spontaneous hypomorphic recessive mutations named: Barthez (*bar*) and follicular dystrophy (*fold*). These mutations correspond to alterations found in patients: p.Arg265Cys, p.Thr389Ile. Hypomorphic mice differ in the disease severity: *bar/bar* is the most severe genotype, followed by *fold/fold*, and *bar/fold*. Phenotypically, homozygous mice exhibit alopecia, growth retardation, lethargy, high ammonia and citrulline values, and a decrease in ASS1 activity. They generally survive 3 weeks or more, due to the 5-10 % of residual ASS1 enzymatic activity (Table 4) (Perez et al., 2010).

Genotype	Ammonia (µg/dl)	Citrulline (µmol/L)	Arginine (µmol/L)	ASS Liver activity (µmol/min/g)
FVB/N-*bar/bar*	530 ± 27	5790 ± 841	97 ± 11	0.06 ± 0.02
	(*n* = 4, P14)	(*n* = 4, P14–P21)	(*n* = 4, P14–P21)	(*n* = 3, P20)
FVB/N-+/+	201 ± 37	145 ± 27	209 ± 49	3.73 ± 2.39
	(*n* = 4, P14)	(*n* = 4, P14–P21)	(*n* = 4, P14-P21)	(*n* = 3, P20)
C57BL/6-*bar/bar*	556 ± 21	N/A	N/A	0.03 ± 0.03
	(*n* = 3, P14)			(*n* = 3, P21)
C57BL/6-*fold/fold*	462 ± 12	2941 ± 1347	171 ± 68	0.12 ± 0.06
	(*n* = 4, P14)	(*n* = 4, P14–P21)	(*n* = 4, P14–P21)	(*n* = 3, P21)
C57BL/6-*bar/fold*	356 ± 22	2076 ± 192	229 ± 41	0.12 ± 0.06
	(*n* = 3, P14)	(*n* = 3, P14–P21)	(*n* = 3, P14–P21)	(*n* = 3, P21)
C57BL/6-+/+	193 ± 35	106 ± 6	271 ± 51	1.23 ± 0.75
	(*n* = 3, P14)	(*n* = 3, P14-P21)	(*n* = 3, P14–P21)	(*n* = 3, P21)
Reference values for human CTLN1 patients	18–2900	1685 ± 1325 (*n* = 24)	71 ± 38 (*n* = 24)	0.02–0.8
	(control range 10–60)	(control range 10–50)	(control range 20–149)	(control range 0.8–3.8)
	(Ref. [25])	(Refs. [15, 25])	(Refs. [15, 21])	(Ref. [34])

Table 4: Characteristics of different CTLN1 mouse models. Plasma ammonia, citrulline, arginine, and ASS liver activity between *bar/bar*, *fold/fold*, *bar/fold*, *wild-type* mice, and human values (Adapted from Perez et al., 2010).

1.6.11. Gene-based therapies for Citrullinemia type I

The first gene therapy treatment for CTLN1 was performed to extend the lifespan of the ASS1 KO mouse model. ASS1 KO mice were injected intravenously with a recombinant adenovirus carrying a human *ASS1* cDNA. The life expectancy with two injections, together with arginine and sodium benzoate therapy, prolonged their life up to 16-36 days (Ye et al., 2000). A second study on the KO ASS1 mouse model was performed with an AAV vector. Mice were injected intra-uterus at days 0, 14, 28 and they reached adulthood if fostered by another mother, who lacked antibodies against the AAV vector. Also, animals received a pharmacological treatment of sodium benzoate and L-arginine (Kok et al., 2013). To rescue the hypomorphic $ASS1^{fold/fold}$ mouse model, mice were injected intraperitoneally with AAV8 expressing *ASS1* cDNA under a liver-specific promoter. With this therapy, mice survived more than 3-weeks with an improvement in biochemical parameters (Chandler et al., 2013). To avoid episomal AAV loss another study was performed on the KO ASS1 mouse model, in which they permanently integrated the *ASS1* cDNA into the genome using a hybrid AAV/*PiggyBac* transposase system. KO mice received an in utero injection with rAAV-ASS1 transposon and rAAV *PiggyBac* transposase at embryonic day 15. Together with the gene therapy, they received L-Arginine therapy every day or 3 times per week. Mice were healthy and survived until adulthood even if biochemical levels were not completely normalized. This approach rescued the severe KO phenotype, but it has a limited application in clinics, as this system is associated with the risk of insertional mutagenesis (Cunningham et al., 2015).

1.7. Hemophilia

Hemophilia is a bleeding disorder in which the bleeding time is prolonged due to the deficiency of inherited coagulation factors. The most common bleeding disorders are hemophilia A (the incidence is 1 in 5000), hemophilia B (the incidence is 1 in 30,000), and Willebrand disease that is affecting 1 in 1000 (Mannucci and Tuddenham, 2001). Hemophilia A and B are X-linked recessive inherited disorders in which there is a

decreased level of functionality of coagulation factors VIII or IX important for the clotting process.

Hemophilia B can be classified as mild, moderate, and severe, according to the residual activity of the coagulation factor present in plasma. The mild form has 6-30 % of factor activity, the moderate form has an activity range from 1-5 %, and in the severe form, activity is lower than 1 %. Severe hemophilic patients often experience bleeding without any cause, while moderate and mild patients experience prolonged bleeding after trauma. Another symptom associated with the severe form is joint bleeding that starts as bleeding into the synovial space and can cause inflammation, followed by pain and swelling. Other serious symptoms are muscle bleeding, and life-threatening internal brain bleeding (Table 5).

The disease is caused by a mutation in the coagulation factor IX gene. 64 % of hemophilic patients represent missense/nonsense mutations, 18 % have small deletions or insertions, 9 % have alteration in splicing system, 6 % are represented by large indels, 2 % have mutated the regulatory components, and 1 % have complex rearrangement. The majority of mutations are causing a decreased activity of the FIX and approximately 40 % of the mutations are involved in a reduction in the FIX levels (Horava and Peppas, 2017, https://www.proteinatlas.org/ENSG00000101981-F9).

Clinical severity	Factor IX clotting activity	Cases by severity	Symptoms	Typical age of diagnosis
Severe	<1%	60%	Frequent spontaneous bleeding (2–5/month); spontaneous joint bleeding; bruises and hematomas not due to trauma	≤2 years
Moderate	1–5%	15%	Rare spontaneous bleeding (1/month–1/year); joint bleeding; bruises and hematomas not due to trauma	<5–6 years
Mild	>5–30%	25%	No spontaneous bleeding (<1/year); often no outward signs	Often later in life

Classifications are based on in vitro clotting activity (1% = 1 IU/dL)

Table 5: Classification of Hemophilia B. Different forms are characterized based on the FIX levels, prevalence, symptoms, and age of manifestation (Adapted from Horava and Peppas, 2017).

1.7.12. Coagulation Factor IX

The factor IX (FIX) is a vitamin K-dependent coagulation glycoprotein, important in the coagulation cascade. It is synthesized in the liver, together with other clotting

factors, and is then released into the bloodstream as a circulating inactive factor. When a vessel is injured two major pathways are triggered to initiate the coagulation cascade: the *extrinsic* and *intrinsic* pathways. Coagulation factor IX is part of the *intrinsic* pathway and is critical in the propagation and thrombin generation. FIX gets proteolytically cleaved and converted in FIXa, which is the catalytically active form. The role of factor IXa is to activate, together with FVIIIa, FX, which is responsible for the initiation of clot formation. Active FXa binds to FVa and is important for converting fibrinogen into a stable covalently cross-linked fibrin thrombus (Figure 10).

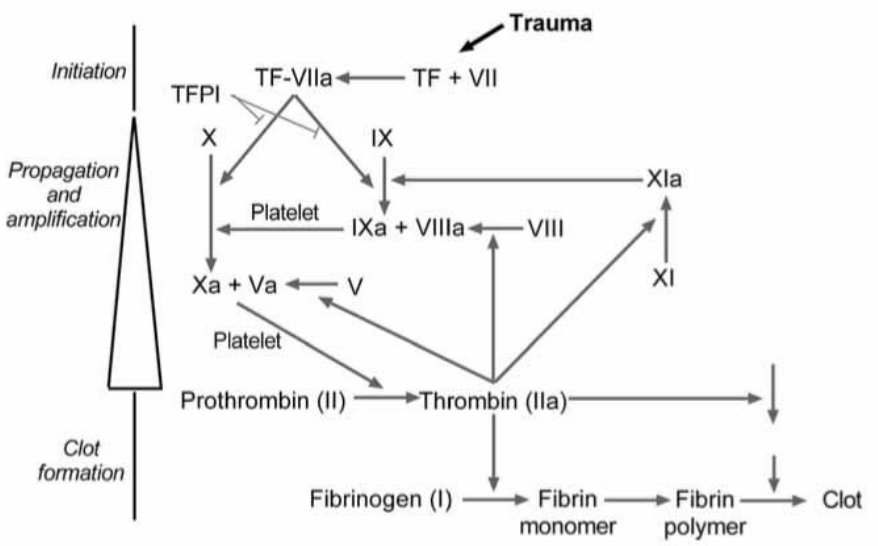

Figure 10: Simplified coagulation cascade pathway. Tissue factors activate factor VII and form a complex TF-VIIa. The complex activates directly factor X and indirectly factor IXa-VIIa. Factor Xa is involved in the activation of thrombin that will initiate the propagation and amplification of the cascade. Factor Xa is inactivated by the tissue factor pathway inhibitor (TFPI). The generation of Xa from IXa-VIIa is important for continuing with the coagulation process. In the propagation phase, thrombin is amplified and fibrinogen is then able to form a fibrin monomer, that will polymerize into a clot (Adapted from Horava and Peppas, 2017).

1.7.13. Treatments for hemophilia B

The first treatment for hemophilia B started in the early 1960s. Fresh frozen plasma from donors was first directly infused into hemophilic patients to ameliorate the bleeding phenotype. Later, concentrates of different clotting factors were obtained by

cryoprecipitation. However, as the therapy was not safe, the transfusions lead to infection with hepatitis and HIV, resulting in 60-70 % of hemophilic patients being infected with HIV. From 1986, the treatment became safe when plasma concentrates underwent specific treatments to inactivate those viruses, which resulted in no more transmission of those diseases. Treatment for hemophilia B made an important step forward when in 1997, the first FIX recombinant protein was approved by the FDA. Recombinant factors are free from infections, but the cost is extremely high, which represents a limitation in the treatment of patients from low-income countries. Coagulation factors have a relatively short half-life in plasma (18-22 h for rFIX) and patients may necessitate 2-3 infusions per week. To increase the half-life, the rFIX was pegylated or fused to a more stable protein, as it is albumin, to increase the stability and decrease the infusion time to once per week. In March 2014, the first rFIX fused to an Fc fusion protein was approved by the FDA. Although it improved drastically the life expectancy and quality of life of hemophilic patients. Another serious complication is the generation of neutralizing antibodies, called inhibitors, against the exogenous enzyme, which decreases the efficacy of the treatment, increasing the risk of bleeding-related morbidity, nephrosis, and mortality (Horava and Peppas, 2017; Mannucci, 2020; Nathwani et al., 2017; Okaygoun et al., 2021; Robles-Rodríguez et al., 2020). An important development in hemophilia treatment is the generation of by-passing agents, such as recombinant factor FVIIa (rFVIIa) and activated prothrombin complex concentrates (aPCC) that are used when hemophilic patients have high titer inhibitors. There have been generated other non-substitutive therapies that represent alternatives to the replacement therapy with recombinant factors and can be used when inhibitors are present or absent. A new approach is based on an RNA interference mechanism that, by targeting the SERPINC1 gene, is lowering antithrombin production. Another method to treat hemophilia is inducing thrombin generation by targeting a tissue factor pathway inhibitor (TFPI), with the use a monoclonal antibody. Those new products are efficient and some of them need only sub-cutaneous injections, which made their administration much simpler. However, despite the positive results of the new therapies, the replacement therapy remains mainly used, requiring intra-venous injections that makes the treatment life-long and expensive (Okaygoun et al., 2021).

1.7.14. Gene therapy and genome editing strategies for Hemophilia B

Hemophilia B became a good candidate for gene therapy treatment. The bleeding time can be significantly reduced by an increase of 1-2 % of active factor IX. Therefore, also gene therapy treatment, even with limited efficiency, can be curative. Many pre-clinical studies showed great success and the therapy quickly proceeded to clinical trials. In one of the first clinical studies, hemophilic patients received an intrahepatic injection of AAV2-hFIX16, which indicated to be efficient at the initial phase, but the efficiency decreased over time, rapidly reaching basal pre-dose levels, as a result of an immune response. All four individuals contained a high titer of neutralizing antibodies against AAV vectors. Despite this, no liver damage was observed, suggesting the safety profile of the therapy (George et al., 2020; Manno et al., 2006).

The AAV8 serotype became more suitable for liver-directed gene therapy, for its lower seroprevalence as AAV2 serotype capsid and higher liver tropism. scAAV2/8 containing a codon-optimized *FIX* cDNA under a liver-specific promoter (scAAV2/8-LP1-hFIXco) was tested on non-human primates. Juvenile male macaques were injected with 2,0E11 vg/kg and after 5 years they maintained hFIX levels around 10 % of the normal FIX levels (Nathwani et al., 2011b). Later, the scAAV2/8-LP1-hFIXco vector was used in a clinical trial in which 6 severe patients were enrolled. The subjects were split in 3 different dosage groups (low – 2,0E11 vg/kg, intermediate – 6,0E11 vg/kg, or high dose – 2,0E12 vg/kg). In all patients, the FIX level increased from less than 1 % to 2-11 % and remained stable for 6 to 16 months. Four patients stopped the prophylaxis treatment without any spontaneous bleeding episodes. Additional four patients were enrolled in the same study and treated with a higher dose. All 10 treated patients demonstrated an increase in FIX of 1-6 % in 3,2 years. In four patients the presence of liver transaminases in the bloodstream was observed, followed by FIX decrease. This was solved by 5 days of glucocorticoid administration. Besides this, no liver damage was observed in any treated subject (Nathwani et al., 2011a, 2014).

In a subsequent clinical trial, 10 hemophilic patients received a single dose of an engineered SPK-9001 AAV vector containing a codon-optimized hyperactive Padua

FIX. Participants reached a mean increase in the FIX levels of 33,7% ± 18,5% with a strong improvement in the bleeding time (George et al., 2017).

Despite all the achievements in treating hemophilic patients, gene therapy has still side effects related to the immune response against the AAV vector. Another problem is the loss of episomal vector due to liver growth, which is a restraint especially in the treatment of pediatric patients (Cunningham et al., 2008; Wang et al., 2012).

Gene targeting studies were performed on hemophilic mice, treating mice in both adult and neonatal periods. A study was performed on 8-week old mice with an AAV encoding h*F9*-specific ZFN pair and a donor containing arms of homology flanking *FIX* cDNA. The treatment resulted in an increase in 23 % of FIX compared to the normal levels at week 60 (Anguela et al., 2013). Another study was performed on hemophilic mice using the more common CRISPR/Cas9 platform together with a partial human factor IX (*FIX*) cDNA carrying the hyperactive FIX Padua mutation. Both adult and neonatal mice were treated and reached an increase in the hFIX level up to 10,9 ± 1,6 % (n=6) in the neonatal group and 8,2 ± 1,2 % (n=5) in the adult group. The FIX levels were stable for 8 months (Wang et al., 2019). Currently, Sangamo Therapeutics has started a clinical trial in which adult severe hemophilic patients received an AAV co-delivery of zinc finger nuclease (ZNF) and a promoterless vector containing the *FIX* gene and homology arms for the albumin locus. This will permanently integrate the transgene overcoming the problem of vector loss, which is important especially for the treatment of pediatric patients (https://www.sangamo.com/, https://clinicaltrials.gov/). Unlike gene therapy treatment, with a gene-targeting approach, a permanent and precise integration can be accomplished, enabling a long-term expression of the transgene.

2. Aims

The gene-targeting approach used in this thesis is based on the permanent integration of the therapeutic transgene into the albumin locus using the CRISPR/*Sa*Cas9 system. This strategy can overcome the loss of vector DNA and, consequently, therapeutic efficacy observed in non-integrative AAV-mediated gene therapy approaches when applied to neonatal and pediatric settings.

To evaluate the clinical potentiality, I tested the approach in two different rare genetic disorders affecting the liver: citrullinemia type I (CTLN1) and hemophilia B, where different correction levels are needed to obtain a therapeutic effect. The treatments were tested in animal models of the disease, mimicking both pediatric and juvenile/adult patients. With the intention of generating a safer and more efficient strategy, we also tested a SaCas9 version nuclease with a self-limiting circuit.

Thus, the aims of this thesis are:

- Compare *in-vivo* a self-limiting CRISPR/SaCas9 system with the normal CRISPR/SaCas9 version
- Evaluate the therapeutic efficacy and long-term stability of gene-targeting and non-integrative gene therapy approaches on the CTLN1 mouse model, performing the treatment at the neonatal and juvenile stages
- Evaluate the therapeutic efficacy and long-term stability of the gene-targeting approach on the hemophilia B mouse model, performing the treatment at the neonatal and adult stages

3. Material and methods

3.1. Chemicals

Name	***Producer***
1 kb Plus molecular weight marker	Invitrogen
2-propanol	Sigma-Aldrich
Boric acid	Sigma-Aldrich
Bovine Serum Albumin	Sigma-Aldrich
Bromophenol blue	
Citric acid	Invitrogen
dNTPs	Rovalab GmbH
DTT	
EDTA	Sigma-Aldrich
Ethanol	Sigma-Aldrich
EuroSafe nucleic acid stain	Euroclone
EDTA	Sigma-Aldrich
Glycine	Sigma-Aldrich
HEPES	Sigma-Aldrich
HPO_4	Sigma-Aldrich
H_2SO_4	
KCl	Sigma-Aldrich
KH_2PO_4	Sigma-Aldrich
Methanol	Sigma-Aldrich
$MgCl_2$	Sigma-Aldrich
Mouse serum albumin	Sigma-Aldrich
NaCl	Sigma-Aldrich
Na_2CO_3	
Na_2EDTA	
$NaHCO_3$	
Na_2HPO_4	Sigma-Aldrich
NaOH	
NP-40	Sigma-Aldrich

OPD	Sigma-Aldrich
PFA	Sigma-Aldrich
Proteinase K	Roche
Ponceau S staining	Sigma-Aldrich
SSC 20X	Sigma-Aldrich
Sharpmass VII Plus	Euroclone
Sucrose	
Tris	Invitrogen
Triton-X 100	Sigma-Aldrich
Tween 20	Sigma-Aldrich

Table 6: List of chemical reagents used in experiments.

3.2. Standard solutions

Standard solution	***Composition***
Blotting Solution 1	200 mM Tris, 10 % v/v Met-OH
Blotting Solution 2	25 mM Tris, 10 % v/v Met-OH
Blotting Solution 3	25 mM Tris, 40 mM Glycine, 10 % v/v Met-OH
Coating Buffer	1.59 g Na_2CO_3, 2,93 g $NaHCO_3$ dissolved in 1 L of dH_2O, pH 9.6
Electrophoresis sample buffer (ESB) 5x	50 % w/v sucrose, 25 % w/v urea, 0.5 % v/v bromophenol blue, 5x TBE in dH_2O
Luria-Bertani (LB) medium	10 g/L Bacto-tryptone, 5 g/L yeast extract, 10 g/L NaCl pH 7.5 dissolved in dH_2O
OPD Substrate	5 mg OPD dissolved in 12 mL substrate buffer, 12 µl 30 % H_2O
PBS 1x	137 mM NaCl, 10 mM Na_2HPO_4, 2.7 mM KCl, 2 mM KH_2PO_4, pH 7.4
Protein lysis buffer	50 mM Hepes, 150 mM NaCl, 1 mM EDTA, 0.5 % NP40

Sample Diluent	5.95 HEPES, 1.46 g NaCl, 0.93 g Na_2EDTA, 2.5 g BSA, 0.25 ml Tween- 20, pH 7.2 in 250 mL of dH_2O
Stopping solution	2.5 M HSO_4
Substrate Buffer	2.6 g citric acid, 6.9 g Na_2HPO_4, dissolved in 500 mL of dH_2O, pH 5.0
TBE 1X	220 mM Tris; 180 mM Boric Acid; 5 mM EDTA; pH 8.3
Wash Buffer	PBS 1X, 0.01 % Tween-20

Table 7: List of standard solutions used in experiments.

3.3. Primer list

Target	***Application***	***Primer***	***Sequence 5'-3'***
mAlb	T7E1 assay	FwStopmALB	GCCACACTGCTGCCTATTAAATACC
		RevStopmALB	CTTACATGAACCACTATGTGGAGTCC
Cas9	T7E1 assay	FwCas9_347	CCTGCTGAAGACACTCTTGC
		RevCas9_1122	CGGCCACGTATTTCTCTTCC
Cas9	VGP	pX602TBGdir	AAGGATCACCCAGCCTCTGC
		pX602TBGrev	CCTGCTGAAGACACTCTTGCCA
pAB288	VGP	pAB_4464_dir	ACTTCTTGTCTCTGTGCTGC
		pAB_4689_rev	TGATTAACCCGCCATGCTAC
pSMD2	VGP	pGG2-906 DIR	GCCACTAAGGATTCTGCAGT
		pGG2-1051 REV	CTGCACTTACCGAAAGGAGT
mAlb	mRNA expression	Alb10F	CTGACAAGGACACCTGCTTC
		Alb11R	TGAGTCCTGAGTCTTCATGTCTT
mAlb-hASS1 WT	mRNA expression	hASS1 WT F1	AGGAGCTGGTGAGCATGAAC
		Alb11R	TGAGTCCTGAGTCTTCATGTCTT

mAlb-hASS1 CO	mRNA expression	hASS1 CO F1	GGAGCTGGTCTCTATGAACG
		Alb11R	TGAGTCCTGAGTCTTCATGTCTT
mAlb-hFIX	mRNA expression	pAB_FIX2868_Dir	AAGGCACCAGCTTTCTGACC
		Alb11R	TGAGTCCTGAGTCTTCATGTCTT
mFIX	mRNA expression	mFIX_339Fw	TTCCTATGAATGCTGGTGCCAAG
		mFIX_520Rev	CTGTTGGTTCACAGGACTTCTGG
mGapdh	mRNA expression	RT-mGAPDH dir	ATGGTGAAGGTCGGTGTGAA
		RT-mGAPDH rev	GTTGATGGCAACAATCTCCA

Table 8: List of primers used to analyze mRNA expression levels, viral genome copies and T7E1 assay.

3.4. Vector construction

3.4.1. Codon-optimization

Human *wild-type* and three codon-optimized versions of the human *ASS1* cDNA were firstly inserted into the pGEM cloning vector. Codon optimized cDNA versions were generated with different optimization algorithms (Genescript, IDT, JCat (Grote et al., 2005), GeneArt). The optimized Kozak sequence was added to all cDNAs, including the WT *hASS1* cDNA. Cryptic splice sites were identified using Splice Site Prediction by Neural Network (fruitfly.org) and manually removed. Alternative reading frames (ARFs) longer than 50 aa were manually removed from both strands, when possible. The cDNAs were synthesized by Genscript and cloned into the pUC57-Kana vector at the SalI and NheI sites.

3.4.2. Vector cloning

hASS1 wild-type and codon-optimized cDNA number 1 were cloned into pSMD2 vector containing the alpha-1-antitrypsin (*hAAT*), liver-specific, promoter and the apolipoprotein E (*ApoE*) enhancer (Ronzitti et al., 2016). *hASS1* WT/CO and *hFIX* cDNAs were inserted using SalI and NheI restriction sites into a donor vector (pAB288). The ATG start codon was replaced with the NheI restriction site. The vector had to be modified as the original was used for a nuclease-free targeting and it contained the PAM site (Barzel et al., 2015). A modified version of the pAB288 vector was generated by mutating the PAM recognition site as described previously (De Caneva et al., 2019; Porro et al., 2017). We further modified the hASS1 donor vectors by removing a polylinker sequence after the P2A and before the *hASS1* coding sequence.

3.4.3. Ligation

In general, 1 µg of the desired vector was digested in a final volume of 50 µl. Enzyme units and incubation time were performed following the enzyme instructions. 1 µg of insert DNA was digested with the same condition. Ligation was performed using T4 DNA ligase (Roche) using 20 ng of vector and 2-7 molar excess of the digested insert with the final volume of 20 µl. The reaction was left overnight at room temperature.

3.4.4. Transformation into X10 gold bacterial cultures

XL10-gold ultracompetent bacterial cells were used to transform plasmids. 80 µl of cells were added to the ligation reaction and incubated for 30 min on ice. A hit-shock was performed at 42°C for 20-40 seconds followed by 2 min on ice. Bacteria were recovered in a 37°C shaker for 1 hour with 500 µl LB medium. Cells were plated on 100 mg/ml ampicillin LB agarose plates for 12 hours at 37°C.

3.4.5. Purification of bacterial DNA

A single colony was inoculated overnight in 5 ml of LB with 100 µg/ml ampicillin in a 37°C shaker. The plasmidic DNA was obtained using the Wizard® Plus SV Minipreps DNA purification system from Promega using manufacturers' instructions. Briefly, bacteria were centrifuged at 7000 xg for 5 min. Pellet was resuspended in 250 µl of Cell Resuspension Solution. 250 µl of Cell lysis solution was added and mixed. After, 10 µl of Alkaline Protease Solution was added and left incubating for 5 min. Last, 350 µl of Neutralization Solution was added, mixed and centrifuged for 10 min at room temperature. The cell lysate was added to the Spin Column centrifuged for 1 min at top speed. The column was washed two times with ethanol. To elute the DNA, 100 µl of DNAse free water was used and centrifuged at top speed for 1 min.

Large-scale DNA purification (Maxi-prep) was performed using Macharey-Nagel™ NucleoBond™ Xtra Maxi Kits following the manufacture's protocol.

DNA was quantified on NanoDrop™. The sequence was analyzed by Eurofins Genomics company by Sanger sequencing.

3.4.6. rAAV vectors production

The recombinant AAV vectors were prepared by AAV Vector Unit at ICGEB Trieste or Genethon Institute in Paris.

3.5. Transient cell transfection

HeLa, HUH7 and HEK cells were maintained in Dulbecco's Modified Eagle Medium (DMEM) with 10 % of Fetal Bovine Serum (FBS) and amphotericin or normomicyn at 37°C.

Transient transfection was performed using Lipofectamine 2000 reagent. Briefly, one day before the transfection a specific number of cells was plated on a multi-well plate reaching 70-80 % confluence. Desired DNA quantity and Lipofectamine 2000 were

diluted in serum reduced Opti-mem medium and left incubating for 5 minutes. Lipofectamine mix was then added to DNA mixes in a ratio of 1:1 and incubated for 30 min. Cells medium was changed to antibiotic free-medium and cells were transfected with transfection mixes. After 5 hours cell antibiotic-free medium was changed to a normal medium.

3.6. Animals

Wild-type and CTLN1 mouse model ($ASS1^{fold/fold}$) were housed in ICGEB bio-experimental facility in Trieste - Italy. All the experimentation was performed following EU Directive 2010/63/EU for animal experimentation, with the previous approval of the Italian Ministry of Health (authorization number 123/2019-PR).
CTLN1 mice, strain B6Ei.PAss1<fold>/GrsrJ, were purchase from The Jackson Laboratory (stock number 006449). The colony was expanded and maintained in the ICGEB experimental facility. Mice were in a temperature-controlled environment with 12/12 hours of light/dark cycles.
FIX KO mouse model (strain B6.129P2-*F9*<tm1Dws>/J) was used for Hemophilia B treatments. Mice were held and treated at the Institute for Myologie in France (Genethon Institute).

3.6.7. Animal diets

In general, mice were fed with a standard diet purchased from Mucedola s.r.l. company (4RF21). For the high protein challenge, a 23 % (EMMA23 from Mucedola s.r.l.) and 51 % (U8959 version 0142 from SAFE Rettenmaier Italia) protein diet were used.
The diet was given to pregnant $ASS1^{fold+/-}$ females. Mice were wined at 30 days of age and the diet was given to them until the end of the experiment. Blood samples were taken at 1-2 months of age.

3.6.8. rAAV treatment of *wild-type* C57 mice

To evaluate the SLiCES system mice were injected with the normal version of the rAAV-SaCa9-H1toCNT or with rAAV-SaCa9-H1toCas (SLiCE system). Mice were treated intravenously with a dosage of 5,0E11 viral genome particles per each pup (vgp/pup) or with PBS1 X (control group) and sacrificed at P10 when liver was collected.

To evaluate the integration rate in adult mice, we used a previously described donor vector expressing the eGFP cDNA with or without the SaCas9 system. Mice at P60 were injected intravenously with rAAV-donor-EGFP (5,0E11 vgp/mouse) with or without the rAAV-SaCa9-sgRNA8 (1,0E11 vgp/mouse). Mice were sacrificed after two weeks (+SaCas9) or 1 month (- SaCas9). A control group was injected with PBS 1X.

3.6.9. rAAV treatments of neonatal ASS1$^{fold/fold}$ mice

ASS1$^{fold/fold}$ pups were genotyped right after birth and treated at post-natal day 2. With the following dosages of integrative donor vector (rAAV8-hASS1WT/CO) and the *Sa*CRISPR/Cas9 vector (rAAV8-SaCas9-sg8):

- 2,0E11 vgp/pup of rAAV8-SaCas9-sg8 and 2,0E11 vgp/pup of rAAV8-hASS1WT/CO
- 2,0E11 vgp/pup of rAAV8-SaCas9-sg8 and 1,0E12 vgp/pup of rAAV8-hASS1WT/CO
- 2,0E11 vgp/pup of rAAV8-SaCas9-sg8 and 2,5E12 vgp/pup of rAAV8-hASS1WT/CO

Blood samples were taken at different time points and mice were sacrificed at 1 month or at 5 months of age.

Mice were also treated with an episomal vector expressing the *hASS1* WT and codon-optimized cDNA. Mice were treated intra-venously at post-natal day 2 with the following doses:

- 2,0E11 of rAAV8-pSMD2-hAAT-hASS1WT or rAAV8-pSMD2-hAAT-hASS1CO
- 2,0E12 of rAAV8-pSMD2-hAAT-hASS1WT or rAAV8-pSMD2-hAAT-hASS1CO

Mice were sacrificed at 1 month of age. A group of untreated ASS1$^{fold/fold}$ mice was injected with PBS 1X and sacrificed at 1 month of age.

3.6.10. rAAV treatments of juvenile ASS1$^{fold/fold}$ mice

1 month old ASS1$^{fold/fold}$ were treated with different combinations of the integrative donor vector (rAAV8-donor-hASS1WT), SaCrispr/Cas9, Fludarabine (9-beta-D-arabinofuranosyl-2-fluoroadenine 5) and only with the episomal hASS1 WT vector, with the following doses:

- rAAV8-pSMD2-hAAT-hASS1 WT (6,0E13 vg/kg)
- rAAV8-donor-hASS1WT (6,0E13 vg/kg)
- rAAV8-donor-hASS1WT (6,0E13 vg/kg) + Fludarabine (3x125 mg/kg)
- rAAV8-donor-hASS1WT (6,0E13 vg/kg) + rAAV8-SaCas9-sg8 (6,0E12 vg/kg)
- rAAV8-donor-hASS1WT (6,0E13 vg/kg) + rAAV8-SaCas9-sg8 (6,0E12 vg/kg) + Fludarabine (3x125 mg/kg)

3.6.11. rAAV treatment of neonatal and adult FIX knock-out (KO) animals

FIX KO mice were treated with a donor vector encoding for hFIX protein and the SaCRISPR/Cas9 system. A neonatal mouse group was injected at postnatal day two and the adult group at 2 months of age.
Neonatal mice were injected intravenously at P2 with rAAV8-SaCas9 (0,6E11 vg/mouse) and rAAV8-donor-hFIX (5,0E11 vg/mouse). Mice were sacrificed at 4 month of age.

Mice at post-natal day 60 (2 months old) were injected in a 1:5 ratio, of rAAV8-SaCas9 (1,0E11 vg/mouse) and rAAV8-donor-hFIX (5,0E11 vg/mouse) and sacrificed two months after the treatment at 4 month of age.

3.7. Tail clip test

Tail clip test on FIX KO mice was performed in the experimental facility at the Institute for Myologie in France. The tip of the mouse tail was cut and the bleeding was monitored over a time period of 20 min. After 20 min the final blood loss volume was measured.

3.8. Biochemical analysis of mice plasma

Mice plasma was obtained by a facial vein puncture of previously anesthetized animals. The blood was collected in a tube containing 1-2 µl of 0.5 M EDTA. The blood was centrifuged at 3,000 xg for 15 min at 4°C and the plasma was stored at -80°C.

3.8.12. Plasma citrulline

Plasma citrulline was evaluated in the Biotechnology Transfer Unit at the ICGEB in Trieste. L-Citrulline was purchased from Merck-Sigma-Aldrich and the isotopically labeled internal standard L-Citrulline-4,4,5,5-d4 was purchased from Cambridge Biolabs.

The quantitative experiments were done using as internal standard the isotopically labeled L-Citrulline-4,4,5,5-d4 in 10 µM concentration both for calibration curve and samples. A typical calibration curve ranged from 0 to 800 µM with excellent linearity (R2>0.99).

The mix was the following:

- 10 µl of *wild-type* plasma (standard curve) or sample plasma (1:5 dilution)

- 10 µl of L-Cit (standard curve) or H_2O (for samples)
- 10 µl of 80 µM D4-Cit
- 50 µl of 0.2 % HCOOH in acetonitrile

Samples were centrifuged for 2 min at 12,000 xg and loaded in Agilent 2 ml vials.
The data was analyzed using the Bruker Compass Data Analysis software.
A Bruker (Bremen, Germany) amaZonSL bench-top ion trap mass spectrometer, equipped with an electrospray source, was employed for this study. The source was operated in positive ion mode with a needle potential of 4500V and nitrogen nebulizer at 44 psi with dry gas 8L/min at 200°C. The chromatographic separations for quantitative experiments were performed using a series 1260 Agilent Technologies (Waldbronn, Germany) HPLC with autosampler controlled from the Bruker Hystar datasystem. An Agilent Zorbax Hilic Plus HPLC column, 2.1x50mm thermostated at 30°C was employed. Column flow rate was 0.5 mL/min and elution was performed using 3 minutes wash time after 5 µl injection and a 10 min gradient from 95% acetonitrile/5% water with 0.1% formic acid to water with 0.1% formic acid.
The retention time of citrulline and internal standard in these conditions was 7.8 minutes.
The MS/MS transitions used for the quantitative experiments (multiple reaction monitoring, MRM) were m/z 176.2 to 159.1 (citrulline) and 180.2 to 163.1 (L-Citrulline-4,4,5,5-d4).
The acquired data were processed using the Bruker Compass Data Analysis 4.2 software and quantified using the Bruker Quant Analysis 2.2 software.

3.8.13. Ammonia assay

Plasma ammonia was analyzed spectrophotometrically with the Ammonia Assay Kit from Sigma-Aldrich (AA0100). 10 µl of plasma was diluted in 10 µl of water to reach a final volume of 20 µl. To each sample, 200 µl of Ammonia Assay Reagent was added. After 5 min of incubation at room temperature, absorbance was read at 340 nm on a multi-plate reader (Perkin Elmer Envision Plate Reader, Walthman, MA). After, 2 µl of

L-Glutamate solution was added to each sample, incubated for 5 min and the absorbance was re-measured at 340 nm.

Plasma ammonia was calculated in mg of NH_4/ml as described in the manufacturer's instructions.

3.8.14. Plasma hFIX and anti-hFIX antibody determination

hFIX levels were analyzed by enzyme-linked immunosorbent (ELISA), using previously reported protocol (Barzel et al., 2015), using antibody an antibody set FIX-EIA provided by Enzyme Research Laboratories, USA. A standard curve was generated using control human plasma from a healthy individual. A 96 well plate (NUNCTM) was used. The capture antibody (Sigma F2645) was diluted 1/1000 in coating buffer and incubated at room temperature for 2 hours. After, the wells were washed 3 times with PBS 1X 0.1 % Tween. Samples were diluted 1/1000 or 1/25 in sample diluent while reference plasma was serially diluted starting from 1/100 (100%) down to 1/3200 (3.13 %).

100 µl/well of diluted plasma was then incubated for 90 minutes at room temperature. After, the plate was washed 3 times with washing buffer. A polyclonal goat anti-human F9 peroxidase-conjugated IgG secondary antibody (Enzyme Research GAFIX-APHRP) was then diluted 1/4200 in sample diluent and 100 µl/well was incubated in the dark for 90 minutes at room temperature. After the washing step, 100 µl/ well of OPD substrate was used to allow the color to develop. After, 5-10 minutes the reaction was stopped by adding 50 µl of 2.5 M H_2SO_4 to each well. The plate was read at a wavelength of 490 nm on a multi-plate reader (Perkin Elmer Envision Plate Reader, Walthman, MA). The hFIX levels were determined by interpolating the absorbance values from the reference curve, considering reference values 5000 ng/ml.

To evaluate the presence of anti-hFIX antibodies we used a previously reported protocol (Nathwani et al., 2007). Briefly, I coated the plate with 1 µg of native hFIX protein (Invitrogen), mouse IgG (Millipore) to generate a standard curve (starting from 100 ng/µl) left incubating over-night. After the blocking step (2% bovine serum albumin in PBS-0.05% Tween-20), we diluted the plasma sample in 1:10 dilution and detected it with an anti-mouse IgG-HRP antibody. The detection was performed as

described above. For the positive control, we incubated the hFIX protein with an anti-hFIX antibody (Sigma Aldrich).

3.9. Genomic DNA extraction from mice tail

DNA extraction from mice tail biopsies was performed with KAPA Express Extract kit from Sigma-Aldrich (KK7103). Approximately 0.5 cm biopsies were incubated in 50 µl of extraction mix containing 5 µl of Kapa Express Extract buffer, 1 µl of Kapa Express Extract enzyme and 44 µl of water. After a lysis incubation for 10 min at 70°C, a 5 min incubation at 95°C was performed to inactivate the enzyme. The extract was diluted 10-fold with 10 mM Tris-HCl (pH 8.0–8.5).

3.10. Genomic DNA extraction from liver tissue

The extraction kit used for this procedure is Wizard® SV Genomic DNA Purification System by Promega following the indication provided. The lysis buffer (200 µl of Nucley Solution, 50 µl of EDTA, 5 µl of RNAse and 20 µl of Proteinase K) was added to each sample containing from 10-20 mg of liver powder and left incubating O/N at 55°C. The next day, samples were shacked to make sure the liver dissolved. The samples were centrifuged for 20 min at 13,000 xg. After, 250 µl of each supernatant and 250 µl of Wizard® SV Lysis Buffer lysis was transferred into a new 1.5 ml tube and incubated at room temperature for 5 minutes. After incubation, 250 µl of the sample lysate was transferred to Wizard® Minicolumn and centrifuged at 13,000 xg for 2 minutes. The remaining liquid in the collection tube was discarded. A column wash solution (CWA) provided in the kit was added in an amount of 650 µl for each sample and centrifuged at 13,000 xg for 1 minute, this was repeated three times. After the last wash, samples were centrifuged at 13,000 xg for 2 minutes. The DNA was eluted with 50-100 µl of Nuclease-Free Water provided in the kit, by incubating for two minutes at room temperature and centrifuged at 13,000 xg for 1 minute. The concentration was quantified on NanoDrop™.

3.11. Taqman real-time PCR for B6Ei.P-ASS1^{fold}/GrsrJ

A real-time PCR was performed in a C1000 Thermal Cycler CFX96 Real-Time System (Bio-Rad). The 15 µl reaction mix contained:

- 7.5 µl of iQ™ Supermix from Bio-Rad
- 0.3 µl of 20 µM Fw 29134
- 0.3 µl of 20 µM Rev 29135
- 0.1 µl of 20 µM WT probe
- 0.1 µl of 20 µM MUT probe
- 1 µl of DNA diluted 1:10

The cycling conditions were the following:

- 1 cycle of 3 min at 95°C
- 40 cycles of 5 seconds at 95°C and 30 seconds at 60°C

3.12. The T7E1 assay

PCR amplicons from mice genomic DNA were performed with specific primers flanking the targeting region (Table 8). The PCR reaction was performed in a final volume of 50 µl contained: 2 µl of 5mM dNTPs, 4 µl of 100 ng/µl Forward primers, 4 µl of 100 ng/µl Reverse primer, 5 µl of 10x Buffer (Roche), 0.3 µl of Taq polymerase (Roche), 29.7 µl of H_2O and 5 µl of DNA diluted 1:10. The PCR was performed with the following cycles: 1 cycle at 94°C for 2 min, 30-35 cycles at 94°C for 30 sec, 60°C for 45 sec, 68°C for 1 min and 1 cycle at 68°C for 7 min. PCR amplicons were purified using Sephacryl S-400 beads (Sigma-Aldrich). For the T7E1 assay amplicons were denatured and self-annealed forming heteroduplex structures in the case of indels. The T7E1 enzyme was added (1 µl for each amplicon) and left incubating at 37°C for 30 min. The enzyme was stopped by adding 0.25 M EDTA. Samples were run on a 2 % agarose gel and visualized with a UV transilluminator.

3.13. Crispr/Cas9 efficiency: TiDE software

CRISPR/Cas9 cleavage efficiency was estimated using TIDE (Tracking of Indels by Decomposition) software. PCR amplicons used previously for the T7E1 assay were sequenced with Eurofins Genomics. The raw sequences were analyzed with the TIDE web tool (https://tide.nki.nl/) (Brinkman et al., 2014).

3.14. Total RNA extraction from liver

Frozen livers were crushed into liver powder and stored at -80°C. RNA was extracted by homogenizing liver powder in NucleoZOL solution (Takarabio) following the supplier protocol "Isolation of total RNA" (https://www.takarabio.com/assets/documents/User%20Manual/NucleoZOL%20RNA%20Isolation%20User%20Manual_Rev_01.pdf). Up to 50 µg of the tissue was homogenized in 500 µl of NucleoZOL using a homogenizer. After, 200 µl of RNAse free water was added, mixed for 15 seconds, and left at RT for 15 minutes. After centrifugation at 12,000 xg for 15 minutes, 500 µl of supernatant was transferred to 500 µl of isopropanol left incubating for 10 minutes and centrifuged for another 10 minutes at 12,000 xg at RT. The RNA pellet was washed 2 times with 500 µl of 75 % ethanol by centrifugation for 3 minutes at RT. The RNA was dissolved in 70 µl of RNAse free water at 56 °C for 10 minutes. The RNA quality was controlled on 1 % agarose gel and by absorbance ratios 260/280 and 260/230 nm measured on a NanoDropTM 1000 spectrophotometer (Thermo Scientific) at 260 nm. The concentration was obtained by the same NanoDropTM measurement.

3.15. Reverse transcription (RT)

1 µg or 300 ng (in case of hemophilia study) of total RNA was reverse-transcribed using M-MLV reverse transcriptase (Invitrogen, Carlsbad, CA, United States)

following suppliers instructions (https://assets.thermofisher.com/TFS-Assets/LSG/manuals/mmlv_rt_man.pdf).

The mix included:

- 5 µl of oligo(dT) (100 µg/mL),
- 1 µl of 300 ng or 1 µg of total RNA
- 1 µl of 10 mM dNTP Mix (10 mM each dATP, dGTP, dCTP and dTTP at neutral pH) distilled water up to the final volume of 12 µL

Samples were incubated at 65°C for 5 min and left cooling on ice for 2 min. Each sample received the second mix that included:

- 4 µl of 5x First-Strand buffer
- 2 µl of 0.1 M DTT
- 1 µl of RNaseOUT™ Recombinant Ribonuclease Inhibitor

Samples were incubated for another 2 minutes at 37°C. After, 1 µl of M-MLV RT (200 units) was added and incubated for 50 min at 37°C. To inactivate the enzyme, samples were heated at 70°C for 15 minutes.

3.16. Comparison of RT-qPCR primer efficiency

Primers efficiency was compared by amplifying the chimeric *hFIX-Alb* or *hASS1-Alb* cDNAs in treated mice and endogenous *mFIX* or *mASS1* cDNA in *wild-type* mice. To obtain the amplicon, a first PCR amplification was performed using the following protocol:

- 5 µl of Buffer Roche 10X,
- 2 µl of 5mM dNTPs,
- 4 µl or forward primer (100 ng/µl),
- 4 µl of reverse primer (100 ng/µl),
- 0.3 µl of taq polymerase Roche,
- 32.2 µl of H_2O and
- 1 µl of cDNA (diluted 1:10).

The amplification was carried in a C1000 Thermal Cycler CFX96 Real-Time System (Bio-Rad) with the following cycles:

- 1 cycle at 94°C for 2 min,

- 30-35 cycles at 94°C for 30 sec, 60°C for 45 sec, 70°C for 1 min
- 1 cycle at 70°C for 7 min

The PCR product was cleaned up or, in the case of double bends, extracted from the gel using a kit NucleoSpin® Gel and PCR Clean-up from Macherey-Nagel company. The amplicons were quantified with nanodrop and the set of primers was tested again on the amplicons using a C1000 Thermal Cycler CFX96 Real-Time System (Bio-Rad).

A master mix with a final volume of 15 µl included:

- 7.5 l of SYBER Green Supermix (Biorad)
- 1 µl of primer forward (100 ng/µl)
- 1 µl of primer forward (100 ng/µl)
- 4.5 µl of dH2O
- 1 µl of the amplicon (serial dilution 1:10 were generated starting from 0.2 ng of the template)

The Cq mean values and the template quantity of the chimeric mRNA in treated mice and the endogenous mRNA levels in *wild-type* mice were plotted in a graph using Prism 8.

3.17. mRNA expression level

mRNA expression levels were measured with a quantitative RT-PCR using a C1000 Thermal Cycler CFX96 Real-Time System (Bio-Rad).

A master mix with a final volume of 15 µl included:

- 7.5 l of iQ SYBER Green Supermix (Biorad)
- 1 µl of primer forward (100 ng/µl)
- 1 µl of primer forward (100 ng/µl)
- 4.5 µl of dH2O
- 1 µl of cDNA diluted 1/10
- Samples were analyzed on a 96-well real-time PCR plate with the following conditions:
- 1 cycle of 30 seconds at 98°C
- 40 cycles of 5 seconds at 95°C and 25 seconds at 62°C

- Melting curves were generated at 95°C for 10 seconds and increased from 65°C to 95°C at 0.5°C/sec

Data were analyzed using the ΔΔCt method.

3.18. Viral genome particle analysis

Viral genome particles were quantified using a quantitative PCR method. Total genomic DNA from the liver was extracted using the previously Wizard SV Genomic Purification System. The pAB288 donor vectors or SaCas9 were analyzed using specific primers listed in the table 8. A master mix included:

- 7.5 l of iQ SYBER Green Supermix (Biorad)
- 1 µl of primer forward (100 ng/µl)
- 1 µl of primer forward (100 ng/µl)
- 4.5 µl of dH2O
- 1 µl of DNA (10-20 ng)

To extrapolate the number of genomic particles per cell a standard curve was generated from the desired vector. The quantification protocol was the following:

- 1 cycle of 30 seconds at 98°C
- 40 cycles of 5 seconds at 95°C and 25 seconds at 62°C

Melting curves were generated at 95°C for 10 seconds and increased from 65°C to 95°C at 0.5°C/sec.

3.19. Histological analysis

Liver lobes of *wild-type* mice treated with rAAV-donor-eGFP were fixed in 4 % PFA in PBS 1X for 24 hours at 4°C and the PFA was then changed with 20 % sucrose 0.02 % sodium azide in PBS 1X and kept at 4°C. Liver lobes were frozen at optimal cutting temperature and cut in a cryostat in 4 µm slices. They were washed twice with PBS and mounted with Vectashield (Vector Laboratories, CA, United States).

3.19.15. eGFP analysis

Slices were washed three times with PBS 1X and nuclei were stained with Hoechst solution for 10 minutes. Slices were washed three more times with PBS 1X, rinsed in water and covered with a coverslip on Mowiol mounting regent. Fluorescent images were taken with NIKON fluorescent microscope. Images were modified using ImageJ software version 2.0.0-rc-69/1.52p.

3.19.16. Fluorescent in-situ hybridization

hASS1 mRNA was detected in liver sections using HRC RNA-FISH Technology kit purchased from Molecular Instruments, using their protocol. Fixed liver cryosections were permeabilized with PBS 1X, 0.1 % Tween, 0.5 % Triton for 20 minutes. 100 µl of hybridization buffer was added to the liver section and was incubated in a humidified chamber for 10 minutes at 37°C. Next, 0.4 pmol of hASS1-specific probes and 100 µl of hybridization buffer were added to the liver section and left incubating overnight in a humidified chamber at 37°C. The next day, probe wash buffer was added to slides and left at 37°C for 10 minutes. Following probe washes at 37°C with:

- 75% of probe wash buffer and 25% 5× SSCT for 15 min,
- 50% of probe wash buffer and 50% 5× SSCT for 15 min,
- 25% of probe wash buffer and 75% 5× SSCT for 15 min,
- 100% 5× SSCT for 15 min

The last wash used 5× SSCT for 5 minutes at room temperature.

To pre-amplify the probe, 100 µl of amplification buffer was added on slides and left incubating in a humidified chamber at 37°C for 30 minutes. In the meantime, 6 pmol of hairpin h1 and 6 pmol of hairpin h2 were activated at 95°C for 90 seconds and left to cool down to room temperature for 30 minutes in dark. Hairpins were mixed to 100 µl of amplification buffer, added to the sample and incubated overnight in a humidified chamber at room temperature.

5× SSCT was used to remove excess hairpins for 2x30 minutes and 1x5min. Nuclei were stained with Hoechst for 5 minutes and washed three times with PBS. Samples

were covered with a coverslip on top of Mowiol mounting reagent. Fluorescent images were taken with a confocal microscope. Images were modified using ImageJ software version 2.0.0-rc-69/1.52p.

3.19.17. Immunostaining of hFIX in liver tissue

Liver lobes from FIX KO were sent frozen. Later they were cut at 8 µm slices in a cryostat. Sections were thawed at room temperature and rinsed in PBS 1X. Fixation and permeabilization step was performed in acetone for 10 min at -20°C. Slices were washed three times with PBS 1X for 5 minutes. Slices were blocked for 90 minutes in a blocking solution containing 10 % normal goat serum (NGS), Triton 0.1 %, PBS 1X. The primary antibody (GAFIX-AP, Affinity Biologicals) was diluted 1/50 in blocking solution and left incubating overnight at 4°C. The next day samples were washed 3 times in PBS 1X for 5 minutes. Slides were incubated with the secondary antibody AlexaFluor 647 IgG at 1/500 in Triton 0.1 %, PBS 1X for 1 hour. After washing the slices 3 times with PBS 1X, slices were incubated with Hoechst 1/5000 in PBS 1X for 10 min and washed 3 times in PBS 1X for 5 minutes. After a rinse in water, slices were covered with a coverslip in Mowiol mounting reagent. Fluorescent images were taken with NIKON fluorescent microscope. Images were modified using ImageJ software version 2.0.0-rc-69/1.52p.

3.20. Protein extraction from mice liver

Proteins were extracted from liver powder by homogenizing the powder in a lysis buffer for protein extraction. For approximately 10 mg of liver powder, 200 µl of lysis buffer was used. Samples were centrifuged at max speed at 4 °C and the supernatant was collected.

Protein concentration was measured with the Bradford assay. Briefly, on a 96 well NUNC plate, 200 µl of Coomassie Brilliant Blue G-250 (CBB) was added to 1 µl of protein lysate and measured absorption at 595 nm using a multi-plate reader (Perkin Elmer Envision Plate Reader, Walthman, MA). To determine protein concentration a

reference curve was made with known concentrations of Bovine Serum Albumin protein (BSA, BioLabs).

3.21. Western blot analysis

Liver protein extract (40 µg in case of FIX and eGFP, 10 µg for hASS1) or plasma diluted 1:50 were run on a precast gel (NuPAGE Bis-Tris 4-12 %, Thermofisher). 10 µl of the sample was added to electrophoretic chambers, after a denaturation step with 1X of protein loading buffer for 5 min at 95°C. After the run, the proteins were transferred to a Polyvinylidene fluoride membrane using a Lightning Blot™ System (Perkin Elmer). A sandwich was made from three Whatmann 3 mm papers soaked in Blotting solution 1, the PVDF membrane activated in methanol and soaked in Blotting solution 2, gel and three 3 mm papers soaked in Blotting solution 3. Proteins were visualized by incubating the membrane with Red Ponceau solution for 5 min. The membrane was washed and blocked in Block-CH (Chemiluminescent Blocker, Millipore) for at least 2 hours.

For hFIX detection, the primary antibody (GAFIX-AP, Affinity Biologicals) was diluted 1/3000 in 5 % milk 0.1 % Tween PBS for 5 hours. After washing the membrane three times for 5 min with PBS 0.1 % Tween, the membrane was incubated with the secondary antibody anti-goat for 1 hour and the washing step was repeated. Enhanced Chemiluminescence (ECL – ThermoFisher Scientific) was added to the membrane for 5 min and the proteins were visualized using a ChemiDoc imaging system (Biorad).

The primary antibody for hASS1, Hsp70, EGFP, was diluted 1/3000, 1/8000, 1/3000 respectively in 5 % milk 0.1 % Tween PBS overnight at 4°C and the membrane was washed three times with PBS 0.1 % Tween. After, the secondary antibody was diluted 1/3000 and added to the membrane for 1 hour. After the washing step, Enhanced Chemiluminescence (ECL – ThermoFisher Scientific) was added to the membrane for 5 min and the proteins were visualized using a ChemiDoc imaging system (Biorad).

Target protein	*Supplier*	*Source*	*Dilution*
eGFP	Santa Cruz	Rabbit	1/3000
GAPDH-HRP	Sigma	Mouse	1/10000
hASS1	Invitrogen	Mouse	1/3000
hFIX	Affinity Biologicals	Goat	1/3000
Hsp70	Enzo	Rat	1/8000

Table 9: Antibodies used for western blot analyses.

3.22. Statistical analysis

Statistical analyses were performed using GraphPad Prism 8.2.1. Data shown in graphs are plotted as mean and standard deviation (SD) or standard error of the mean (SEM). For the statistical analysis of two groups, Student's t-test was used. For the comparison of more than two groups one-way or two-way ANOVA was used following Tukey's test. Mantel-Cox test was used for survival analysis. A p-value below 0.05 was considered significant (* $p<0.05$, ** $p<0.01$, *** $p<0.001$).

4. Results

4.1. Self-limiting Crispr/Cas9

To prevent long-term expression of the CRISPR/Cas9 system in the organism and all side-effects it brings along, a self-limiting CRISPR/SpCas9 circuit was developed by Petris et al. (2017), with the Staphylococcus pyogenes Cas9, to ensure safety and specificity. The SLiCES (Self-limiting Cas9 Circuit for Enhanced safety and Specificity) system consists of the simultaneous delivery of a Cas9 endonuclease, a single guide RNA that targets a specific genome region and a second gRNA that targets the coding sequence of the *Cas9* cDNA. Self-targeting mediates a knockdown of the endonuclease, reducing its expression and, subsequently, the possibility of having an off-target activity (Petris et al., 2017). I compared the normal SaCas9 and SLiCES system (Petris et al., 2017b) *in vivo* on *wild-type* FVB mice. In the first group of mice, we delivered a rAAV8 vector encoding the SaCas9 with a guide RNA targeting the albumin locus. The second group was treated with the SLiCES version: a SaCas9 with two guides RNA, one targeting the albumin locus and the other targeting the *Cas9*. Mice were treated intravenously with 3,20E11 vgp/pup with AAV8 encoding SaCas9 or self-limiting SaCas9 at post-natal day 2. Mice were sacrificed at P10 and liver was collected (Figure 11).

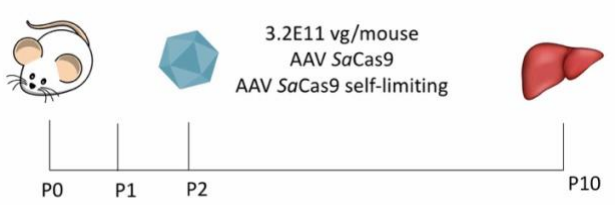

Figure 11: Experimental plan for the evaluation of the self-limiting Cas9 system *in vivo*. Newborn mice were injected i.v. with rAAV8 Sacas9 gRNA 8 or rAAV8 SaCas9 sgRNA8 and sgRNACas9.

I extracted genomic DNA from liver homogenates and evaluated viral genome particles per cell. Both experimental groups showed a similar amount of *Sa*Cas9 (Figure 12).

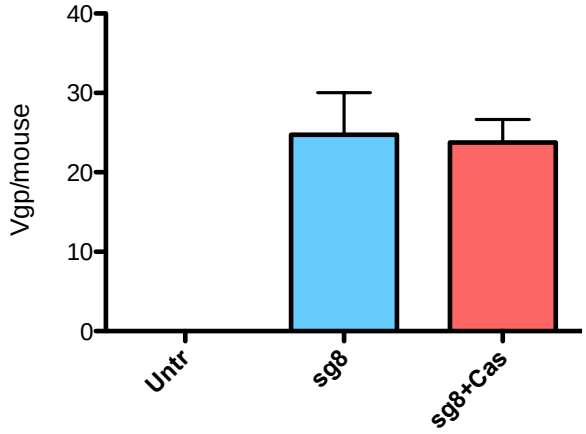

Figure 12: Viral genome particles analysis of AAV8 SaCas9 and AAV8 SaCas9 self-limiting. Vgp were measured at post-natal day 10, 8 days after injection.

Next, I evaluated the cleavage efficiency in genomic DNA of both *Sa*Crispr/Cas9 with T7E1 assay and TiDE software (Figure 13). T7E1 assay consists of generating a PCR fragment containing the edited locus. The T7 endonuclease cuts the DNA in the edited region in a single-stranded region present in heterodimers formed between edited and WT fragments. Both analyses showed a similar cleavage activity of the two *Sa*Cas9 versions. Animals A8191, A8192, A8194, A8195 were injected with the normal version of AAV8 *Sa*Cas9, containing only the guide RNA targeting the albumin locus. Mice A8196, A8197, A8198, A8199 were treated with the self-limiting version of the *SaCas9* (Figure 13).

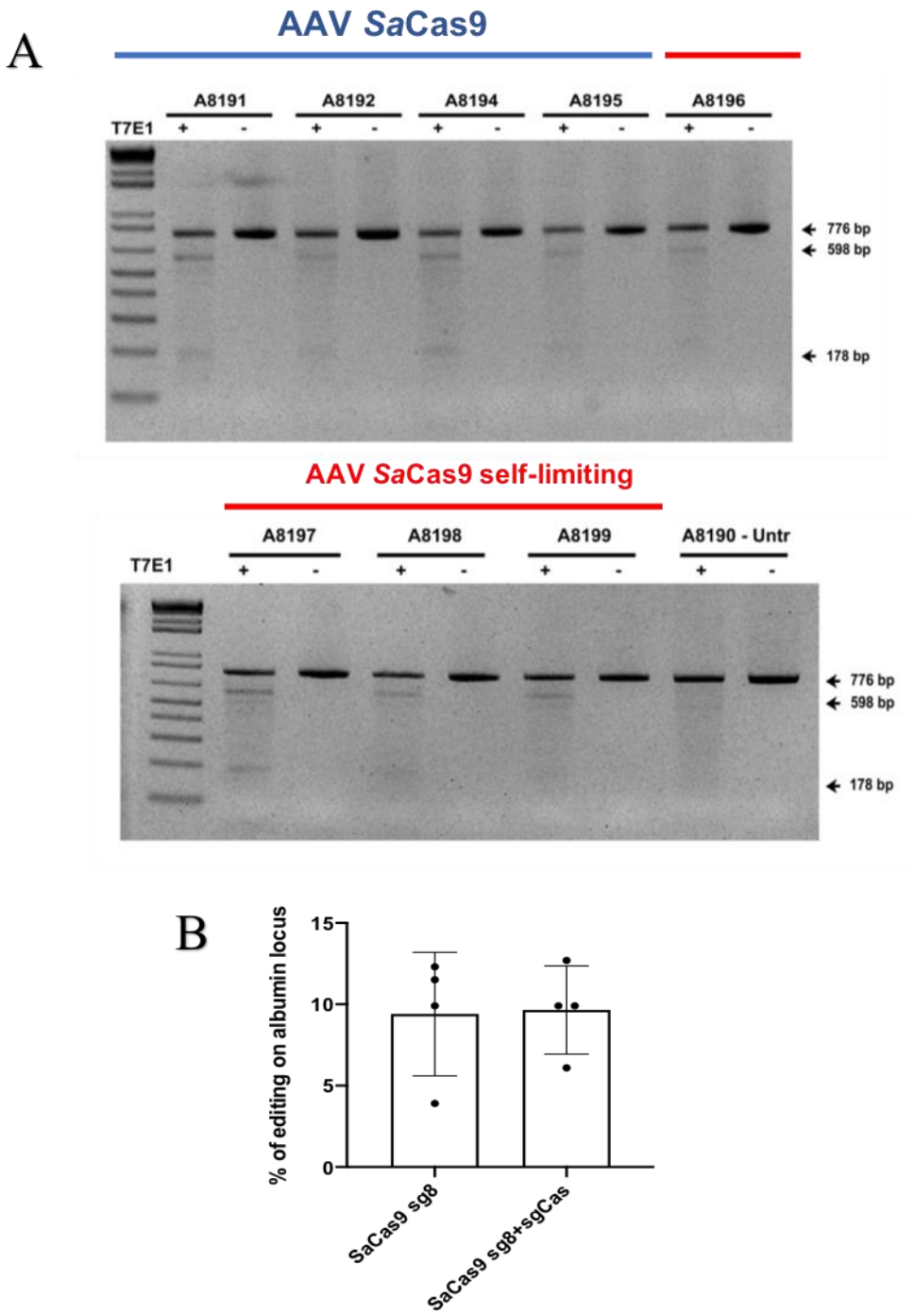

Figure 13: Evaluation of the guide RNA cleavage efficiency for the albumin locus. SaCas9 and self-limiting SaCas9 *in vivo* cleavage efficiency with (A) T7E1 assay and (B) TiDE software showing editing efficiency (in %) in the albumin genomic DNA.

Unexpectedly, mice injected with the SLiCE system had a similar vgp/cell as mice injected with normal Cas9. I hypothesized that the sgRNA targets the Cas9 gene but the AAV DNA may not be degraded by the cell, as it may be repaired by the NHEJ repair

mechanism. To evaluate this possibility, I performed a T7E1 assay evaluating the presence of InDels in the Cas9 gene. I did not observe any cleavage activity by agarose gel electrophoresis, as no fragments were detected. The TiDE software instead showed a cleavage activity of the second guide (Figure 14). We suppose that the guide RNA that targets the Cas9 was not efficient enough in the *in vivo* experiments, in contrast with the previous data generated in transfected tissue culture cells. However, the T7E1 assay is not sensitive enough to detect a small percentage of edited DNA. For further experiments, we decided not to use the self-inactivating system but the normal SaCas9 nuclease.

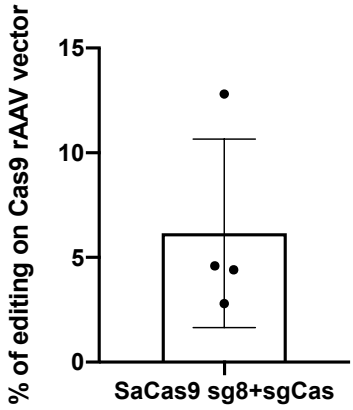

Figure 14: Evaluation of the guide RNA cleavage efficiency for the Cas9 gene: Cleavage efficiency of the gRNA targeting the Cas9 gene was evaluated with TiDE software.

4.2. The "GeneRide" targeting strategy coupled with the Crispr/Cas9 platform

Gene replacement therapy has shown many successes in the treatment of monogenic liver metabolic diseases both in pre-clinical studies and clinical trials especially when treating adult patients. However, important limits are present in neonatal/pediatric settings, as many of those diseases have a pediatric onset and due to liver proliferation the rAAV episomal vector is lost over time. Re-administration in most cases is not possible due to the formation of neutralizing antibodies. Thus, conditions with active

cell division may require a strategy resulting in the permanent modification of the genome by correcting the mutated gene or by integrating a corrected cDNA into the genome, by gene editing or genome targeting.

The "GeneRide" strategy was developed in Mark Kay's Lab to treat the Hemophilia B mouse model and consists of a donor vector containing a promoterless therapeutic *hFIX* cDNA with arms of homology for the albumin gene. The donor DNA is delivered to hepatocytes with an AAV vector and mediates a site-specific integration by homologous recombination mechanism, without the use of engineered nucleases. The transgene is inserted right upstream the stop codon, in-frame with the ORF of albumin, without disrupting its coding sequence, producing a chimeric mRNA that will be translated into two separate proteins: albumin and therapeutic protein (Barzel et al., 2015). In the Mouse Molecular Genetics laboratory (ICGEB, Trieste) this strategy was applied to a mouse model of the Crigler-Najjar Syndrome (CNS) by inserting the human uridine glucuronosyltransferase A1 (UGT1A1) cDNA into the mouse albumin locus. However, even if this strategy was able to rescue mice from neonatal lethality, the levels of toxic bilirubin did not reach *wild-type* levels (Porro et al., 2017).

To increase the targeting rate of the "GeneRide" strategy, the Crispr/SaCas9 nuclease was co-delivered with a modified version of the donor vector. The PAM sequence present in the vector was mutated to avoid vector cleavage (Figure 15). This strategy on the CNS mouse model showed a complete rescue of the diseased phenotype, lowering plasma bilirubin levels to normal *wild-type* values until 10 months of age. Animals did not present any liver abnormality and Illumina sequencing on predicted SaCas9 off-target sites resulted in no off-target activity. This strategy confirmed its efficacy in the rescue of neonatal lethality of a liver metabolic disease and also demonstrated a safety profile (De Caneva et al., 2019).

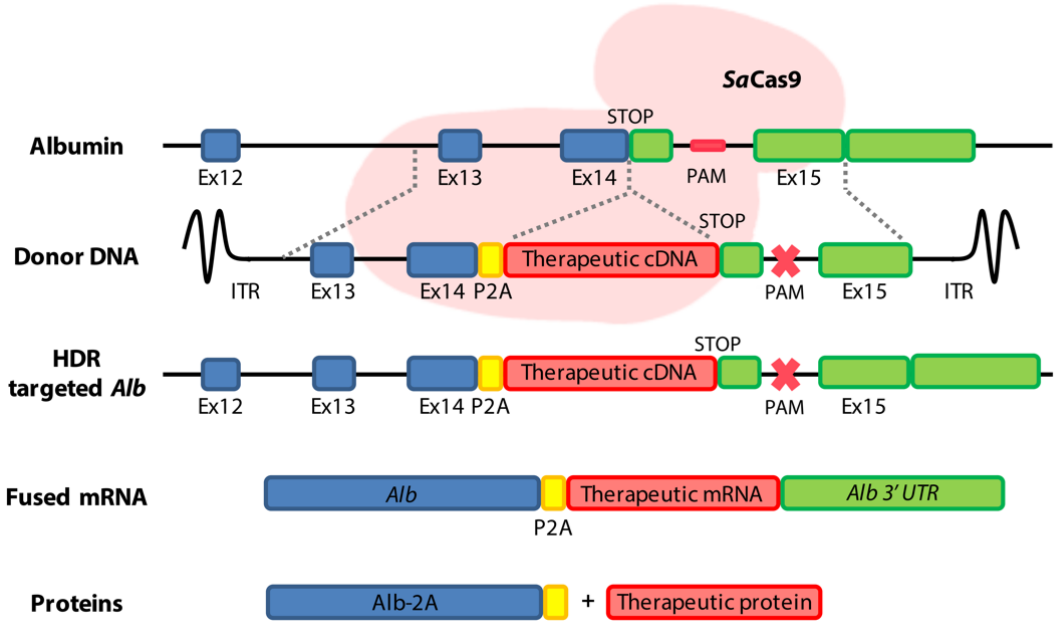

Figure 15: "GeneRide" coupled with SaCas9 nuclease. This strategy targets a therapeutic vector into the albumin locus. The therapeutic cDNA is preceded with the 2A-peptide and flanked with the albumin homology arms. After recombination, the transgene is integrated before the stop-codon signal. *Albumin* and a therapeutic cDNA are transcribed in one hybrid mRNA molecule, but after translation two different proteins are produced. The *Sa*Crispr/Cas9 performs a double-strand break downstream of the albumin stop codon, enhancing the homologous directed repair rate.

Citrullinemia type I study

Different mouse models for Citrullinemia type I have been generated and employed to study the disease, and to find potential treatments to cure this metabolic disorder. A mouse model representing a milder form of the disease was generated and described by Perez and colleges (Perez et al., 2010). Those mice have a $ASS1^{fold/fold}$ hypomorphic mutation in the *ASS1* gene resulting in an amino acid change, causing a decrease in the ASS1 activity and leading to the accumulation of citrulline and toxic ammonia. $ASS1^{fold/fold}$ mice can be recognized by their lack of fur at 10 days of age and their smaller size compare to the *wild-type* littermates. According to the reported characterization of $ASS1^{fold/fold}$ mice, approximately 50 % die within 21 days, with plasma ammonia levels around 270 µM (Perez et al., 2010).

We obtained the ASS1$^{fold/fold}$ mouse stain from the Jackson laboratories (Strain N. 006449). However, in our laboratory, the homozygous mutant animals survived more than 21 days when fed with a normal protein-content chow diet (18% of protein), even until day 164 (Figure 16A). Those results showed that the ASS1$^{fold/fold}$ colony present in our facility displays a less severe form than the one originally described by Perez and colleges (Perez et al., 2010). Proteins were extracted from the liver homogenate and western blot using a human-specific anti-ASS1 antibody was performed. We purchased and tested anti human ASS1 antibodies from different companies and observed that these antibodies were able to also recognize the murine ASS1 protein, and no significant difference in ASS1 protein levels between *wild-type* and homozygote ASS1$^{fold/fold}$ mice was observed (Figure 16B-C). This happened because the ASS1$^{fold/fold}$ mice produce similar amounts of a less active ASS1 protein compared to *wild-type* mice (Perez et al., 2010).

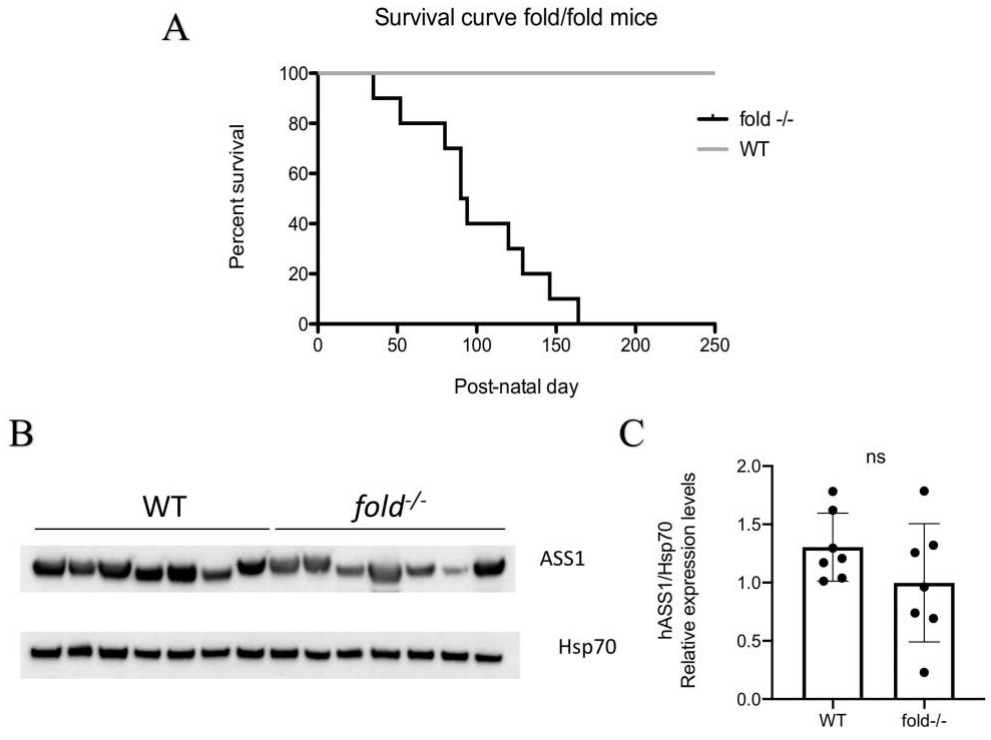

Figure 16: Characterization of ASS1$^{fold/fold}$ mice. A) Kaplan-Meier survival curve. Evaluation of the mortality rate of ASS1$^{fold/fold}$ mice (black) and *wild-type* (grey). **B) Western blot analysis.** Comparison of the ASS1 protein levels in *wild-type* and ASS1$^{fold/fold}$ mice. **C) WB quantification.** hASS1/Hsp70 relative protein levels from western blot analysis. Data are shown as mean ± SEM and statistically analyzed by one-way ANOVA with Tukey's multiple comparison test.

To increase the severity of the diseased phenotype, we fed the ASS1$^{fold/fold}$ mice with diets containing increasing protein content, expecting that high protein levels in mice with an altered urea cycle would lead to an accumulation of ammonia in their bloodstream and a more severe phenotype will be displayed. We fed mutant ASS1$^{fold/fold}$ mice with different protein-content diets: 18 % (standard diet), 23 % (enriched diet for enhanced breading) and 51 % (high protein diet) of proteins and monitored survival of mice. Mice fed with an enriched diet did not show an increase in the mortality rate compared with the mice fed with the standard diet. In contrast to what we expected, mice fed with a 51 % diet had an increase in the survival rate up to 1 year (Figure 17).

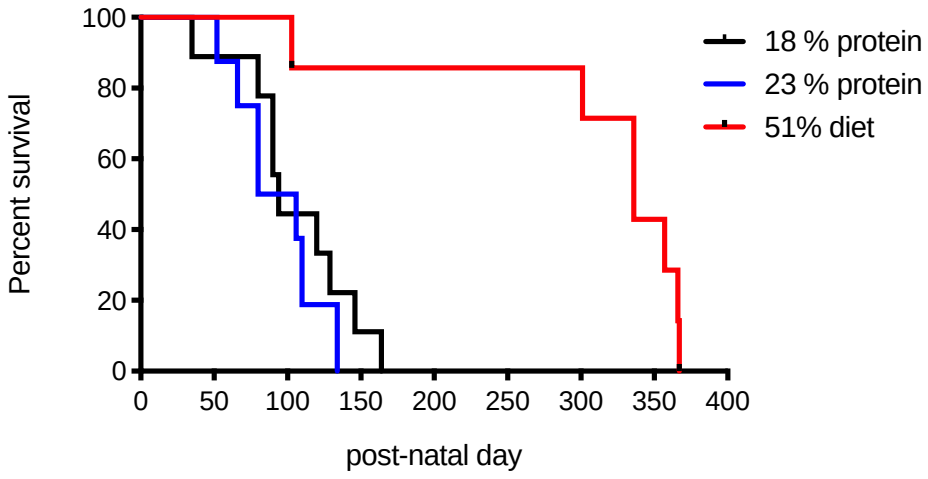

Figure 17: Kaplan-Meier survival curve of ASS1$^{fold/fold}$ mice treated with different diets. A standard 18 % protein diet survived until the post-natal day (P) 164 (n=4). Mice treated with a 23 % protein diet survived until P 134 (n=5). One mouse treated with a 51 % diet died at P103, the others are still alive (n = 6).

Plasma citrulline analysis showed a citrulline increase in all three groups reaching an average citrulline level of 400 µM, ranging from 200–800 µM, in 1-2 months old mice, while in the *wild-type* animals citrulline was between 0-50 µM (Figure 18A).

Compared to the *wild-type* mice, the ASS1$^{fold/fold}$ mice fed with a 51 % protein diet had a higher increase in ammonia levels than ASS1$^{fold/fold}$ mice fed with an 18 % protein diet. The statistical comparison of ammonia levels of ASS1$^{fold/fold}$ animals fed with 18 % and 51 % showed no statistical significance. A significantly higher increase had animals given the enriched diet (23 % protein diet) with an average of 400 µM NH_4 levels when compared to animals given the 18 % protein diet (Figure 18B). All animals had from 1-2 months of age.

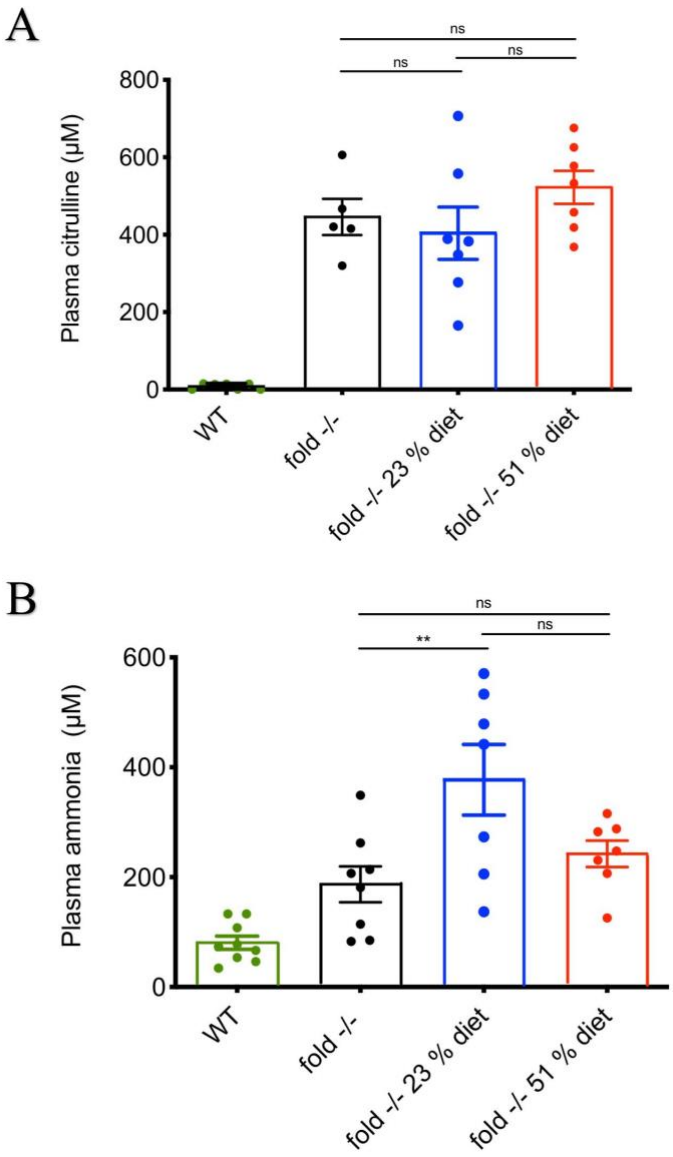

Figure 18: Plasma analysis of mice treated with different protein-content diets. Citrulline (A) and ammonia (B) levels from plasma samples of ASS1$^{fold/fold}$ animals treated with different diets. *Wild-type* mice were treated with a standard 18 % protein diet. Plasma from the ASS1$^{fold/fold}$ mice, treated with 18 %, 23 % and 51 % protein diet from birth was analyzed at 1-2 months of age. Data are shown as mean ± SEM and statistically analyzed by one-way ANOVA with Tukey's Multiple comparison test: ** P<0.01.

4.2.1. Evaluation of *hASS1* codon optimization versions

We designed different codon-optimized versions of the *hASS1* cDNA and evaluated their expression *in vitro*. HeLa cells were transfected with four codon-optimized versions and the *wild-type* version of the *hASS1* cDNA (Figure 19A). Proteins were extracted 24 hours post-transfection and a western blot was performed to analyze protein expression (Figure 19B-C). The band detected in the cells transfected with codon-optimized vector 1 was almost 3-fold more abundant than the one resulting from the *wild-type* cDNA. After this result, we selected the *hASS1 wild-type* and codon-optimized version 1 as candidates for further *in vivo* experiments. The two *hASS1* cDNA variants were cloned into a modified version of the donor pAB288 vector. To compare the efficacy of the integrative approach with the classic episomal one, the same *hASS1* cDNAs were also cloned into an episomal pSMD2 vector containing a strong liver-specific promoter (α1AAT and ApoE enhancer, Ronzitti et al., 2016) (Figure 20). AAV vectors were produced in Genethon (France) or ICGEB AAV facilities (Trieste).

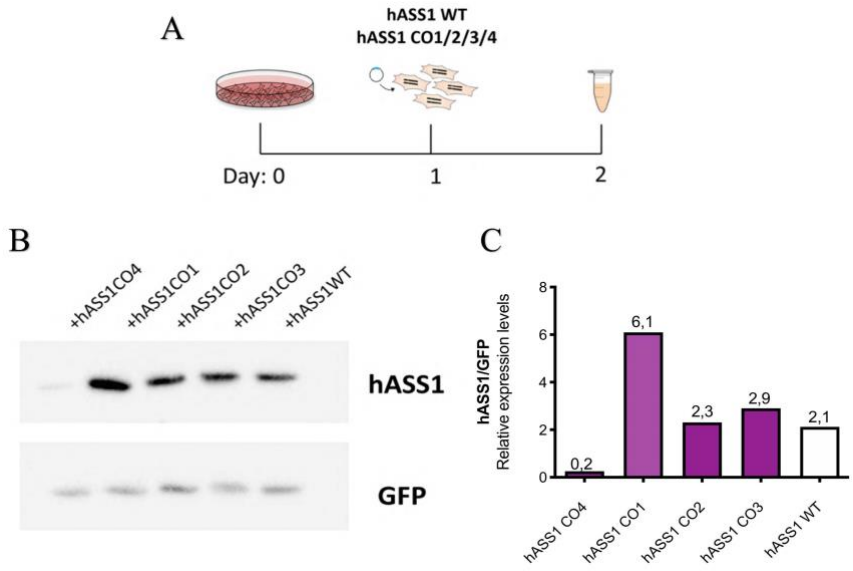

Figure 19: Evaluation of *hASS1 wild-type* and codon-optimized cDNAs. A) Experimental plan: Transfection of HeLa cell line with four codon-optimized versions of *hASS1* and the *wild-type* version. **B) Western blot analysis** of four codon-optimized versions and *wild-type* version of hASS1 protein. **C) Quantification of hASS1/eGFP** protein levels from western blot analysis.

For the treatment of neonatal CTLN1 mice we selected two gene-based therapies:

- Gene therapy with an episomal rAAV vector encoding *hASS1* cDNA
- GeneRide with the CRISPR/Cas9 approach composed of a rAAV *Sa*Cas9 endonuclease coupled with integrative donor vector containing *hASS1* cDNA flanked with arms of homology of the albumin locus

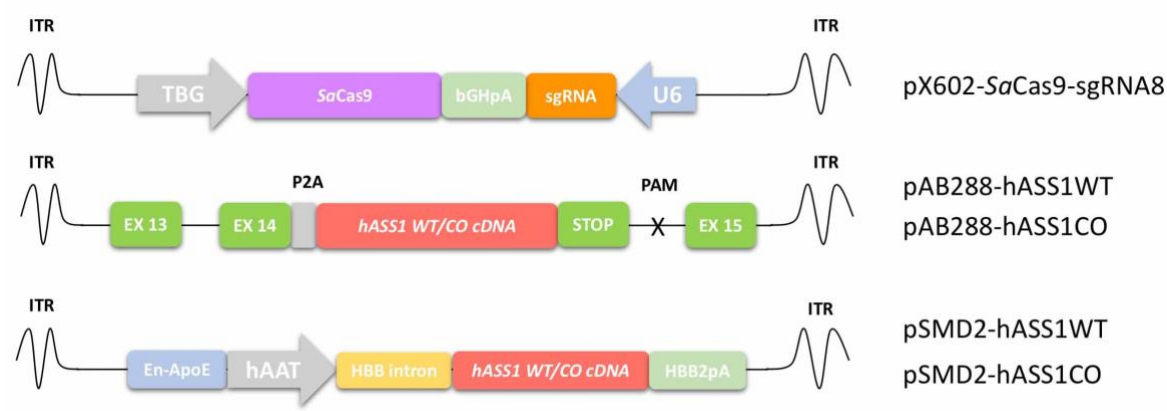

Figure 20: AAV8 vectors used in citrullinemia type I treatments.

4.2.2. Treatment of neonatal CTLN1 mouse model

Mice were treated at post-natal days two with the following rAAV8 vectors:

Gene targeting (integrative) approach:

- rAAV8-SaCas9 (2,0E11 vg/pup) + rAAV8-donor-hASS1WT (2,0E11 vg/pup)
- rAAV8-SaCas9 (2,0E11 vg/pup) + rAAV8-donor-hASS1CO (2,0E11 vg/pup)

Gene therapy (non-integrative) approach:

- rAAV8-pSMD2-hAAT-hASS1 WT (2,0E11 vg/pup)
- rAAV8-pSMD2-hAAT-hASS1 CO (2,0E11 vg/pup)

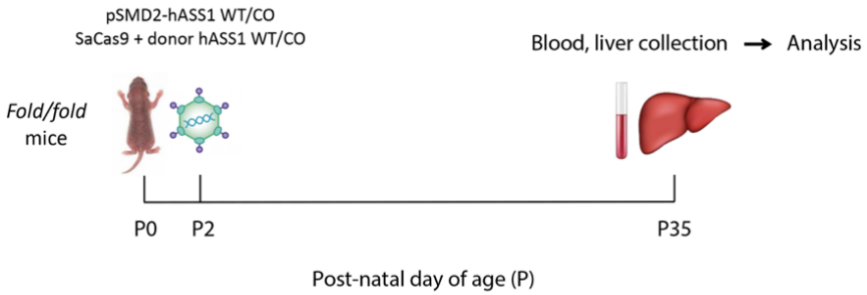

Figure 21: Experimental plan for gene targeting and non-integrative gene therapy for CTLN1 mice: treatment of four groups of ASS1$^{fold/fold}$ newborn mice with rAAV8-donor-hASS1 WT or CO (2,0E11 vgp/pup) together with rAAV8-SaCas9 (2,0E11 vgp/pup) and episomal rAAV8-pSMD2-hAAT-hASS1 WT or CO (2,0E11 vgp/pup). Mice were sacrificed at 35 days.

4.2.2.1. Biochemical analysis of mice plasma

Blood from treated mice was collected at 1 month of age and analyzed for citrulline and ammonia levels. Mice treated with the integrative gene targeting approach had a significant decrease in plasma citrulline level compared to the untreated ASS1$^{fold/fold}$ mice. On the contrary, mice treated with the episomal gene therapy approach showed a smaller decrease in plasma citrulline which was not statistically significant (Figure 22A). Plasma ammonia was analyzed using an ammonia assay kit. Plasma ammonia in all treated groups showed no statistical difference compared to the untreated ASS1$^{fold/fold}$ group, suggesting that none of the treatments were effective in lowering ammonia levels (Figure 22B).

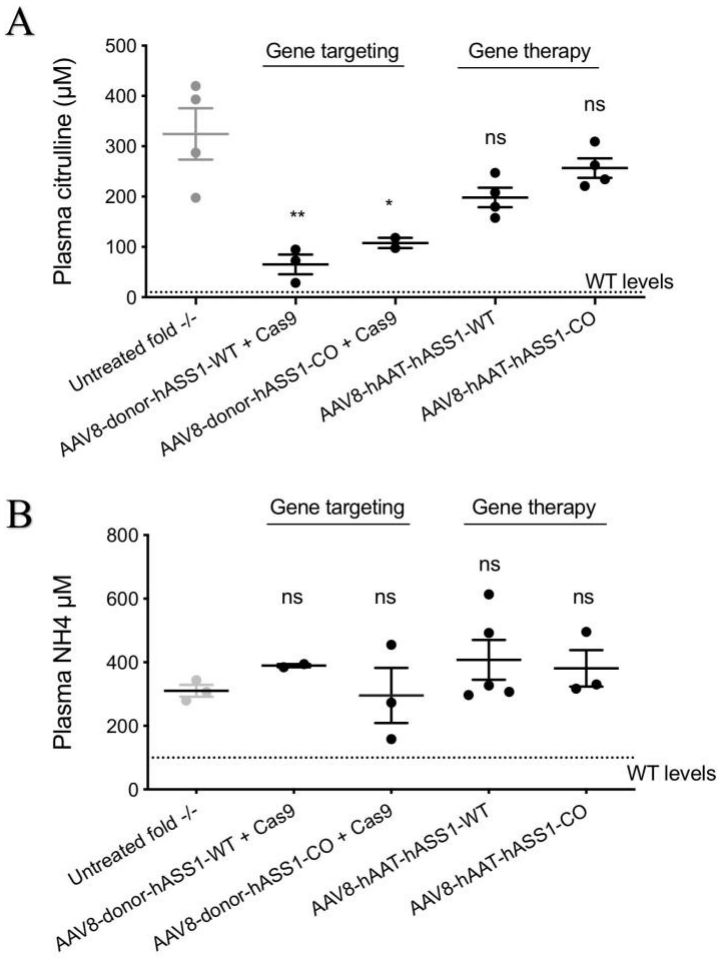

Figure 22: Plasma analysis after CTLN1 mice treatment: A) Plasma citrulline levels were analyzed at P35. Untreated $ASS1^{fold/fold}$ mice were used as a control group. Data are shown as mean ± SEM and statistically analyzed by one-way ANOVA with Tukey's Multiple comparison test: * $p<0,05$, ** $p<0,01$. **B) Plasma ammonia levels** were analyzed at P35. Untreated $ASS1^{fold/fold}$ mice were used as a control group. A grid line represents ammonia levels in healthy wild-type mice. Data are shown as mean ± SEM and statistically analyzed by one-way ANOVA with Tukey's Multiple comparison test: ns>0,05.

4.2.2.2. Viral genome particles in mouse livers

Since the gene targeting treatment efficiently lowered the citrulline levels but didn't have a significant effect on ammonia levels, I performed a quantitative PCR to determine the number of viral genome particles present in each cell in order to assess

potential differences in transduction efficiency between the two rAAV8 vectors. Thus, two qPCR were performed: one amplifying the TBG promoter present in the AAV8 vector that encodes the *Sa*Cas9; and the other qPCR on a region specific to the pAB288 donor template. With this analysis, the presence of the viral genome in liver cells was confirmed at similar levels in all the treated groups (Figure 23).

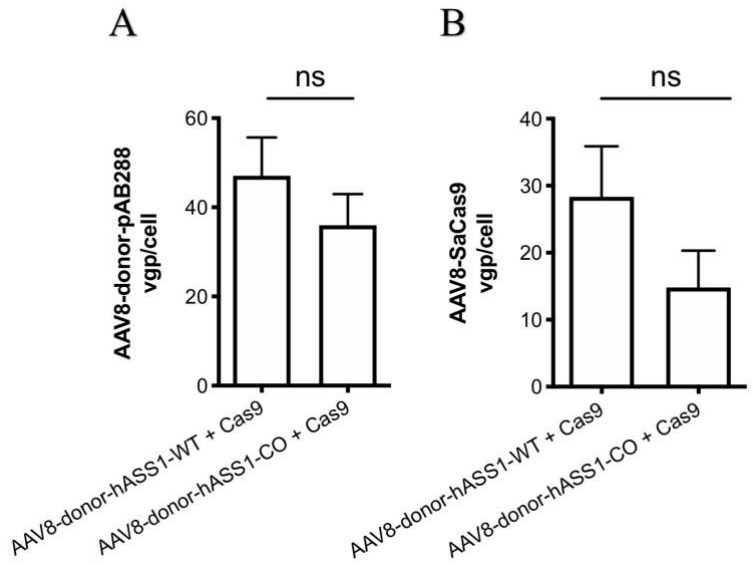

Figure 23: Viral genome particle analysis of AAV8 vectors after CTLN1 mice gene-targeting treatment: A) donor hASS1 WT/CO and B) SaCas9 in treated $ASS1^{fold/fold}$ hASS1 mice. Data are shown as mean ± SEM and statistically analyzed by Student's *t-test.*

4.2.2.3. Chimeric *Alb-hASS1* mRNA expression levels

After confirming the presence of the viral DNA in mouse livers, I analyzed the production of the *Alb-hASS1* chimeric mRNA, as an indicator of the donor hASS1 integration (*wild-type* and codon-optimized versions). cDNAs were evaluated by analyzing mRNA expression levels of the hybrid *Alb-hASS1* mRNA using a set of primers complementary for the albumin exon and the *hASS1* WT/CO cDNA to specifically amplify the targeted genomic region and not the donor vector. This primer pair is not able to amplify any endogenous mRNA or residual donor vector. To compare the expression levels of the transgenic *hASS1* with the endogenous *mASS1* present in

wild-type mice, I amplified the treated mice cDNA and *wild-type* mice cDNA with a template-specific set of primers to obtain a template DNA from each variant. Since it is necessary to calculate the primer efficiency in order to be able to compare the levels of different templates, I then tested the efficiency of each pair of oligos by using them on a qPCR with serial dilutions of the specific template. The analysis showed that both pairs of oligos had the same efficiency in amplifying the template (Figure 24A). The presence of high expression levels of the chimeric mRNA confirmed donor DNA integration into the albumin locus. The expression levels of the two chimeric mRNAs were similar (Figure 24B).

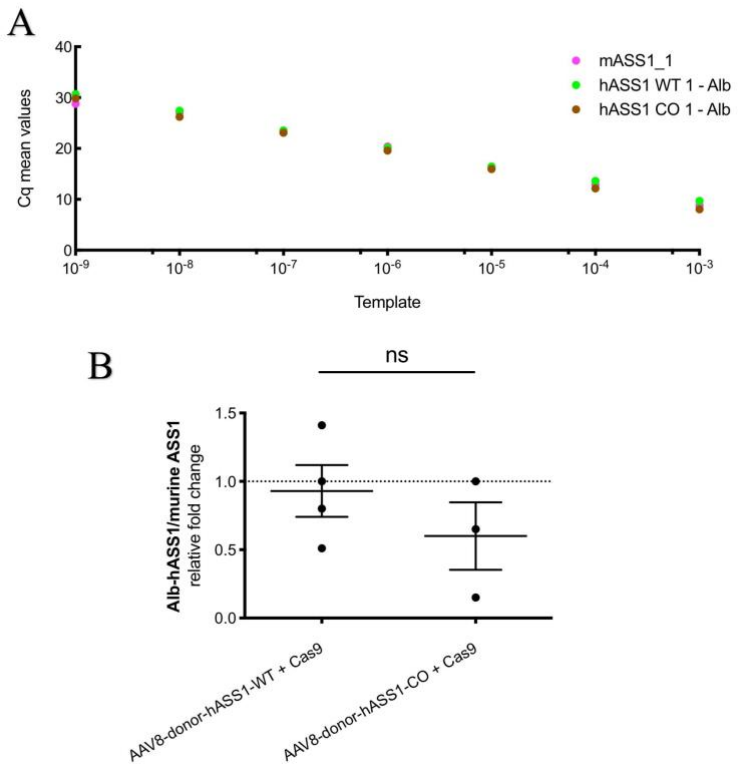

Figure 24: mRNA analysis after CTLN1 mice gene-targeting treatment A) Primer efficiency comparison. Specific primers for *hASS1WT-Alb*, *hASS1CO-Alb* and *mASS1* were analyzed with qPCR starting from the same amount of template following with 1:10 dilutions. Template in ng and Cq mean values are plotted in the graph. **B) Hybrid mRNA *Alb-hASS1* expression level**. Comparison between expression levels of the donor *hASS1 wild-type* and codon-optimized versions. Values were normalized with endogenous murine *ASS1* mRNA expression levels in *wild-type* mice. On the graph each dot represents an analyzed animal, with mean±SEM and was statistically analyzed with student's *t-test.*

4.2.2.4. Evaluation of hASS1 protein by western blot or immunohistochemistry

We wanted to specifically analyze the human ASS1 produced by our transgene, by western blot and immunofluorescence using an anti-human ASS1 antibody. However, it was not possible to discriminate the human ASS1 protein from the endogenous murine one as the species-specificity of the antibody was much broader than declared by the producers, and both proteins were recognized. We purchase and tested different anti-human ASS1 antibodies, but none could detect the human version specifically. The reason was probably related to the high degree of homology between the human and mouse proteins (89 % homology between murine and human cDNA and 97 % of homology between the two protein primary sequences (Figure 25).

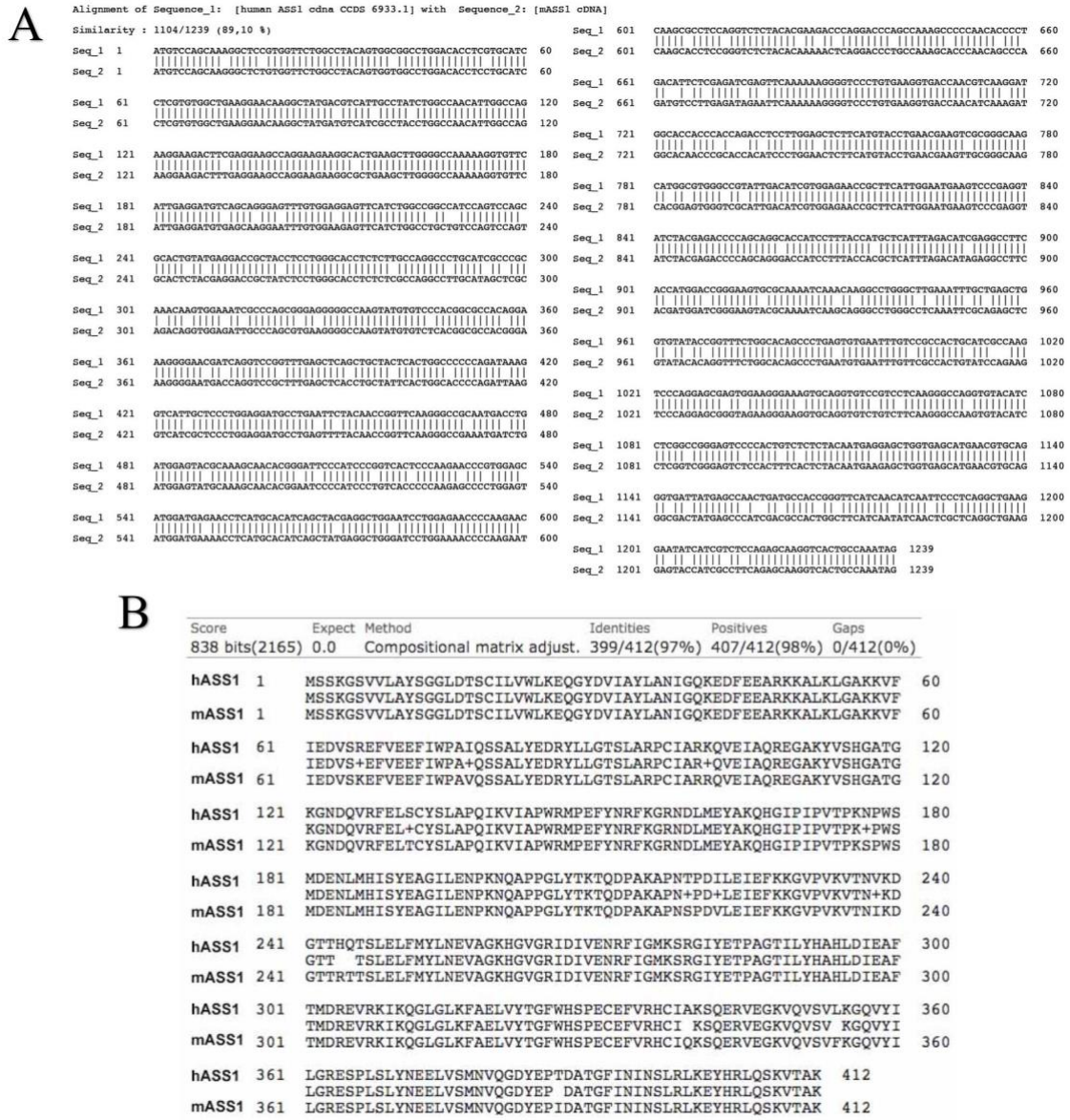

Figure 25: Comparison between human and murine *ASS1* cDNA and protein sequence. A) Alignment of the two *ASS1* cDNAs (murine and human). The homology between the two cDNA is 89 %. **B) Alignment of ASS1 protein primary sequence.** The homology between human and murine ASS1 protein is 97 %. + sign is a positive match (considering it as conservative substitution), white space is a match with a zero or negative score.

4.2.3. Treatment of neonatal ASS1$^{fold/fold}$ mice: short-term experiment with a high dose

We hypothesized that the dose we administer was not high enough to achieve complete therapeutic levels, which should result in a reduction of the toxic metabolites, especially ammonia. We planned another experiment increasing the dosage of the donor vector to 1,0E12 vgp/pup. The *Sa*Cas9 dosage remained the same, as previous studies showed, this dosage (2,0E11 vgp/pup) resulted in efficient editing of the albumin locus in *wild-type* mice injected with *Sa*Cas9 and donor-eGFP and in treating the Ugt1 KO mice with *Sa*Cas and donor-hUGT1A1 (De Caneva et al., 2019).

Also, the conditions tested in the non-integrative approach were not efficient in lowering plasma ammonia levels and, for this reason, we decided to repeat the experiment increasing the dose of the two rAAV8-pSMD2 vectors. ASS1$^{fold/fold}$ animals were injected at post-natal days 2 and 4 with 1,0E12 vgp/pup of rAAV8-PSMD2-hAAT-hASS1-WT or rAAV8-PSMD2-hAAT-hASS1-CO. For evaluating the gene targeting approach animals were injected with half dose of the donor vectors at day 2 and half the dose was administer at day 4. The Cas9 AAV8 vector was given only at day 2. The dose was halved and given in two days to reduce the injected volume in small animals. Blood for ammonia and citrulline analysis was collected on day 30. Mice were then sacrificed at P30 and the liver was collected for molecular analysis (Figure 26).

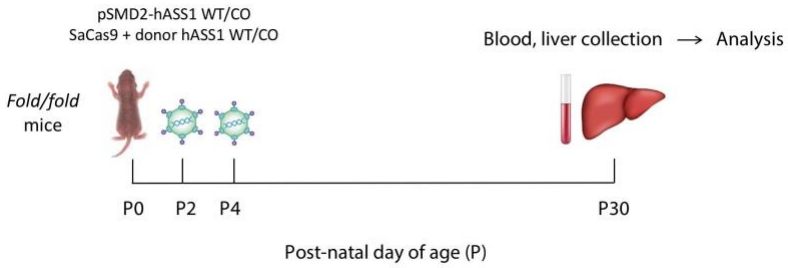

Figure 26: Experimental plan for CTLN1 high dose treatment. Animals were transduced at post-natal day (P) 2 with 2,0E11 vgp/pup of rAAV8-*Sa*Cas9 and at day 2 and 4 with 1,0E12 vgp/pup of rAAV8-donor-hASS1-WT and CO or 1,0E12 vg/pup of rAAV8-PSMD2-hAAT-hASS1-WT and CO. The dose was split into two days (P2 and P4). At P30 mice were sacrificed when blood and liver were collected.

4.2.3.1. Biochemical analysis of mice plasma

Metabolites in mice plasma were analyzed at 1 month of age. Similar to the previous experiment, plasma citrulline levels significantly decreased in mice treated with the gene-targeting approach, reaching 117 µM in the group treated with the donor hASS1 WT and 143 µM in animals treated with the codon-optimized version. Mice treated with the non-integrative approach did not present a decrease in citrulline levels (Figure 27A). However, ammonia levels in animals treated with the gene targeting treatment did not show the same decrease and remained high. Mice treated with the episomal gene therapy seemed to have a reduction in ammonia levels (Figure 27B). However, when we analyzed blood ammonia, the levels were highly variable in the treated groups and also in untreated $ASS1^{fold/fold}$ and wild-type mice. Therefore, we can't conclude that a reduction in blood ammonia is a consequence of the episomal gene therapy treatment. In conclusion, the high citrulline levels in the episomal gene therapy group is probably associated with the loss of episomal AAV vector during liver growth and, therefore, confirming that the gene-targeting approach is the most suitable treatment during the neonatal period.

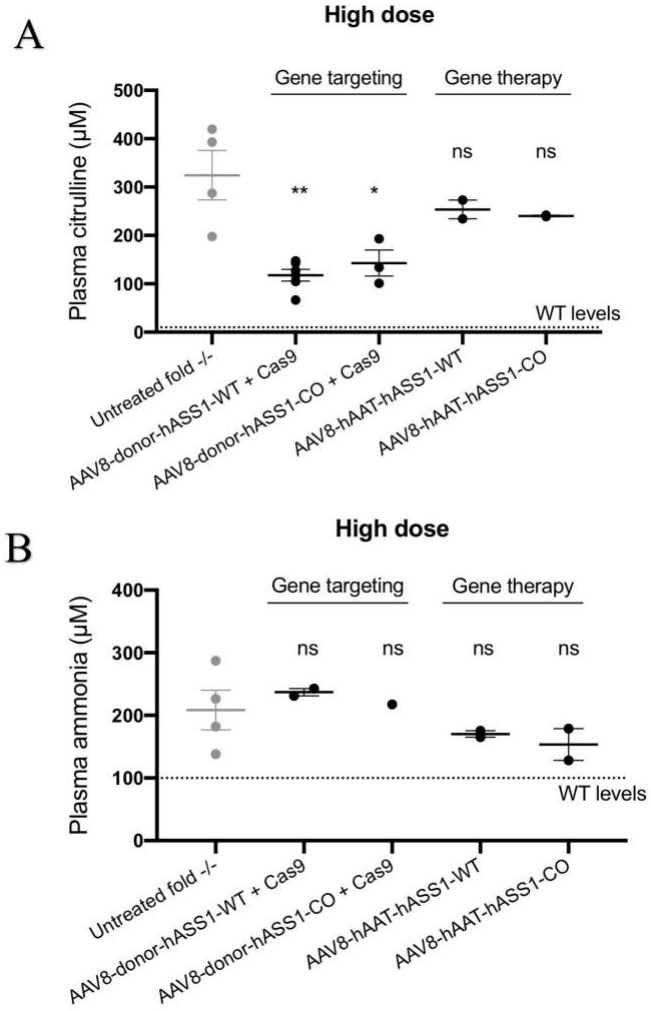

Figure 27: Plasma analysis after CTLN1 high dose treatment. A) Plasma citrulline levels were analyzed at P30. Untreated $ASS1^{fold/fold}$ mice were used as a control group. Data are shown as mean ± SEM and statistically analyzed by one-way ANOVA with Tukey's Multiple comparison test: * $p<0,05$, ** $p<0,01$. **B) Plasma ammonia** levels were analyzed at P30. Untreated $ASS1^{fold/fold}$ mice were used as a control group. A grid line represents ammonia levels in healthy *wild-type* mice. Data are shown as mean ± SEM and statistically analyzed by one-way ANOVA with Tukey's Multiple comparison test: ns>0,05.

4.2.3.2. Viral genome particles and chimeric mRNA analysis

To assess the presence of the viral genomes in the livers and the presence of the chimeric mRNA, I repeated the same qPCR assays performed in the previous section for the animals treated with the integrative strategy.

qPCR analysis of viral particles confirmed the presence of the viral DNA in liver cells of treated mice (Figure 28A). I also confirmed the presence of the chimeric mRNA (Figure 28B). The analysis revealed a higher expression in the group treated with the *wild-type* version of the *hASS1* cDNA, but the difference was not statistically significant. However, the *hASS1* expression in both groups was not significantly lower than levels of endogenous *ASS1* present in *wild-type* animals.

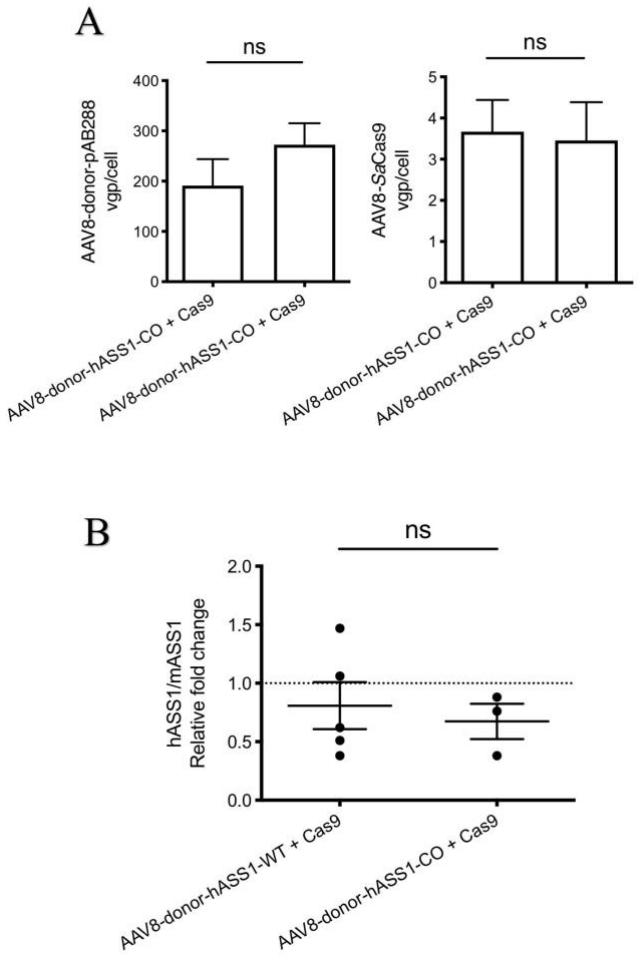

Figure 28: Viral genome particle and chimeric mRNA expression levels analysis after CTLN1 high dose treatment. A) Viral genome particles analysis: SaCas9 and donor hASS1 WT/CO in ASS1$^{fold/fold}$ hASS1 mice. Data are shown as mean ± SEM and statistically analyzed by Student's *t-test.* **B) Hybrid *Alb-hASS1* mRNA expression level**. Comparison between expression levels of the donor *hASS1 wild-type* and codon-optimized versions. Values were normalized with endogenous murine *ASS1* mRNA expression levels in *wild-type* mice. On the graph each dot represents an analyzed animal, with mean±SEM and was statistically analyzed with student's *t-test.*

4.2.4. Survival study of neonatal ASS1$^{fold/fold}$ mice after gene-targeting treatment

We have seen that CTLN1 neonatal mice treated with the gene targeting approach showed a significant decrease in citrulline, a marker of the disease (Figure 22A and 27A). However, plasma ammonia, the main metabolite causing disease toxicity, was not significantly decreased. Metabolites in CTLN1 ASS1$^{fold/fold}$ mice accumulate in time until they reach extremely high levels causing the death of mice. To evaluate if the gene targeting treatment could rescue mice from the lethality of the disease, we decided to perform a 5 month long experiment. I used only the donor vector encoding the *hASS1 wild-type* cDNA, since the codon-optimized version of the *hASS1* cDNA did not show the same efficiency as in *in-vitro* studies, where its efficiency was 3-times higher. We decided to use only one donor vector also to reduce the number of experimental groups. I treated mutant mice with the previous doses of donor vector (2,0E11 vgp/pup and 1,0E12 vgp/pup) and included a third group with an even higher dose (2,5E12 vg/pup). The last group was added to verify if very high levels of donor vector could have an impact on targeting rate and therefore, lower plasma ammonia.

CTLN1 ASS1$^{fold/fold}$ mice were treated i.v. at P2 and P4 with the following doses:

- Cas9 2,0E11 vg/pup + donor hASS1 WT 2,0E11 vg/pup
- Cas9 2,0E11 vg/pup + donor hASS1 WT 1,0E12 vg/pup
- Cas9 2,0E11 vg/pup + donor hASS1 WT 2,5E12 vg/pup

Mice were sacrificed at 5 months of age and citrulline levels were monitored at different time points (Figure 29).

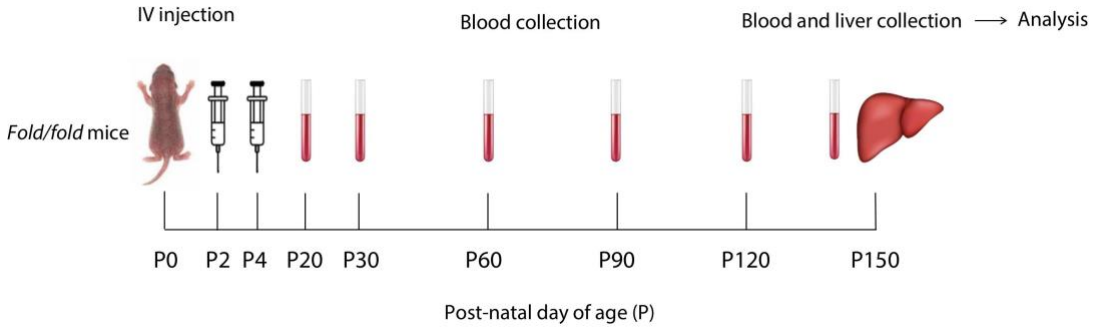

Figure 29: Experimental plan for CTLN1 mice survival study after gene-targeting treatment: Mice were injected at P2 with AAV-SaCas9 (2,0E11 vg/pup) and at P2 and P4 with different doses of AAV-donor-hASS1 WT (2,0E11 vg/pup, 1,0E12 vg/pup, 2,5E12 vg/pup). Blood withdrawal was performed at P20, 30, 60, 90, 120 and the experiment was terminated at 5 months of age (P150).

4.2.4.1. ASS1$^{fold/fold}$ mice survival rate after gene targeting treatment

All treated animals, except for one that died at post-natal day 138, survived until the end of the experiment reaching 5 months of age. Only 10 % of untreated ASS1$^{fold/fold}$ mice reached 5 months of age, while the survival rate of treated mice was 92 % (Figure 30A). The mouse that died had decreased citrulline levels, ranging from 95-200 µM from blood analyzed at P20, P30, P60 and P90, suggesting that the treatment was efficient and the reason for the death may not be related to the disease. This suggests that the treatment with a gene targeting strategy at a neonatal age was efficient in rescuing mice from disease lethality. Treated animals had also a statistically significant increase in their body weight reaching approximately 20 grams, while untreated ASS1$^{fold/fold}$ mice weighed about 10 grams or less (Figure 30B).

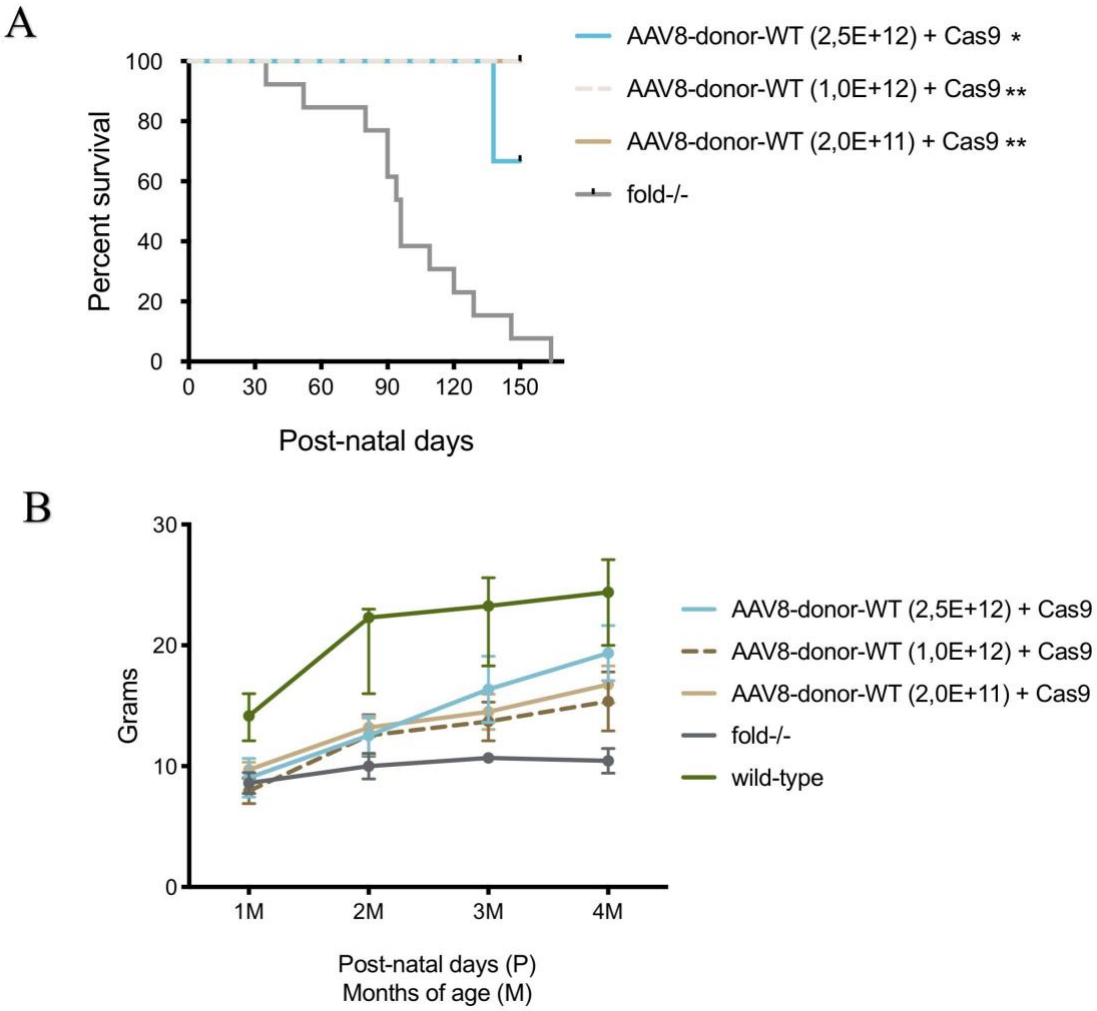

Figure 30: Survival and body weight evaluation until 5 months of age after neonatal treatment. A) Kaplan-Meier: In the curve are represented mice treated with different AAV-donor-hASS1 WT doses together with the AAV-Cas9 and untreated ASS1$^{fold/fold}$. 100 % of survival had mice treated with donor vector doses 2,0E11 (n=6) and 1,0E12 (n=4). Mice treated with the highest donor dose, 2,5E12, had 75 % of survival (n=4.) More than 90 % of untreated ASS1$^{fold/fold}$ mice died by 5 months. Analyzed with Long-rank (Mantel-Cox). **B) Growth curve**. Bodyweight mean values ± SEM of the three treated groups, untreated *wild-type* and ASS1$^{fold/fold}$ mice. The growth is measured at different points, showing body weight gain of treated ASS1$^{fold/fold}$ mice compared to the untreated. Two-way ANOVA: Time ***, Treatment ***, Interaction ns.

4.2.4.1. Biochemical analysis of mice plasma

Plasma citrulline was analyzed at different time points. Levels of citrulline were higher compared to healthy *wild-type* animals (0-50 µM). However, while citrulline started to accumulate in the untreated ASS1$^{fold/fold}$ control group, in animals treated with different doses of our gene targeting therapy it remained stable and ranged from 130 and 300 µM. Consistently, we observed a dose-response pattern, as the group injected with the highest dose (donor 2,5E+12) had a greater decrease in citrulline, ranging from 130-200 µM, while the group injected with the lower donor-hAAS1 dose presented the highest values (Figure 31A). Serum ammonia in all treated groups at 5 months of age was non-significantly lower compared to untreated 2-4 months old mice (Figure 31B). Aged matched controls couldn't be analyzed as animals died before reaching the final timepoint. The data demonstrate that with gene targeting treatment plasma citrulline decreased, compared to untreated controls, to life-compatible levels resulting in a rescue in the disease mortality.

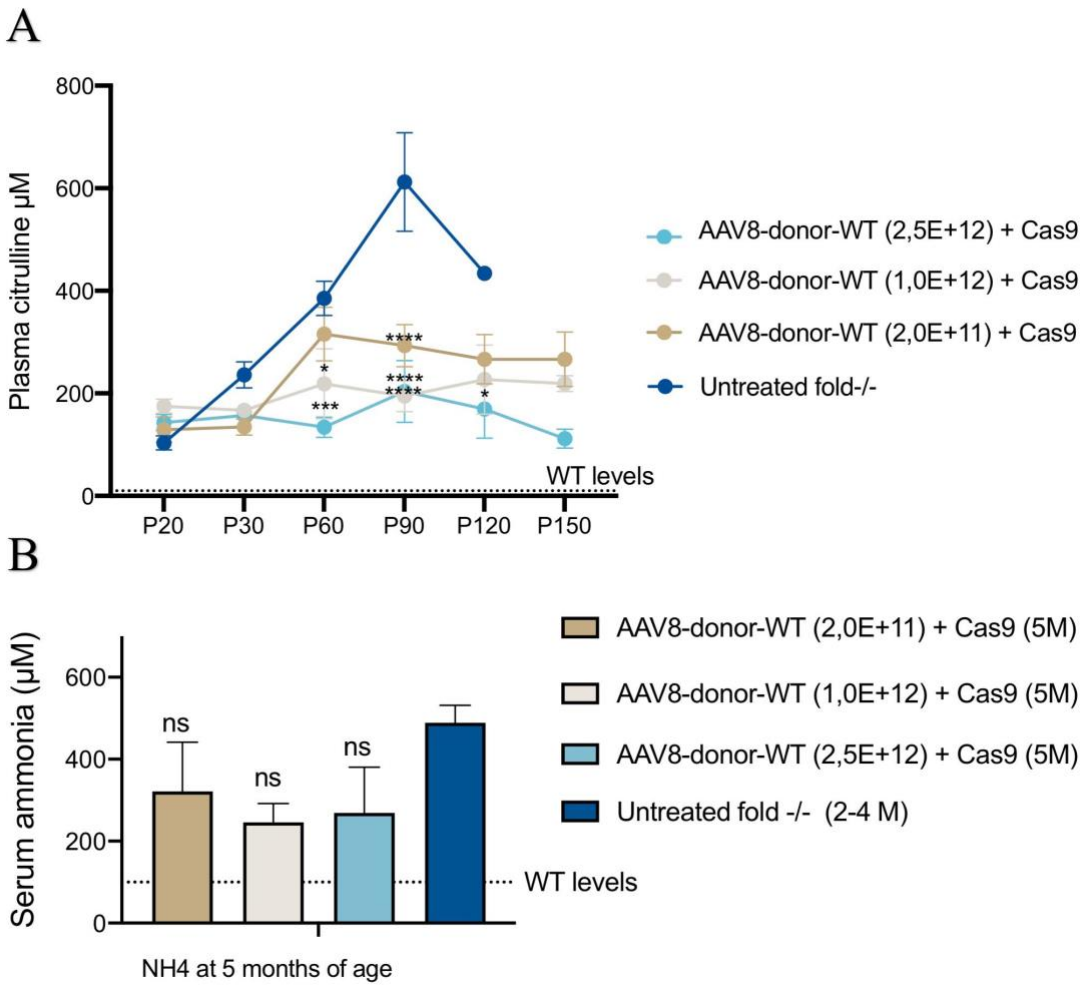

Figure 31: Plasma analysis after neonatal gene-targeting treatment in a 5 month period. A) Plasma citrulline: Plasma citrulline analyzed at different time points. In the graph are represented treated mice with different AAV-donor-hASS1 WT vector doses and untreated ASS1$^{fold/fold}$ group. Two-way ANOVA, Treatment, **, Time, ***, Interaction, ***. **B) Serum ammonia:** Ammonia levels were determined at 5 months of age in animals with gene targeting treatment. For the control group, untreated ASS1$^{fold/fold}$ mice from 2-4 months of age were used. Data are shown as mean ± SEM and statistically analyzed by one-way ANOVA with Tukey's multiple comparison test.

4.2.4.2. ASS1 protein levels

We wanted to evaluate if animals treated with the gene-targeting approach had an increase in the ASS1 protein levels, compared to untreated mice. However, since the

expression of the endogenous ASS1 protein in mutant mice was very high, we could not detect any significant increase in any of the treated groups (Figure 32).

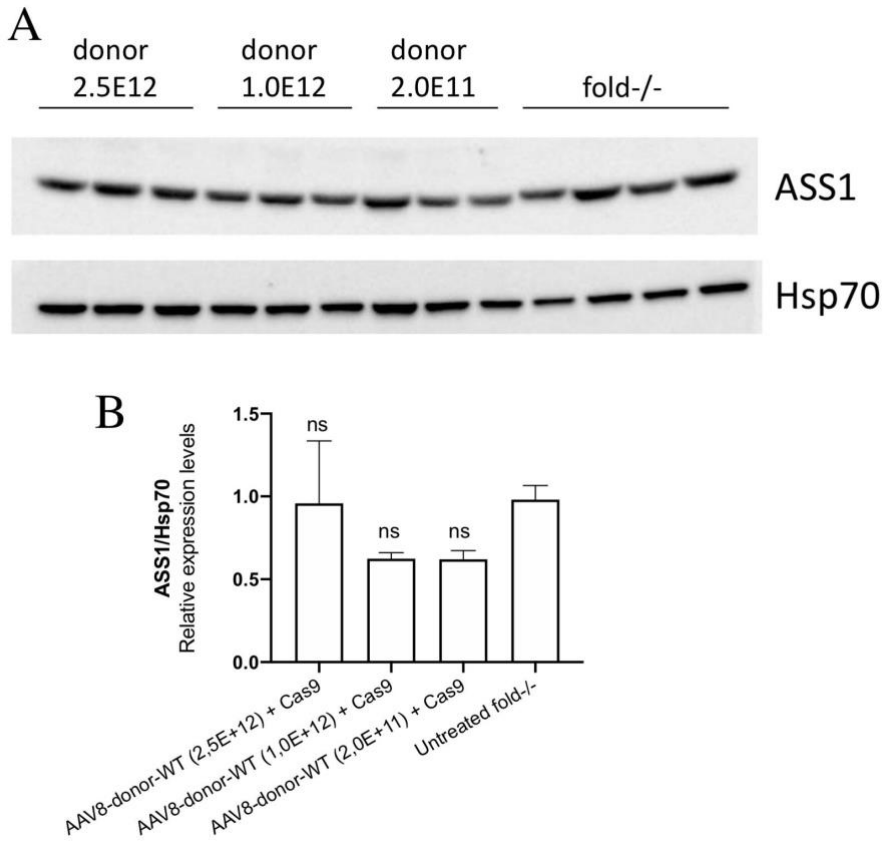

Figure 32: ASS1 protein levels after 5 month post-treatment. A) ASS1 western blot analysis. Three mice from each treatment group and four untreated $ASS1^{fold/fold}$ were analyzed for ASS1 protein levels from liver lysate. **B) Quantification of the western blot.** Data are shown as mean ± SEM and statistically analyzed by one-way ANOVA with Tukey's multiple comparison test.

4.2.4.3. Recombinant hepatocytes rate after neonatal gene-targeting

To estimate the percentage of targeted hepatocytes, I performed an RNA in-situ hybridization analysis on liver sections of mice treated with the highest donor dose (2,5E+12 vg/mouse), detecting specifically the human ASS1 mRNA by using 3 sets of probes designed for hASS1-specific regions. The quantification showed an approximate

value of 7,4 % of transduced hepatocytes (ranging from 3 to 12,5 %), per total nuclei count. However, the value is approximal, as polynuclear hepatocytes were not considered. Edited cells were detected in clusters of hASS1 positive cells, suggesting that the targeted insertion was stably maintained in daughter cells (Figure 33).

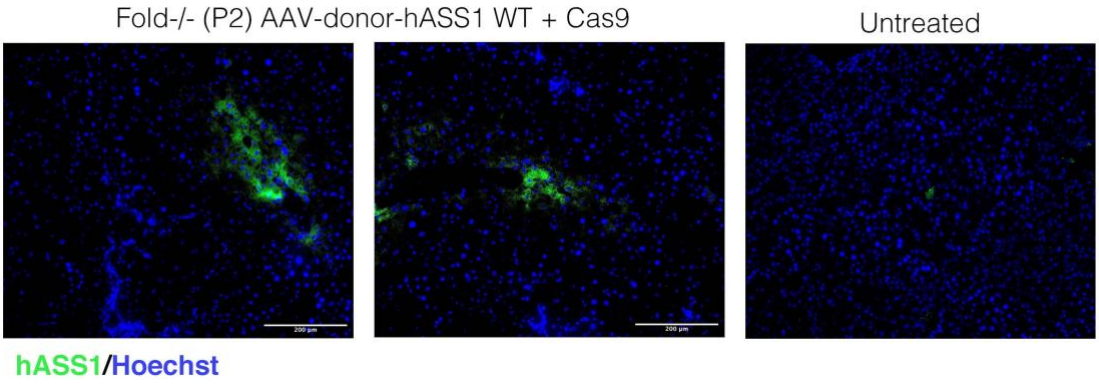

Figure 33: FISH analysis for hASS1-positive hepatocytes in CTLN1 mice. Liver sections were analyzed with fluorescence in-situ hybridization for human ASS1 mRNA in animals treated with gene targeting strategy (Cas9 and donor-hASS1-WT) at P2 and analyzed at 5 months of age. hASS1 mRNA is represented in green and nuclei are stained with Hoechst (blue). Approximately 7 % of hepatocytes were positive for hASS1 WT mRNA. hASS1 positive hepatocytes normalized for total cell count. In the graph are plotted mean values of hASS1-positive liver sections of mice treated with the highest dose (n=3). 2-5 liver sections were analyzed for each treated mouse.

4.2.5. Treatment of juvenile ASS1$^{fold/fold}$ mice

We hypothesized that the episomal gene therapy vector, if dosed in the juvenile period, may have higher potentiality than at the pediatric stage, as the proliferation rate of hepatocytes is much lower than in neonates, without resulting in the loss of vector DNA in liver cells and ensuring a long-lasting effect. On contrary, the gene-targeting strategy in juvenile mice has lower efficiency, as cells are not actively proliferating and the preferred double-strand break repair mechanism is NHEJ rather than HDR. To exploit both treatments, we proceeded by treating juvenile animals with the previously described gene therapy and gene targeting approach, but using a compound, fludarabine, that increases the recombination in combination or not with the

Crispr/Cas9 nuclease. This compound in previous studies showed to be very effective in increasing the recombination rate (Tsuji et al., under revision). Therefore, it could be possible to substitute the Cas9 nuclease avoiding serious concerns, such as off-target activity and immune response, obtaining similar recombination efficiency. For this reason, we tested different gene-targeting approaches with Cas9 and fludarabine or combining the two approaches (Figure 34).

Five groups of 1 month old ASS1$^{fold/fold}$ mice were injected with the following treatments:

- rAAV8-pSMD2-hAAT-hASS1 WT (6,0E13 vg/kg)
- rAAV8-donor-hASS1WT (6,0E13 vg/kg)
- rAAV8-donor-hASS1WT (6,0E13 vg/kg) + Fludarabine (3x125 mg/kg)
- rAAV8-donor-hASS1WT (6,0E13 vg/kg) + rAAV8-SaCas9-sg8 (6,0E13 vg/kg)
- rAAV8-donor-hASS1WT (6,0E13 vg/kg) + rAAV8-SaCas9-sg8 (6,0E13 vg/kg) + Fludarabine (3x125 mg/kg)

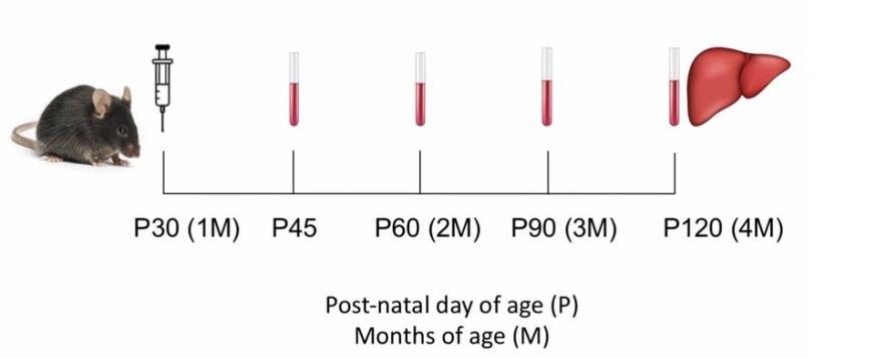

Figure 34: Experimental plan for juvenile CTLN1 mice treatments. Juvenile ASS1$^{fold/fold}$ mice were injected with different treatments at P30. Blood was collected at different time points. The experiment was terminated after 3 months when animals reached adulthood (4 months of age), and liver was collected.

4.2.5.1. ASS1$^{fold/fold}$ mice survival after treatment with non-integrative or gene targeting therapy at juvenile age

Three out of four untreated ASS1$^{fold/fold}$ mice died before reaching the final time point. The same outcome was observed in animals treated only with the donor hASS1 vector. The other treatments, which combined the donor vector with an HDR enhancer (Cas9 or fludarabine) showed improved survival. Only 1 animal out of 4 died before reaching 4 months in the "donor + Cas9" and "donor + Cas9 + fludarabine" groups, while animals treated with "donor vector + fludarabine" and the group with the episomal gene therapy vector resulted in complete rescue of all animals (Figure 35A). The only treatment that significantly corrected the bodyweight was the episomal gene therapy vector, while with other treatments the animals weight was similar weight to the untreated ASS1$^{fold/fold}$ mice (Figure 35B).

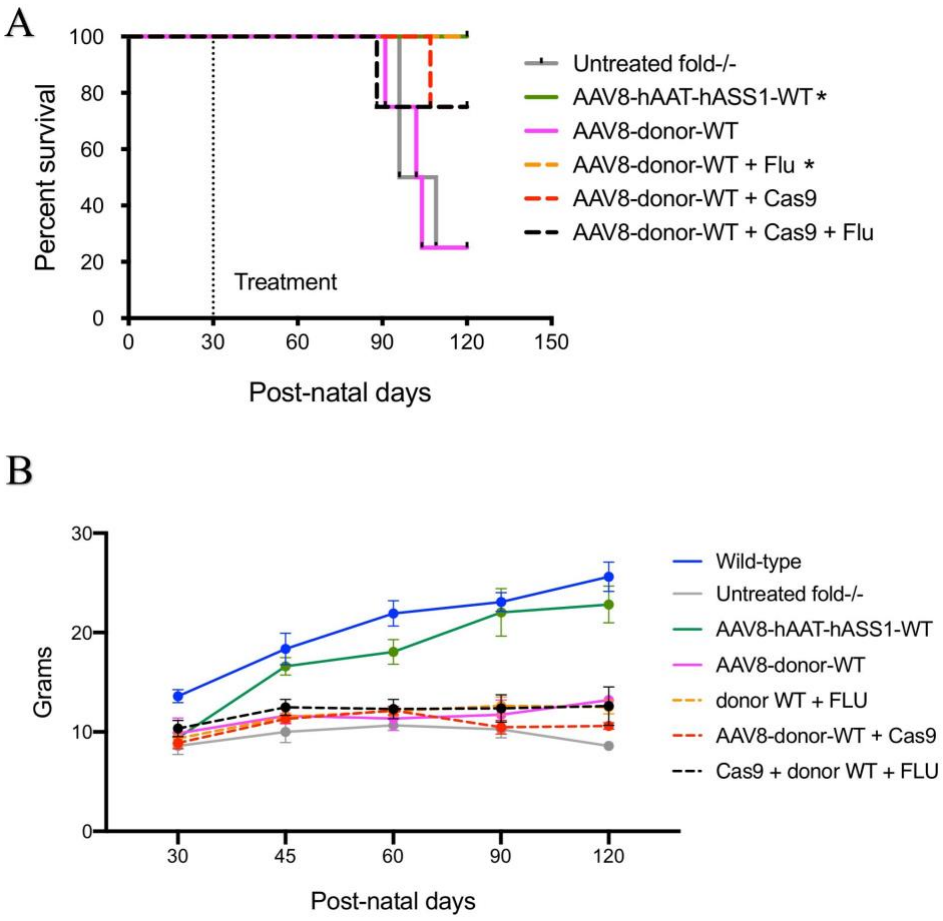

Figure 35: Survival rate and body weight evaluation after juvenile CTLN1 mice treatments. **A) Kaplan-Meier curve**. 100 % of survival was achieved in mice treated with episomal pSMD2-hAAT-hASS1 WT (n=4) vector and donor "hASS1 WT + fludarabine" (n=4). 75 % of survival was obtained with mice treated with "donor hASS1 WT + Cas9" (n=4) and "donor WT + Cas9 + fludarabine" (n=4). Mice treated with only donor hASS1 WT (n=4) and the untreated group had a 25 % of survival rate (n=4). Analyzed with Long-rank (Mantel-Cox). **B) Growth curve**. Body growth was measured through all the experiment. In the graph are represented mice's weight with mean ± SEM of each experimental group, the untreated group (control) and healthy *wild-type* animals.

4.2.5.2. Citrulline and ammonia levels after juvenile treatments

Plasma citrulline was analyzed at different time points (Figure 36A). Compared to the untreated control group, only the animals treated with the episomal gene therapy vector containing the hAAT-hASS1-WT cDNA had a significant decrease in citrulline levels,

which were low until the end of the experiment. The other groups showed high levels of plasma citrulline that were not statistically different from the untreated controls.

In line with other analyses, the group treated with the episomal gene therapy vector had a decrease also in plasma ammonia levels. Ammonia blood concentrations at 4 months of age reached *wild-type* levels and were significantly lower compared to the untreated mutant mice. Mice treated with different gene-targeting treatments had a slight decrease in plasma ammonia level compared to older ASS1$^{fold/fold}$ mice, which was not statistically significant, however, it had a positive impact on their lifespan (Figure 36B). Treated mice were compared to 2-4 month old untreated mutants, as the majority of untreated ASS1$^{fold/fold}$ mice are not able to survive until this time point.

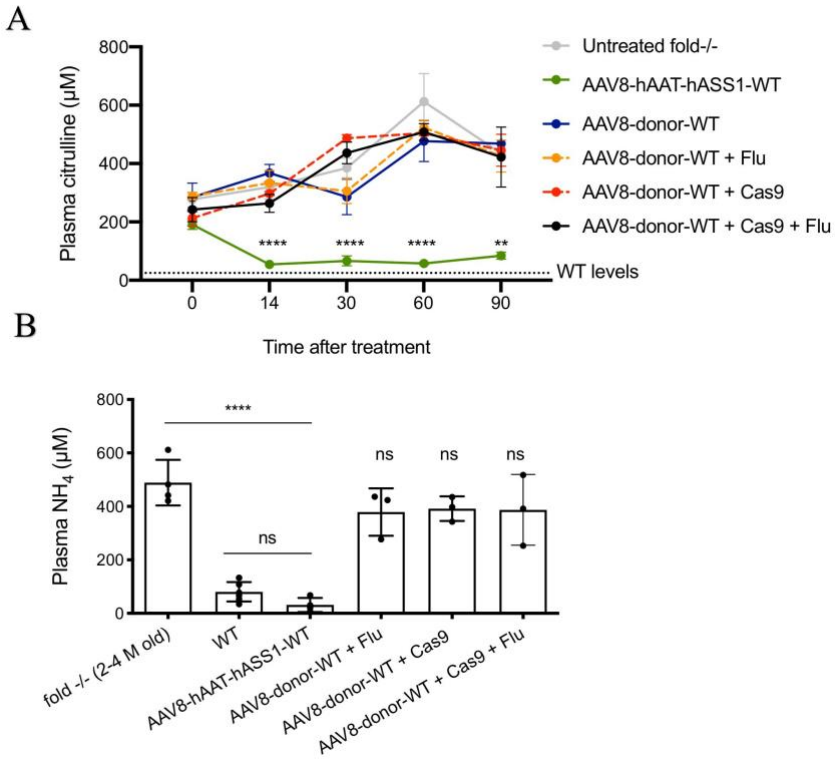

Figure 36: Plasma analysis after CTLN1 mice juvenile treatments. A) Plasma citrulline analyzed at different time points. The treatment with the episomal pSMD2-hAAT-hASS1 WT vector leads to a significant decrease in citrulline levels compared to the untreated group. Data are shown as mean and statistically analyzed by two-way ANOVA, Treatment, ***, Time, ***, Interaction, ***. **B) Plasma ammonia levels.** NH_4 was analyzed at 4 months of age (3 months after the treatment). The only group treated with the episomal pSMD2-hAAT-hASS1 WT vector had a significant decrease of ammonia plasma levels, reaching *wild-type* levels. Data are shown as mean ± SEM and statistically analyzed by one-way ANOVA with Tukey's Multiple comparison test: *** p<0,001.

4.2.5.3. ASS1 protein levels after juvenile treatment

The analysis of protein levels by western blot showed a significant increase in the amount of ASS1 protein only in the group treated with the episomal gene therapy vector (Figure 37). Therefore, we can confirm a higher production of the hASS1 protein, which was able to convert the diseased phenotype to *wild-type*, normalizing both citrulline and ammonia concentration in plasma.

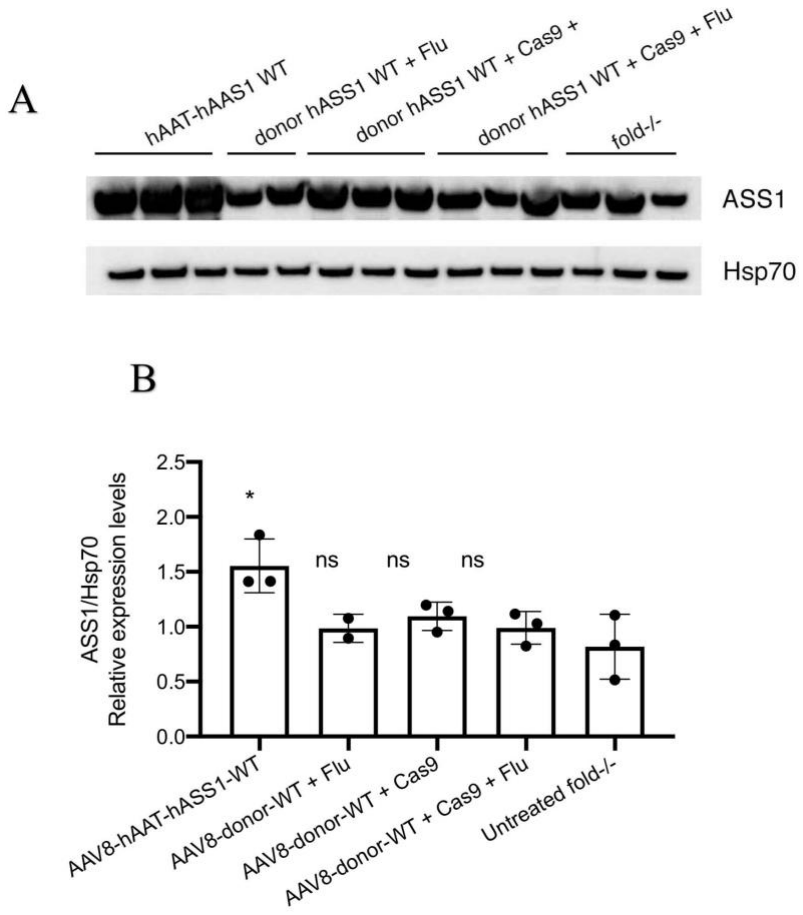

Figure 37: ASS1 protein after juvenile treatments. A) Western blot analysis. ASS1 was detected in liver extracts of treated and untreated $ASS1^{fold/fold}$ mice, using an antibody that recognizes both the human and endogenous ASS1 protein. **B) Quantification of WB**. Animals treated with the pSMD2 episomal gene therapy vector had a significant increase in the amount of ASS1 protein in the liver compared to the untreated $ASS1^{fold/fold}$ group. Data are shown as mean ± SEM and statistically analyzed by one-way ANOVA with Tukey's Multiple comparison test: * $p<0,05$.

4.2.5.4. Transduction rate after juvenile non-integrative treatment

Quantification of the hASS1 *wild-type* positive hepatocytes by RNA-FISH in mice treated with episomal gene therapy vector showed that about 20 % of the hepatocytes have been successfully transduced and have an active production of the hASS1 mRNA (Figure 38).

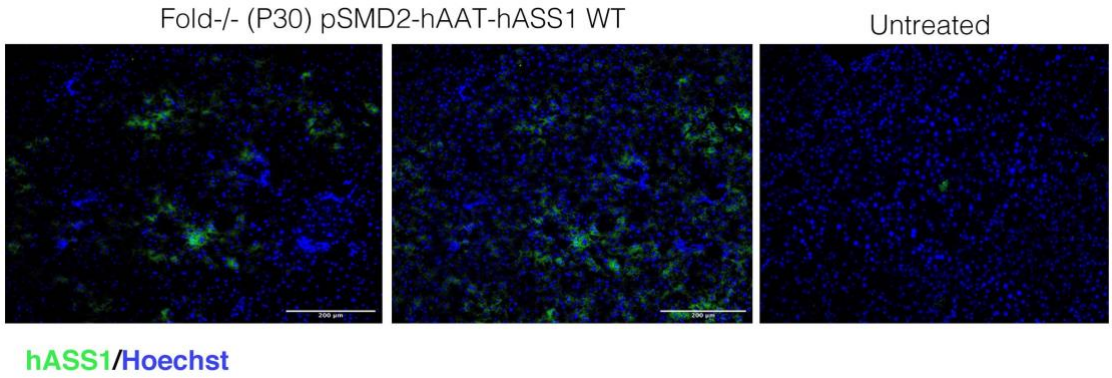

Figure 38: Transduced hepatocytes with non-integrative gene therapy treatment on juvenile CTLN1 mice. Liver sections were analyzed with fluorescence in-situ hybridization for human ASS1 mRNA in animals treated at P30 with episomal rAAV8 pSMD2-hAAT-hASS1 WT vector. hASS1 mRNA is represented in green and nuclei are stained with Hoechst (blue). About 20 % of hepatocytes were positive for hASS1 mRNA. hASS1-positive cells are normalized for total cell count and represented with dots. In the graph are plotted mean values of analyzed liver sections of mice treated with pSMD2-hAAT-hASS1 WT (n=4).

4.3. Hemophilia B study

4.3.6. Treatment of *wild-type* neonate mice with a hFIX gene-targeting approach

In order to test a CRISPR/Cas9-mediated gene targeting strategy for hemophilia, we used a modified version of the pAB288 and the SaCas9 nuclease. The original pAB288 vector originally contains a human version of the coagulation factor IX (FIX) cDNA (Barzel et al., 2015). Here, we mutated the *Sa*Cas9 PAM8 site of the pAB288 donor vector to avoid self-targeting. In previous experiments of the laboratory, we had transduced neonatal *wild-type* mice with the donor vector, containing the human FIX cDNA, together or without the *Sa*Cas9 that targets the albumin locus. Plasma from treated mice was analyzed with a human-specific FIX ELISA, which uses an antibody specifically recognizing the human FIX and not the endogenous murine FIX. The analysis showed an increase from 100% to 200 % of human FIX, compared to the normal human levels (Figure 39). FIX levels were stable until 10 months of age, which proves an efficient and long-term therapy.

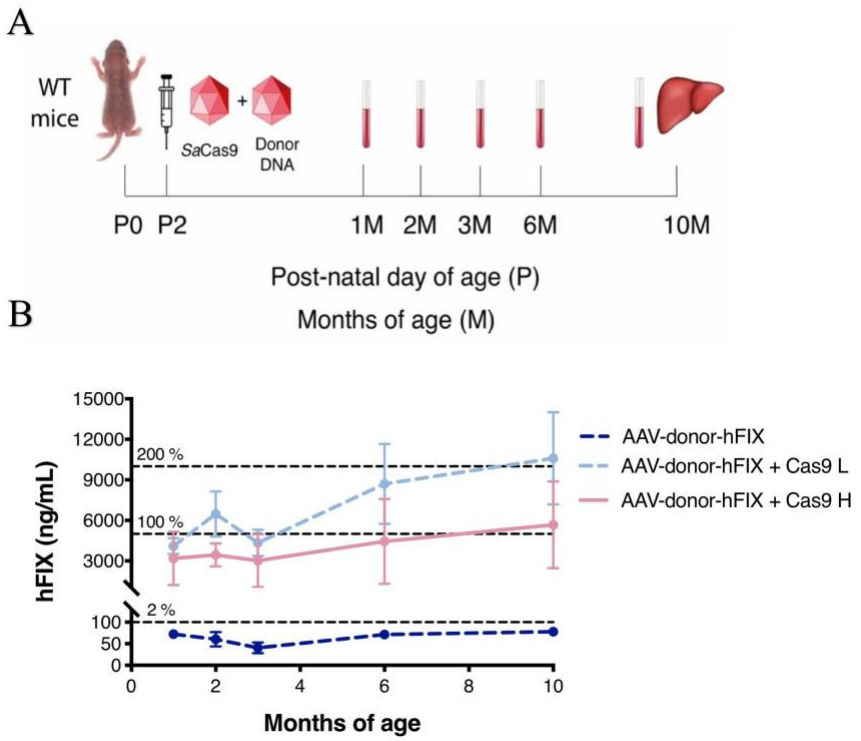

Figure 39: Treatment of *wild-type* neonate mice with a *hFIX* gene-targeting approach. A) Experimental plan: neonatal *wild-type* mice were treated with only rAAV8-donor-hFIX (2,0E11 vg/mouse) or with rAAV8-donor-hFIX combined to different rAAV8-*Sa*Cas9 doses (6,0E10 vg/mouse, L; or 2,0E11 vg/mouse, H). Blood was collected at different time points and mice were sacrificed at 10 months of age. **B) Plasma hFIX** was analyzed at 1, 2, 3, 4, 6 and 10 months of age. 5000 ng/ml represents 100 % of the hFIX level in the healthy human population. Values are represented with mean±SD (Alessia De Caneva, unpublished data).

4.3.7. Treatment of neonatal FIX KO mice with a gene targeting approach

Due to the potentiality of those results, we initiated a collaboration project with a research group from Genethon Institute in Paris, which had in their animal facility, a FIX knock-out mouse model for the study of Hemophilia B.

The comparison between gene therapy and gene targeting was not carried out in hemophilia B study, as there are already different successful clinical trials for

hemophilia B adult patients and, since we wanted to treat neonatal mice, we focused on apply only the gene targeting strategy.

We produced mega preps of the two plasmids (*Sa*Cas9 and pAB288-donor-FIX) and the ICGEB AAV facility generated the rAAV8 vector stocks, which were sent to Genethon in France to be dosed into the FIX mutant mice.

Since injections were performed at P2, it was not possible to perform the genotype analysis on newborn mice at birth due to the risk of bleeding and being killed or not accepted by the mother. In consequence, all the pups obtained from the breeding of a heterozygous female and a mutant homozygous male were injected.

Two-day old pups were injected with the two rAAV8 vectors with rAAV8-SaCas9 (0,6E11 vg/mouse) and rAAV8-donor-hFIX (5,0E11 vg/mouse). The donor and SaCas9 vector doses were previously determined with eGFP and hFIX donor vectors in experiments with WT mice. Blood was taken at months 1, 2, 3 and mice were sacrificed at 4 months of age (Figure 40A). The plasma and liver of all treated animals (*wild-type*, heterozygote and knock-out) were sent back to our laboratory for molecular analysis. The plasma of all treated mice was analyzed at 1, 2 and 4 months of age. The ELISA showed an increase in hFIX from 100 % to 140 % of normal human values (Figure 40B). In the untreated FIX KO mice the human FIX levels were not detected (not shown). These results were present and stable in all treated mice and were similar to what we obtained in the preliminary experiment in *wild-type* mice (Figure 39B). We also checked the hFIX levels in the blood by western blot analysis (Figure 40C), confirming the results obtained with ELISA.

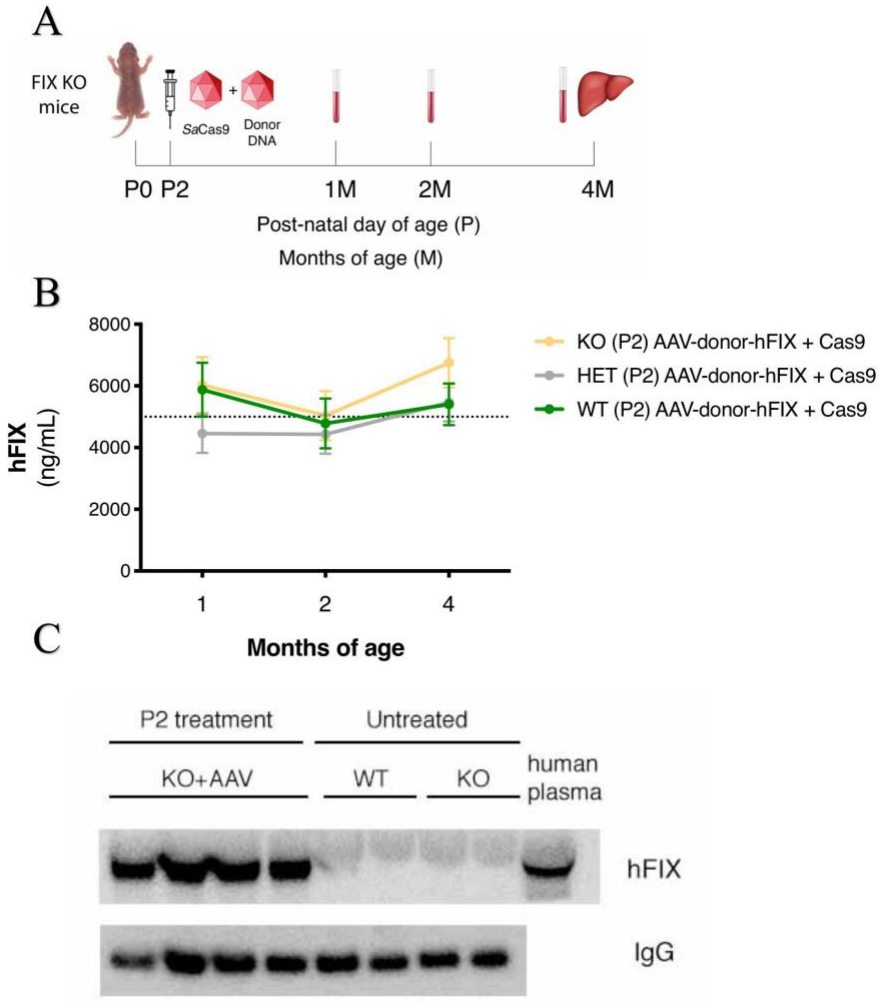

Figure 40: Treatment of neonatal FIX KO mice with a gene targeting approach A) Experimental plan. FIX KO neonatal mice were injected at postnatal day (P) 2 with with 0,6E11 vg/mouse of AAV8-SaCas9 and 5,0E11 vg/mouse of AAV8-donor-hFIX. Bleeding was performed at 1 and 2 months (M), and mice were sacrificed at 4 months. The liver was collected for molecular analysis. **B) Plasma hFIX levels** in mouse transduced with *Sa*Cas9 and donor-hFIX treated at post-natal (P) day 2. hFIX concentration obtained from blood samples at months 1, 2 and 4. 5000 ng/mL corresponds to the normal FIX plasma levels in healthy individuals in the human population. **C) Western blot analysis for hFIX** in treated FIX KO mice plasma. Untreated WT and KO mice were used as a negative control, while human plasma was used as a positive control.

To analyze the rescue of the phenotype with a functional test, a tail clip test assay to evaluate the clotting activity was performed in the animal facility in Paris (Genethon). Treated FIX KO mice had the same coagulation efficiency compared to the *wild-type*

mice littermates, as the bleeding time had no significant difference. This data suggest that the treatment leads to a complete rescue of the bleeding phenotype (Figure 41).

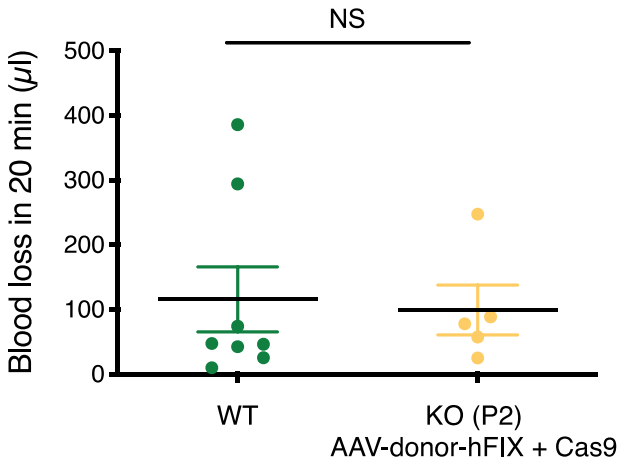

Figure 41: Tail-bleeding assay. The coagulation time was evaluated in neonatally treated FIX KO mice and their *wild-type* littermates.

Immunohistochemistry of liver sections revealed the presence of hFIX positive hepatocytes in treated KO animals, with no signal in untreated mice. The positive cells were present in clusters, suggesting that recombination was an early event and daughter hepatocytes maintained the transgene, forming groups of hFIX-positive hepatocytes (Figure 42).

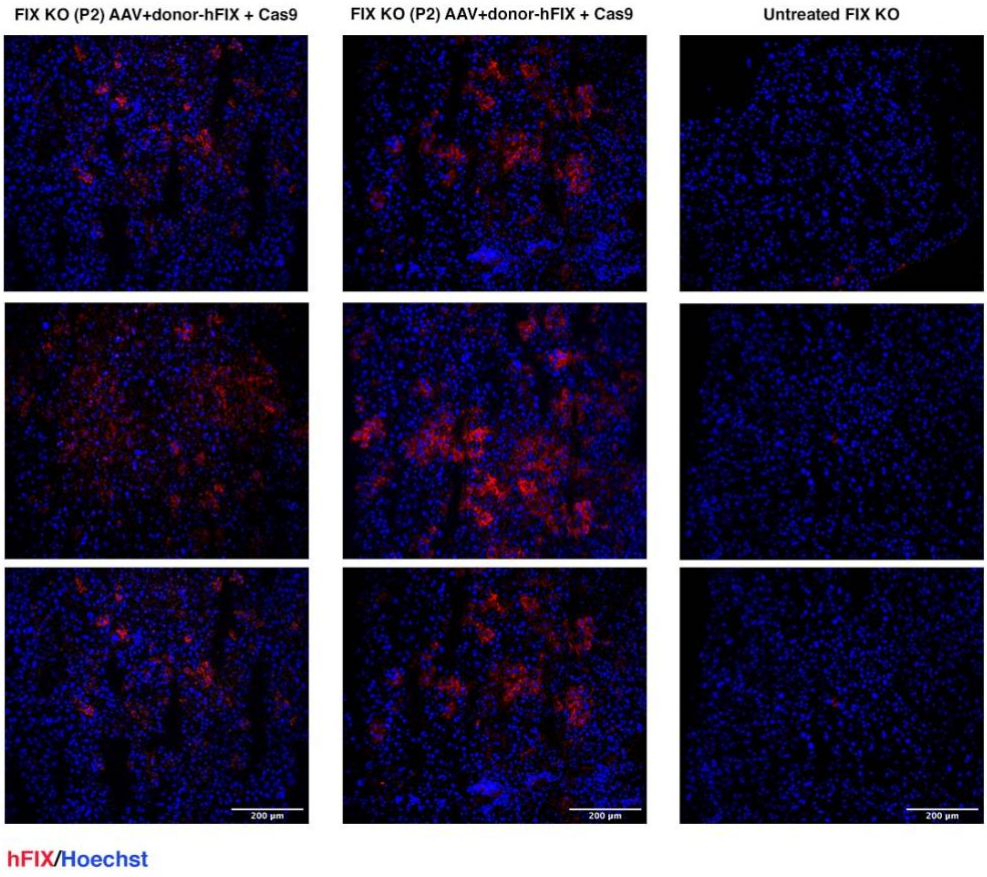

Figure 42: Immunohistochemistry analysis. Liver sections of treated FIX KO mice at P2 were analyzed for hFIX protein.

4.3.8. Treatment of adult *wild-type* mice with eGFP reporter

Next, we decided to perform a preliminary experiment to evaluate the recombination rate in adult mice, using a donor vector encoding the eGFP. I treated adult *wild-type* animals with two rAAV8 vectors: the rAAV8-*Sa*Cas9 and the rAAV8-donor-EGFP, which has the homology arms for the albumin locus flanking the *eGFP* cDNA. Two month old mice were injected with rAAV8-*Sa*Cas9 (1,0E11 vg/mouse) and rAAV8-donor-EGFP (5,0E11 vg/mouse). We used doses that were previously reported to be effective and safe, especially to avoid inactivation of the albumin locus and off-target activity, consequent to a long-term Cas9 activity (Wang et al., 2019). Mice were sacrificed after 2 weeks and the liver was collected for further analysis (Figure 43).

Figure 43: Experimental plan for the treatment of adult *wild-type* mice with eGFP reporter. Mice were transduced with AAV8-SaCas9 (1,0E11 vg/mouse) and AAV8-donor-eGFP (5,0E11 vg/mouse) at postnatal day (P) 60 and liver was collected after 2 weeks post-injection.

I extracted the proteins from the liver homogenate and performed a western blot using an antibody for the eGFP protein. In the western blot analysis, I also included control samples from previous experiments in which adult *wild-type* mice had been injected with only the rAAV8-donor-eGFP and the liver collected after 1 month, 1 untreated *wild-type* animal and the positive control was a mouse treated at P2 with the rAAV8-*Sa*Cas9 + rAVV8-donor-eGFP and sacrificed after 2 weeks. Adult mice treated with the GeneRide and *Sa*Cas9 treatment showed a higher eGFP expression, compared to the animal treated with only the donor eGFP, although the levels were much lower than in the animal treated as a neonate. eGFP protein in the group treated with only the donor eGFP, was under the detectable level of the western, as the bands were barely visible (Figure 44).

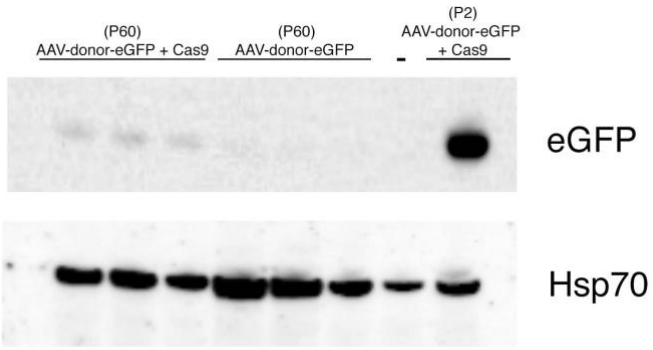

Figure 44: Western blot of eGFP protein after adult treatment from mice transduced with rAAV8-*Sa*Cas9 and rAAV8-donor-eGFP. Liver extract from animals treated with donor-eGFP+SaCas9, donor-eGFP (no nuclease), untreated mouse (-) and a positive control treated at P2 with donor-eGFP+SaCas9 (+).

I evaluated the presence of rAAV8 particles per cell and confirmed the efficient transduction of both rAAV8 vectors (Figure 45).

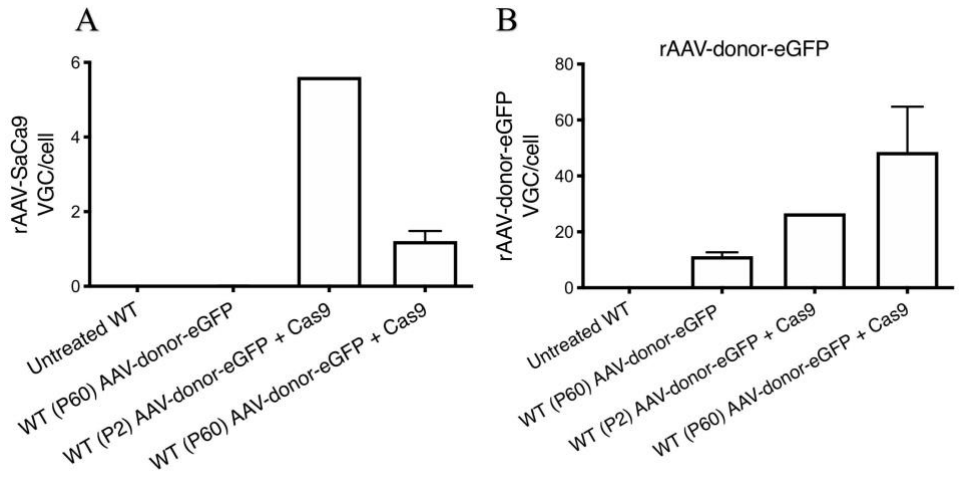

Figure 45: Viral genome particle analysis after adult treatment. Quantification of viral genome particle/cell from the liver extract. Mice were treated with rAAV8-SaCas9 and rAAV-donor-eGFP. The untreated group are the control *wild-type* animals.

In addition, I quantified eGFP positive cells on liver sections (Figure 46). The percentage of eGFP positive hepatocytes was about 0,33 %. Since targeted cells can produce very high levels of recombinant protein, which is secreted in the bloodstream, and even a 1 % increase of the clotting factor can lead to an amelioration of the phenotype, we decided to proceed with the treatment of FIX KO adult mice.

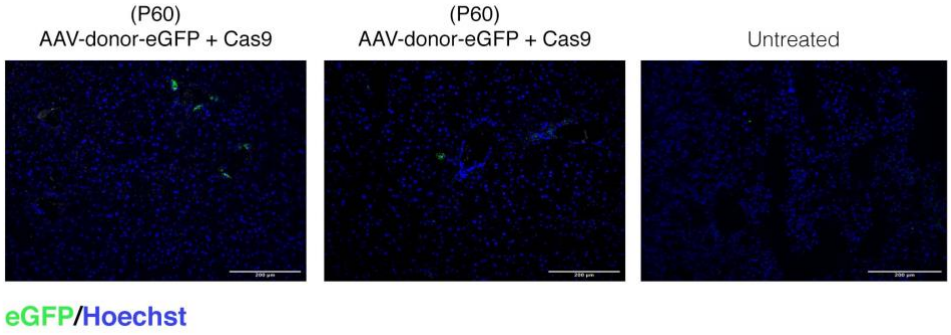

Figure 46: eGFP-positive hepatocytes after adult treatment. Histological analysis. *Wild-type* mice treated at P60 with SaCas9 and donor-eGFP were analyzed for the presence of eGFP positive hepatocytes.

Adult FIX KO mice were injected at post-natal day 60 (2 months old) with rAAV8-*Sa*Cas9 (1,0E11 vg/mouse) and rAAV8-donor-eGFP (5,0E11 vg/mouse) and were sacrificed at 4 month of age (2 months post-treatment) (Figure 47).

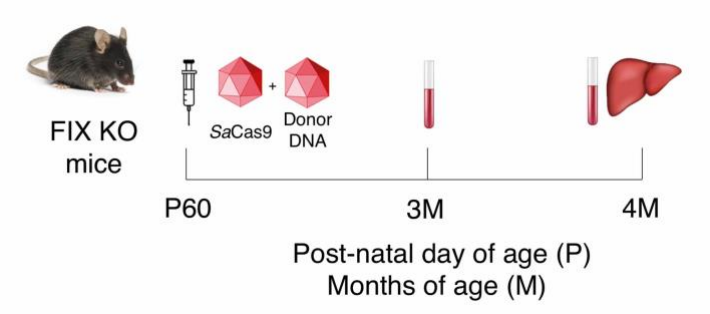

Figure 47: Experimental plan for the treatment of adult FIX KO mice. FIX KO adult mice were injected at 2 months of age with 1,0E11 vg/mouse of AAV8-SaCas9 and 5,0E11 vg/mouse of AAV8-donor-hFIX**.** Blood was collected before injections, 1 month after and at end of the experiment (2 months after treatment).

I analyzed the human FIX levels from the plasma of treated mice with the ELISA. The plasma of FIX KO mice treated at the adult stage showed a concentration of approximately 50 ng/ml of hFIX, which is only a 1-2 % increase, while treatment at the neonatal stage resulted in a 100-140 % increase. Therefore, the neonatal treatment was approximately 150 times more efficient than the treatment at an adult stage (Figure 48).

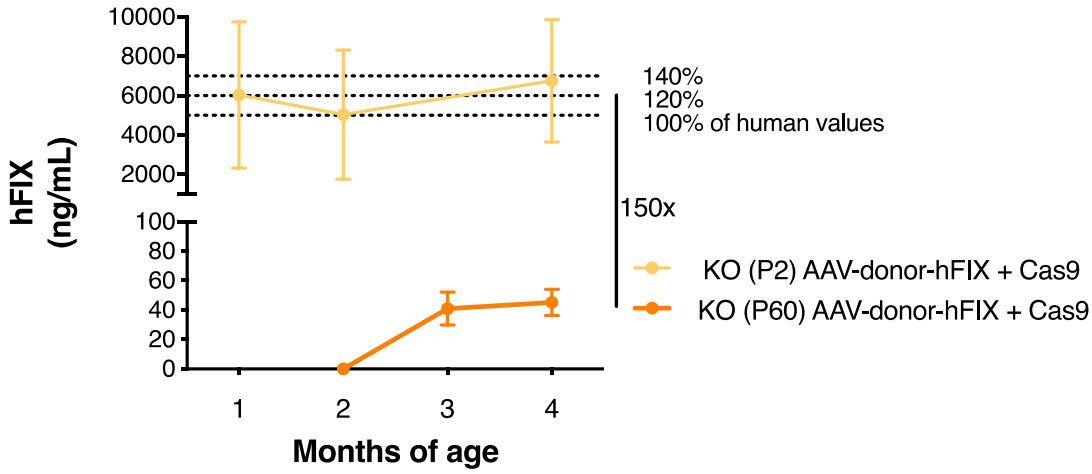

Figure 48: Comparison of plasma hFIX levels between neonatal and adult treatments. Mice were transduced with *Sa*Cas9 and donor-hFIX AAV8 vectors at post-natal (P) day 2 and 60. hFIX concentration obtained from blood samples at months 1, 2 and 4 (P2 treatment) and 2, 3 and 4 months (P60 treatment). 5000 ng/mL corresponds to the normal FIX plasma levels in healthy individuals in the human population.

Mice treated at P60 did not show an important rescue in the bleeding phenotype. There was an amelioration in the tail clip assay compared to the untreated control group, but the difference was not statistically significant (Figure 49). Therefore, the treatment did not reach therapeutic levels in terms of corrections of the bleeding phenotype.

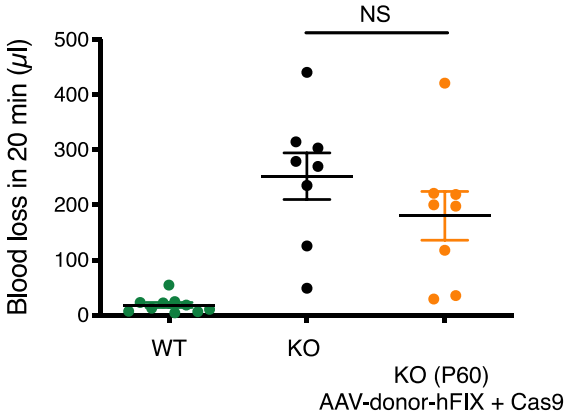

Figure 49: Tail-bleeding assay after adult FIX KO treatment. Bleeding time was evaluated in adult FIX KO mice and compared with untreated *wild-type* and FIX KO mice. Data are shown as mean ± SEM and statistically analyzed by one-way ANOVA with Tukey's multiple comparison test.

In line with other hFIX analyses also western blot both from mouse plasma showed a higher expression in the neonatal group compared to the adult group. In mice plasma, the presence of the hFIX was approximately 63 times higher in the neonatal group, although the western blot cannot be precisely quantified due to saturation of the hFIX band in mice treated at P2 (Figure 50).

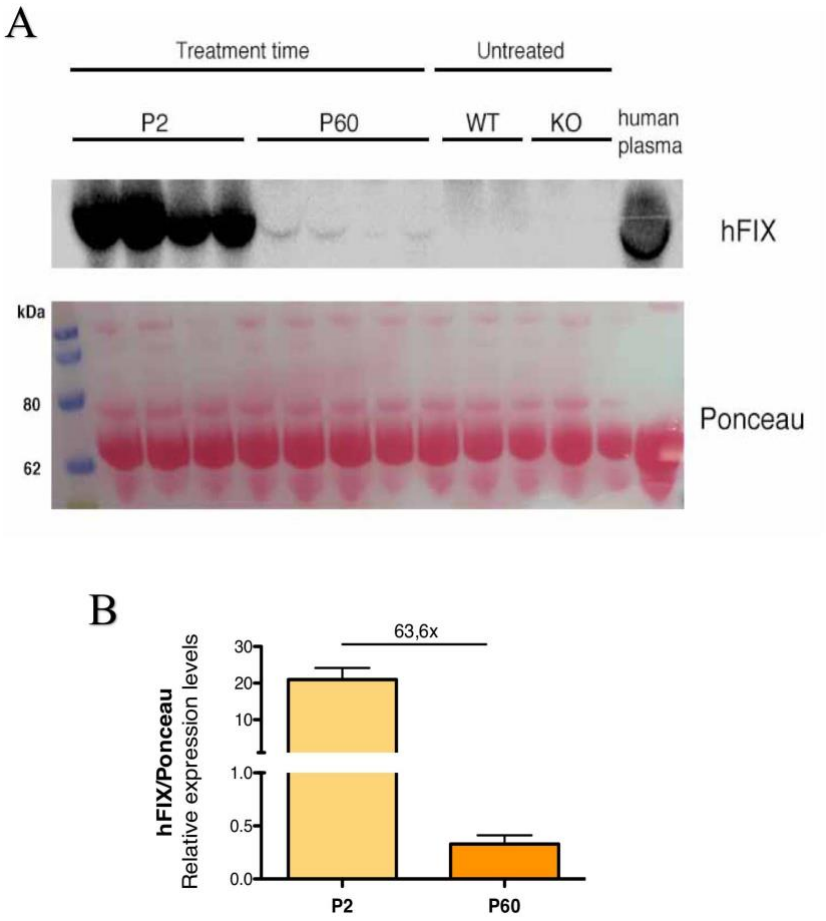

Figure 50: Comparison of plasma hFIX protein levels between neonatal and adult treatments. A) Western blot analysis. Plasma hFIX in FIX KO mice treated at neonatal and adult age with SaCas9 and donor-hFIX. Untreated *wild-type* and FIX KO were used as a negative control and human plasma was used as a positive control. **B) Quantification** of hFIX of the western blot.

To evaluate the *hFIX* expression levels in both treated groups, I performed an RT-qPCR analysis by amplifying the chimeric mRNA and comparing it to endogenous *mFIX* levels of *wild-type* mice. We confirmed the presence of the *Alb-hFIX* mRNA in both groups and detected again a much higher expression in the animals treated in the neonatal stage compared to the animals treated in adulthood. The neonatal group (P2)

had about 150-fold higher expression levels compared to the expression of endogenous murine *FIX* in healthy *wild-type* mice. Surprisingly, the adult group showed a 2-fold increase of the chimeric *Alb-hFIX* expression compared to the normal *FIX* expression in *wild-type* mice (Figure 51A). To evaluate if both sets of primers amplified the target sequence with the same efficiency we tested their efficiency by serially diluting the template and compare the Cq values of the two products. With this analysis, we confirmed that both set of primers had the same efficiency in the amplification of their templates (Figure 51B).

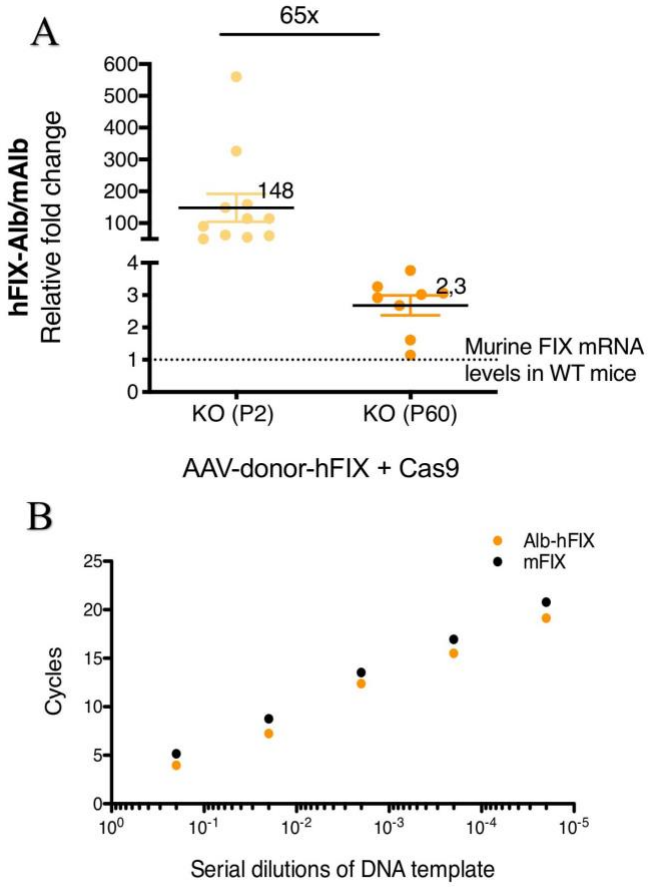

Figure 51: Comparison of *Alb-hFIX* mRNA levels between neonatal and adult treatments. A) Hybrid mRNA *Alb-hASS1* expression level. Comparison between *Alb-hFIX* expression levels in FIX KO mice treated at P2 and P60. Values were normalized with endogenous murine mFIX mRNA expression levels in *wild-type* mice. **B) Primer efficiency comparison**. Specific primers for *Alb-hFIX* and *mFIX* were analyzed with qPCR starting from the same amount of template following with 1:10 dilutions. Template in ng and Cq mean values are plotted in the graph.

To better understand those results, we decided to check the presence of viral genome particles in hepatocytes, to confirm an efficient delivery of the rAAV8 vectors. I performed a qPCR analysis of genomic DNA by using specific primers for the detection of the rAAV8-*Sa*Cas9 and rAAV8-donor-hFIX. With this analysis, I confirmed an efficient delivery as both treated groups had both AAV8 particles (Figure 52).

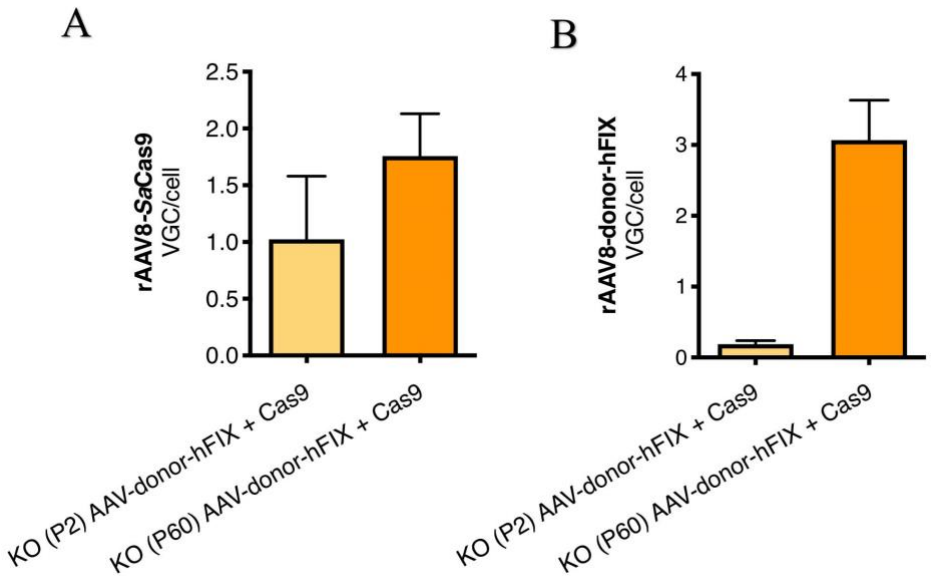

Figure 52: Viral genome particles in FIX KO mice treated at neonatal and adult age. The presence of rAAV8-*Sa*Cas9 and rAAV8-donor-hFIX was analyzed in both treated groups (P2 and P60).

Since the absence of correlation between the mRNA levels and protein levels was unexpected, to exclude the presence of neutralizing antibodies in adult animals, which could clear out the human FIX protein, I performed an ELISA to detect neutralizing antibodies against the hFIX protein. With this analysis, we were not able to detect neutralizing IgG in treated adult mice at any time-point, excluding an activated immune response against the hFIX protein and its potential clearance of the protein from the blood (Figure 53).

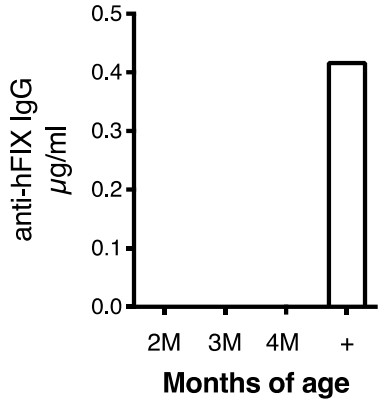

Figure 53: Anti-hFIX IgG assay in adult treated FIX KO mice. The plasma of FIX KO mice treated at P60 was analyzed at different time points. A commercial anti-hFIX antibody was used as positive control.

To evaluate whether the differences between mRNA and protein levels could be related to inefficient hFIX secretion into the bloodstream, I performed a western blot of liver lysate and analyzed the presence of hFIX accumulation inside the liver. The western blot showed much lower hFIX protein levels in the adult treatment compared to the neonatal, which is in line with previous results (Figure 54), suggesting that only a small fraction of chimeric mRNA was efficiently translated into protein. Furthermore, in the P2 treatment, there is a high molecular weight band at 130 kDa, which corresponds to a fused Alb-hFIX chimeric protein at much lower levels than the hFIX band, suggesting efficient ribosomal skipping during translation of the chimeric *Alb-hFIX* mRNA. This band in the adult treatment was under the detection level or absent.

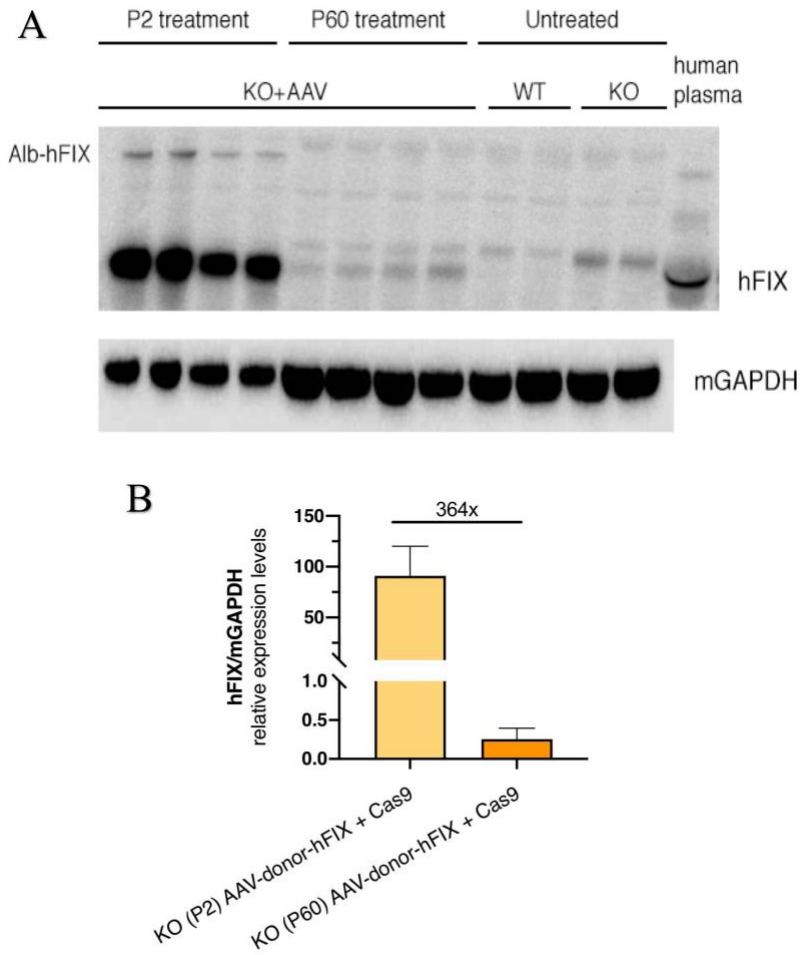

Figure 54: Comparison of hFIX protein levels in liver extracts of neonatal and adult treated mice. A) Western blot analysis. hFIX in liver extracts of hFIX in FIX KO mice treated at neonatal and adult age with rAAV8-*Sa*Cas9 and rAAV8-donor-hFIX. Liver lysates of untreated *wild-type* and FIX KO were used as a negative control and human plasma was used as a positive control. **B) Quantification** of hFIX westernblot normalized for mGAPDH housekeeping protein.

5. Discussion

5.1. Gene targeting therapeutic approach

Gene editing approaches are promising gene-based treatments for liver-mediated monogenic disorders, as they permanently modify the genome, allowing the transfer of the therapeutic transgene to daughter cells and maintaining it over time. There is no loss of information during cell duplication, as it occurs with episomal strategies and, thus, there is no requirement to re-administer the therapeutic vector (Barzel et al., 2015; Chen et al., 2019; De Caneva et al., 2019; De Giorgi et al., 2021; Sharma et al., 2015; Yang et al., 2016). The gene-editing strategies can be applied to disorders using different approaches: for example, by adding a functional gene or correcting the not functional one (Cox et al., 2015).

Different gene targeting approaches have been developed using the albumin locus as a "safe-harbor locus" for transgene integration. The first intron of the *albumin* gene can be a potential target site, as it encodes for a secretory protein that is cleaved post-translationally. The strong albumin promoter was also used to target therapeutic transgenes using ZNF in a clinical trial for Hemophilia B and Mucopolysaccharidosis type I (Ou et al., 2020; Sharma et al., 2015)

A promising gene targeting strategy was developed by Barzel and colleges, and it is based on the integration of a therapeutic transgene into the albumin locus, downstream of the albumin coding sequence. This strategy has several advantages, one of them is inserting a promoterless cDNA into the albumin locus, minimizing the risk related to insertional mutagenesis. When the *hFIX* was targeted downstream the albumin coding sequence, in FIX KO (hemophilia B) mouse model, a 5-20 % increase of hFIX levels was observed in both neonatal and adult mice (Barzel et al., 2015). The same strategy was used in the Mouse molecular genetics laboratory, to target the Ugt1A1 gene in the Crigler-Najjar mouse model, rescuing neonatal lethality, but not normalizing bilirubin levels (Porro et al., 2017). To increase the recombination rate, the same strategy was coupled with the CRISPR/Cas9 platform. One major limitation of using the CRISPR/Cas9 system stands in its long-term expression, potentially leading to off-target cleavage and risk of tumorigenesis. Four predicted potential off-target sites were evaluated by deep sequencing for possible SaCas9 activity, resulting in the manifestation of InDels or SNPs, by deep sequencing. All analyzed sites did not present any change, suggesting a safe and specific SaCas9 activity. Furthermore, analyzing the

safety profile of the approach, no changes were detected in albumin levels, immune response, liver abnormalities, or tumorigenesis (De Caneva et al., 2019). Importantly, this strategy may be applied to different disease-causing mutations by changing the therapeutic cDNA in the donor vector. However, the recombination efficiency may change depending on the transgene in the donor vector. In our laboratory, the highest HDR rate was achieved with the donor vector containing the eGFP cDNA, which was probably related to its shorter length, resulting in a higher integration rate into the albumin locus. A less efficient integration was achieved with the Ugt1a1 donor vector where only 3-4 % of hepatocytes were recombinant, while with the donor eGFP vector approximately 15 % were recombinant (De Caneva et al., 2019). The approach, however, is more suitable for diseases such as hemophilia B, where the therapeutic protein is secreted, as the expression of targeted transgenes is very high, but limited to a small percentage of hepatocytes. Diseases of the urea cycle, where higher levels of enzyme activity are needed to restore the phenotype, may be more difficult to treat.

5.2. Self-limiting CRISPR/Cas9 system

In this study, we exploited the use of the gene targeting approach in combination with the CRISPR/SaCas9 platform. There have been generated different nucleases, but the CRISPR/Cas9 system has shown very promising results both *in vitro* and *in vivo* studies (Chen et al., 2019; Wang et al., 2019; Xue and Greene, 2021; Yang et al., 2016; Yin et al., 2014b). The two main Cas9 nucleases used so far derive from *Staphylococcus pyogenes* (*Sp*) and *Staphylococcus aureus* (*Sa*) bacteria. The *Staphylococcus aureus* Cas9 has some characteristics that provide some advantages, like its small size that can be fit together with the guide RNA into one AAV8 vector, and has also a more complex PAM (NNGRRT) sequence that ensures a more specific cleavage, as the off-target sites are less common compared to the *Staphylococcus pyogenes Cas9,* which has a PAM composed of an NGG sequence, while its catalytic activity is similar to that of the more popular *Staphylococcus pyogenes* Cas9 (Ran et al., 2015).

The SaCas9 used in this work was tested for off-target activity, but no InDels, except for those present at the on-target site, were observed, resulting in a very specific and safe tool. Despite those promising results, off-target activity may be present if Cas9

expression is maintained for longer periods, especially because the episomal AAV-Cas9 DNA can be detected even 10 months after the treatment (De Caneva et al., 2019). Therefore, different approaches have been developed to increase the Cas9 safety profile by limiting the nuclease persistence. One is the self-inactivating Cas9 system, using a gRNA targeting the desired genome sequence and another guide cleaving the Cas9 gene, deactivating the Cas9 (Chen et al., 2016; Petris et al., 2017b). In this work, the SLiCES (Self-limiting Cas9 Circuit for Enhanced safety and Specificity) system developed by Petris and colleges (2017) was tested *in vivo*. Both Cas9 nucleases had similar cleavage efficiency of the guide RNA targeting the albumin locus. However, when I analyzed the self-limiting proprieties, by examining the cleavage efficiency of the second guide RNA, only a small % of InDels were observed in the Cas9 gene, suggesting that even if the Cas9 DNA was cleaved it may be repaired and maintained in the cell. Probably the second guide was less efficient in cleaving the Cas9 gene, compared to the one targeting the albumin locus. Therefore, since we were not able to detect off-target activity with the normal Cas9 nuclease (De Caneva et al., 2019), we decided to use it for further gene targeting experiments. In the future, however, this approach may be improved by selecting more effective guides RNA to eliminate the Cas9 nuclease more efficiently, but always ensuring an efficient cleavage of the target site (Chen et al., 2016; Li et al., 2019). Another possibility to limit the presence of the nuclease in the cell nucleus is by delivering it as mRNA or ribonucleoprotein, which already proved to be effective and safe in different *in vitro* and *vivo* studies (Finn et al., 2018; Lee et al., 2017; Liu et al., 2019; Wang et al., 2016; Zuris et al., 2015).

5.3. Citrullinemia type I mouse model

Citrullinemia type I, unlike disorders as Crigler-Najjar or Hemophilia B, where a smaller increase in the inactive protein is enough to rescue the phenotype, requires a higher protein level to achieve the same results (Yang et al., 2016). In fact, ASS1 knock-out mice die within 24-48 hours after birth, while $ASS1^{fold/fold}$ mice, carrying a hypomorphic mutation in the ASS1 gene, develop a milder form of the disease and it was reported that 50 % survive for only 21 days (Patejunas et al., 1994; Perez et al., 2010). However, in our facility, $ASS1^{fold/fold}$ mice survived until 5 months of age while

given a normal 18 % protein diet, which was by far a longer lifespan than previously reported (Perez et al., 2010). To increase the disease severity, we fed mice with a high protein diet, in order to get an augmented accumulation of citrulline and ammonia. Contrary to our predictions, ASS1$^{fold/fold}$ animals fed with a 51 % diet had an increased survival rate and were able to live up to 1 year, while animals fed with an 18 % and 23 % diet survived until 5 months of age. Mice fed with a 51 % diet had blood ammonia and citrulline levels very high and were not different from mice treated with an 18 % protein diet, yet they had a prolonged lifespan. This was unexpected, as previous studies reported that *spf^{ash}* mice, a mouse model for OTC deficiency, another urea cycle disorder, start developing hyperammonemia and die within 1 week after receiving a high protein diet if they are not treated (Wang et al., 2019; Yang et al., 2016). However, it has been also reported in different studies that a response to an increased protein intake can lead to an increased expression of urea cycle genes, but the mechanism of ASS1 gene regulation is not completely understood (Heibel et al., 2019; Morris, 2002; Nuzum and Snodgrass, 1971). One of the treatments for urea cycle disorders involves a low protein diet. However, the body can adapt to a low protein intake which can subsequently lead to a decreased urea cycle genes production, followed by hyperammonemia (Heibel et al., 2019; Oliva et al., 2019). We suppose that in our case, the increase in high protein intake leads to an increased expression of urea cycle genes (including the not functioning gene), and subsequently, this influenced positively on the survival rate.

5.4. Gene targeting treatment for Citrullinemia type I

We applied the gene targeting approach (Cas9 and donor hASS1 cDNA) and the non-integrative gene therapy on neonatal and juvenile CTLN1 ASS1$^{fold/fold}$ mouse models.
We used also a codon-optimized version of the hASS1 cDNA which may improve treatment efficiency, as *in vitro* studies showed that the codon-optimized cDNA1 had a 3-fold increase in expression compared to the *wild-type* hASS1 cDNA. Unfortunately, it did not show the same efficiency *in-vivo*, probably due to the optimization for a human codon usage bias that is different from the mouse one.

The non-integrative gene therapy treatment on 1 month old juvenile ASS1$^{fold/fold}$ mice was able to completely revert the citrullinemic phenotype. It rescued them from disease lethality and lowered plasma ammonia and citrulline to *wild-type* levels. Importantly, with the FISH analysis, we specifically detected the human ASS1 mRNA in the liver section and were able to estimate that the transduced hepatocytes were approximately 20 %, which was enough to have a systemic reduction in toxic ammonia levels. Another study, performed on a complete ASS1 knock-out mouse model, reported that when delivering four doses of episomal AAV8 ASS1 vector, 22 % of hepatocytes were expressing the ASS1 protein leading to mouse survival until adulthood. Despite an increased survival and low ammonia levels, mice still had significantly higher citrulline levels (Kok et al., 2013). In our case, we used a hypomorphic mouse model, and to achieve the complete rescue of the phenotype, we had 20 % of hASS1-positive hepatocytes added to the 10 % of endogenous mASS1 residual activity in each hepatocyte.

Mice treated at a neonatal stage with the non-integrative gene therapy treatment did not have any decrease in plasma citrulline or ammonia levels 1 month after, suggesting an inefficient treatment, probably related to the loss of episomal vector DNA correlated to hepatocyte proliferation (Bortolussi et al., 2012; Cunningham et al., 2009; Wang et al., 2012).

We treated neonatal mice with our gene targeting approach composed of the donor vector encoding the hASS1 cDNA (*wild-type* or codon-optimized) and the CRISPR/Cas9 platform. With the gene targeting approach on neonatal mice, we were able to rescue the lethality of the diseases and efficiently lower plasma citrulline, within all the tested conditions (donor vector doses 2,0E11, 1,0E12, 2,5E12 vgp/pup). There was a dose-response pattern, as mice treated with the higher dose had a higher decrease in citrulline levels. One mouse out of all injected died at almost 4 months, however, since it had decreased citrulline levels in previous time-points it may have died from another unknown cause. Neonatal treated mice had about 7,4 % of recombinant hepatocytes, which were not enough to lower blood ammonia on a systemic level. However, there was a significant reduction in citrulline level and, importantly, a rescue in the mortality of the mutant animals. While 50 % of untreated ASS1$^{fold/fold}$ mice die by the 3rd month of age and the rest die within 5 months, treated mice lived until the end of the experiment, reaching 5 months of age and increasing their body weight. In a short-term study, we detected the presence of AAV8 vectors in mice liver suggesting efficient

transduction. After, we analyzed the hybrid *Alb-ASS1* mRNA expression level, which was just below normal levels observed for the *mASS1* in *wild-type* mice. However, our gene targeting approach targets the transgene under the strong albumin promoter reaching high expression levels, but this was limited to less than 10 % of hepatocytes, and despite the high expression levels observed in treated animals, it was not sufficient to significantly decrease toxic ammonia from the liver. We hypothesize that reversion of the diseased phenotype may require a higher number of ASS1-positive cells since the expression levels of the other components of the urea cycle are unaffected.

We tested the gene targeting approach on juvenile mice to mimic the treatment of the late-onset form of the disease. The treatment on 1 month old mice was not efficient, due to a low integration rate, that couldn't be estimated, as was under the detection limit of the RNA FISH analysis. Metabolites remained high as in untreated controls, but there was a rescue in the mortality rate when the donor was transduced together with the Cas9 or fludarabine. Fludarabine in a previous study was evaluated for enhancing HR with the same gene targeting strategy used here, but with a donor vector containing an eGFP reported gene. They showed that fludarabine was able to increase HDR efficiency from 1,8 % (Cas9 + donor-eGFP) to 5,7 % (Cas9 + donor-EGFP + Fludarabine), using the same doses of donor vector and Cas9 applied here (6,0E12 vg/kg of Cas9 and 6,0E13 vg/kg of donor DNA) (Tsuji et al., 2020, under revision). However, in this study, they used a donor vector encoding an eGFP reporter cDNA which we observed being more efficient in homologous recombination compared to the donor vector containing the UgtA1A cDNA (De Caneva et al., 2019).

The doses used in the treatment of CTLN1 were higher than the doses used in previous studies on CTLN1, hemophilia B, or hemophilia B clinical trials (Chandler et al., 2013; George et al., 2017; Nathwani et al., 2011a, 2014), raising concerns in the safety aspects of the treatment. However, this study presents the basis that our gene targeting strategy can treat at a pediatric stage, a urea cycle disorder, where higher enzyme levels are needed. Also, this was a first attempt to efficiently treat CTLN1 mice with a gene targeting approach using the CRISPR/Cas9. Still, some improvements on gene targeting efficiency should be obtained to achieve a recombination rate able to completely revert the phenotype.

5.5. Gene targeting treatment for Hemophilia B

In the second part of this PhD thesis, I focused on the development of a gene targeting strategy for hemophilia B disease. In this case, we used a donor vector containing the *hFIX* cDNA together with the SaCas9 nuclease. When WT neonatal mice were treated we observed a very promising result, as hFIX levels had up to a 200 % increase compared to normal hFIX levels in the human population with a stable protein up to 10 months of age. Comparing the treatment with the only donor vector treatment (no nuclease), we observed a 100-fold increase when the nuclease was used. This is in line with previously reported studies, suggesting that the presence of a DNA strand break can enhance the HDR significantly (De Caneva et al., 2019; Rouet et al., 1994a; Smih et al., 1995). FIX KO mice treated at P2 have shown the same coagulation activity as *wild-type* animals, determined by the tail-clip test assay. The treatment given neonatally was very efficient, with long-term stability, completely reverting the hemophilic phenotype in FIX KO mice.

The high hFIX levels observed in P2-treated mice are the result of a high HDR rate obtained with the SaCas9 platform, further increased by the higher translation rate of the *FIX* codon-optimized cDNA. In addition, this transgene carries a triple mutation, V86A, E227A and R338L-Padua hyperactive mutation, which was reported to have a 15-fold increase activity compared to the *wild-type FIX* (Kao et al., 2013).

To go one step further, we decided to treat adult hemophilic mice. In a preliminary experiment, we treated WT mice with an eGFP donor vector together with the SaCas9. We detected about 0,3 % of eGFP positive hepatocytes in adults, while the same system using the SaCas9 and donor-eGFP in neonates resulted in a recombination rate up to 24 % (De Caneva et al., 2019). This result confirms a significantly lower efficiency in adults compared to neonates. However, we proceeded with the treatment of Hemophilic mice, as it was reported in a previous study on hemophilia B mice that 0,5 % of hFIX-positive hepatocytes, expressed under the control of strong albumin promoter, are enough to reach a therapeutic effect (Barzel et al., 2015), and circulating FIX levels of ≥ 2 % should be sufficient to improve the hemophilic phenotype, switching it from a severe to a mild form (Nathwani et al., 2017). With our treatment using the GeneRide with the Cas9 nuclease, we could detect only 1 % of FIX in mice plasma. Coagulation activity measured with a tail clip assay showed a non-significant decrease compare to

untreated FIX KO mice. The low efficiency of gene targeting could be related to the post-mitotic state of the adult liver, which repairs the DSB by the NHEJ mechanism rather than HR (Xue and Greene, 2021). Further improvements are required to increase the homologous recombination rate, such as AAV dose, as in a previously reported study, using a donor vector dosage of 5,0E12 (10-fold higher than the dose we used), had an increase of about 8 % in hFIX levels, reaching a therapeutic effect (Wang et al., 2019). Other possible improvements may involve targeting a different targeting region of the albumin gene or targeting other highly expressed genes, such as the ApoA1 gene. For example, Sharma and colleagues targeted the *hFIX* DNA to the 1st intron, reaching 50-75 % of FIX levels in adult animals. This approach, however, results in the inactivation of the albumin allele (Sharma et al., 2015). Also, other loci, like the ApoA1 gene, showed that the treatment of adult hemophilic animals lead to an approximate increase in 2-5 % of FIX levels, which was enough to ensure clinical benefits (De Giorgi et al., 2021).

After, I measured the *Alb-hFIX* mRNA expression levels of both treated groups and compared them with the endogenous *FIX* in *wild-type* mice. The group treated at a neonatal stage had a major increase in the expression rate compared to the untreated group, but unexpectedly, the group treated at P60 had a 2-fold increase in *hFIX* mRNA expression compared to *mFIX* mRNA levels of healthy *wild-type* mice. This suggests that even after an efficient integration and transcription, the translation process was less efficient. I performed a set of experiments with which I tried to understand this data. First, I compared the efficiency of primers used for the RT-qPCR analysis, and they resulted to have the same efficiency to amplify *Alb-hFIX* and *mFIX* mRNAs. I performed a western blot from liver lysates and excluded an abnormal accumulation of hFIX in the liver. Also, we were not able to detect neutralizing antibodies against the hFIX protein at any time point analyzed, excluding the clearance of the hFIX protein by an active immune response against the human protein. This low protein production may be a consequence of inefficient ribosomal skipping caused by the 2A peptide, which is used for the production of *Alb* and *hFIX* from one chimeric mRNA transcript, with the consequent translation of a fusion albumin-hFIX protein. However, this possibility was also discarded, as we did not observe any high molecular weight band in the adult-treated animals. Importantly, we detected a high molecular weight band in the animals treated at P2, although it was at a much lower abundance than the cleaved hFIX band. This suggests that 2A-skipping is not 100 % efficient, even if we used the *teschovirus-1*

2A peptide that has the highest efficiency compared to peptides from other viruses (Kim et al., 2011).

Even if several successful studies are using non-integrative vectors for hemophilia B adult patients, clinical trials data still suggest that transgene expression can decline over time (Nathwani et al., 2011a). Therefore, developing gene targeting treatments has the key advantage of genome modification resulting in long-term therapeutic efficiency in both pediatric and adult patients.

6. Conclusions

In this PhD work, we evaluated the therapeutic potential of a gene targeting approach coupled to the Crispr/SaCas9 platform two genetically-inherited disorders: citrullinemia type I and hemophilia B. The gene targeting treatment was very promising when applied on hemophilia B neonatal mice, resulting in a long-lasting therapeutic efficacy. The treatment was also efficient on citrullinemia type I neonatal mice, where higher correction levels are needed, significantly improving the phenotype to life-compatible levels. A non-integrative vector, when applied to CTLN1 neonate animals, had no therapeutic effect, while treatment of juvenile mice was able to completely rescue the diseased phenotype.

Altogether, we proved that our gene targeting approach may be applied to different liver disorders, rescuing or significantly improving the diseased phenotype, especially when dosed to neonatal animals. The gene targeting approach still needs further improvements for adult treatments, as the non-integrative treatment efficiency can decline over time. Further studies will be still required to fully understand the safety aspect of the treatment, avoiding long-term effects of the SaCas9 nuclease, and therefore, evaluating alternative Cas9 delivery systems or to develop nuclease-free approaches using other HDR enhancers.

7. References

Adam, R., Karam, V., Delvart, V., O'Grady, J., Mirza, D., Klempnauer, J., Castaing, D., Neuhaus, P., Jamieson, N., Salizzoni, M., et al. (2012). Evolution of indications and results of liver transplantation in Europe. A report from the European Liver Transplant Registry (ELTR). J. Hepatol. *57*, 675–688.

Aiuti, A., Biasco, L., Scaramuzza, S., Ferrua, F., Cicalese, M.P., Baricordi, C., Dionisio, F., Calabria, A., Giannelli, S., Castiello, M.C., et al. (2013). Lentiviral Hematopoietic Stem Cell Gene Therapy in Patients with Wiskott-Aldrich Syndrome. *341*, 13.

Anguela, X.M., Sharma, R., Doyon, Y., Miller, J.C., Li, H., Haurigot, V., Rohde, M.E., Wong, S.Y., Davidson, R.J., Zhou, S., et al. (2013). Robust ZFN-mediated genome editing in adult hemophilic mice. Blood *122*, 3283–3287.

Aravalli, R.N., and Steer, C.J. (2018). CRISPR/Cas9 therapeutics for liver diseases. J. Cell. Biochem. *119*, 4265–4278.

Baganate, F., Beal, E.W., Tumin, D., Azoulay, D., Mumtaz, K., Black, S.M., Washburn, K., and Pawlik, T.M. (2018). Early mortality after liver transplantation: Defining the course and the cause. Surgery *164*, 694–704.

Barrangou, R., Fremaux, C., Deveau, H., Richards, M., Boyaval, P., Moineau, S., Romero, D.A., and Horvath, P. (2007). CRISPR Provides Acquired Resistance Against Viruses in Prokaryotes. Science *315*, 1709–1712.

Baruteau, J., Waddington, S.N., Alexander, I.E., and Gissen, P. (2017). Gene therapy for monogenic liver diseases: clinical successes, current challenges and future prospects. J. Inherit. Metab. Dis. *40*, 497–517.

Barzel, A., Paulk, N.K., Shi, Y., Huang, Y., Chu, K., Zhang, F., Valdmanis, P.N., Spector, L.P., Porteus, M.H., Gaensler, K.M., et al. (2015). Promoterless gene targeting without nucleases ameliorates haemophilia B in mice. Nature *517*, 360–364.

Blaese, R.M., Culver, K.W., Miller, A.D., Carter, C.S., Fleisher, T., Clerici, M., Shearer, G., Chang, L., Chiang, Y., Tolstoshev, P., et al. (1995). T Lymphocyte-Directed Gene Therapy for ADA- SCID: Initial Trial Results After 4 Years. Science *270*, 475–480.

Bordignon, C., Notarangelo, L.D., Nobili, N., Ferrari, G., Casorati, G., Panina, P., Mazzolari, E., Maggioni, D., Rossi, C., Servida, P., et al. (1995). Gene Therapy in Peripheral Blood Lymphocytes and Bone Marrow for ADA- Immunodeficient Patients. *270*, 6.

Borel, F., Tang, Q., Gernoux, G., Greer, C., Wang, Z., Barzel, A., Kay, M.A., Shultz, L.D., Greiner, D.L., Flotte, T.R., et al. (2017). Survival Advantage of Both Human Hepatocyte Xenografts and Genome-Edited Hepatocytes for Treatment of α-1 Antitrypsin Deficiency. Mol. Ther. *25*, 2477–2489.

Bortolussi, G., Zentilin, L., Baj, G., Giraudi, P., Bellarosa, C., Giacca, M., Tiribelli, C., and Muro, A.F. (2012). Rescue of bilirubin-induced neonatal lethality in a mouse model of Crigler-Najjar syndrome type I by AAV9-mediated gene transfer. FASEB J. *26*, 1052–1063.

Brinkman, E.K., Chen, T., Amendola, M., and van Steensel, B. (2014). Easy quantitative assessment of genome editing by sequence trace decomposition. Nucleic Acids Res. *42*, e168–e168.

Brunetti-Pierri, N., and Lee, B. (2005). Gene therapy for inborn errors of liver metabolism. Mol. Genet. Metab. *86*, 13–24.

Bryson, T.E., Anglin, C.M., Bridges, P.H., and Cottle, R.N. (2017). Nuclease-Mediated Gene Therapies for Inherited Metabolic Diseases of the Liver. Yale J. Biol. Med. *90*, 553–566.

Calcedo, R., and Wilson, J.M. (2016). AAV Natural Infection Induces Broad Cross-Neutralizing Antibody Responses to Multiple AAV Serotypes in Chimpanzees. Hum. Gene Ther. Clin. Dev. *27*, 79–82.

Carroll, D. (2014). Genome engineering with targetable nucleases. Annu. Rev. Biochem. *83*, 409–439.

Ceccaldi, R., Rondinelli, B., and D'Andrea, A.D. (2016). Repair Pathway Choices and Consequences at the Double-Strand Break. Trends Cell Biol. *26*, 52–64.

Chakrapani, A. (2001). Detection of inborn errors of metabolism in the newborn. Arch. Dis. Child. - Fetal Neonatal Ed. *84*, 205F – 210.

Chandler, R.J., and Venditti, C.P. (2016). Gene therapy for metabolic diseases. Transl. Sci. Rare Dis. *1*, 73–89.

Chandler, R.J., Tarasenko, T.N., Cusmano-Ozog, K., Sun, Q., Sutton, V.R., Venditti, C.P., and McGuire, P.J. (2013). Liver-directed adeno-associated virus serotype 8 gene transfer rescues a lethal murine model of citrullinemia type 1. Gene Ther. *20*, 1188–1191.

Chandler, R.J., Sands, M.S., and Venditti, C.P. (2017). Recombinant Adeno-Associated Viral Integration and Genotoxicity: Insights from Animal Models. Hum. Gene Ther. *28*, 314–322.

Charlesworth, C.T., Deshpande, P.S., Dever, D.P., Camarena, J., Lemgart, V.T., Cromer, M.K., Vakulskas, C.A., Collingwood, M.A., Zhang, L., Bode, N.M., et al. (2019). Identification of preexisting adaptive immunity to Cas9 proteins in humans. Nat. Med. *25*, 249–254.

Chen, H., Shi, M., Gilam, A., Zheng, Q., Zhang, Y., Afrikanova, I., Li, J., Gluzman, Z., Jiang, R., Kong, L.-J., et al. (2019). Hemophilia A ameliorated in mice by CRISPR-based in vivo genome editing of human Factor VIII. Sci. Rep. *9*, 16838.

Chen, Y., Liu, X., Zhang, Y., Wang, H., Ying, H., Liu, M., Li, D., Lui, K.O., and Ding, Q. (2016). A Self-restricted CRISPR System to Reduce Off-target Effects. Mol. Ther. *24*, 1508–1510.

Concolino, D., Deodato, F., and Parini, R. (2018). Enzyme replacement therapy: efficacy and limitations. Ital. J. Pediatr. *44*, 120.

Cong, L., Ran, F.A., Cox, D., Lin, S., Barretto, R., Habib, N., Hsu, P.D., Wu, X., Jiang, W., Marraffini, L.A., et al. (2013). Multiplex Genome Engineering Using CRISPR/Cas Systems. Science *339*, 819–823.

Cox, D.B.T., Platt, R.J., and Zhang, F. (2015). Therapeutic genome editing: prospects and challenges. Nat. Med. *21*, 121–131.

Cunningham, S.C., Dane, A.P., Spinoulas, A., and Alexander, I.E. (2008). Gene Delivery to the Juvenile Mouse Liver Using AAV2/8 Vectors. Mol. Ther. *16*, 1081–1088.

Cunningham, S.C., Spinoulas, A., Carpenter, K.H., Wilcken, B., Kuchel, P.W., and Alexander, I.E. (2009). AAV2/8-mediated Correction of OTC Deficiency Is Robust in Adult but Not Neonatal Spfash Mice. Mol. Ther. *17*, 1340–1346.

Cunningham, S.C., Siew, S.M., Hallwirth, C.V., Bolitho, C., Sasaki, N., Garg, G., Michael, I.P., Hetherington, N.A., Carpenter, K., de Alencastro, G., et al. (2015). Modeling correction of severe urea cycle defects in the growing murine liver using a hybrid recombinant adeno-associated virus/ *piggyBac* transposase gene delivery system: STEATOHEPATITIS/METABOLIC LIVER DISEASE. Hepatology *62*, 417–428.

Daya, S., and Berns, K.I. (2008). Gene Therapy Using Adeno-Associated Virus Vectors. Clin. Microbiol. Rev. *21*, 583–593.

De Caneva, A., Porro, F., Bortolussi, G., Sola, R., Lisjak, M., Barzel, A., Giacca, M., Kay, M.A., Vlahoviček, K., Zentilin, L., et al. (2019). Coupling AAV-mediated promoterless gene targeting to SaCas9 nuclease to efficiently correct liver metabolic diseases. JCI Insight *4*, e128863.

De Giorgi, M., Li, A., Hurley, A., Barzi, M., Doerfler, A.M., Cherayil, N.A., Smith, H.E., Brown, J.D., Lin, C.Y., Bissig, K.-D., et al. (2021). Targeting the Apoa1 locus for liver-directed gene therapy. Mol. Ther. - Methods Clin. Dev. *21*, 656–669.

Dennis, J.A., Healy, P.J., Beaudet, A.L., and O'Brien, W.E. (1989). Molecular definition of bovine argininosuccinate synthetase deficiency. Proc. Natl. Acad. Sci. *86*, 7947–7951.

Deveau, H., Barrangou, R., Garneau, J.E., Labonte, J., Fremaux, C., Boyaval, P., Romero, D.A., Horvath, P., and Moineau, S. (2008). Phage Response to CRISPR-Encoded Resistance in Streptococcus thermophilus. J. Bacteriol. *190*, 1390–1400.

Deyle, D.R., and Russell, D.W. (2010). Adeno-associated virus vector integration. 11.

Diez-Fernandez, C., Wellauer, O., Gemperle, C., Rüfenacht, V., Fingerhut, R., and Häberle, J. (2016). Kinetic mutations in argininosuccinate synthetase deficiency: characterisation and in vitro correction by substrate supplementation. J. Med. Genet. *53*, 710–719.

Diez-Fernandez, C., Rüfenacht, V., and Häberle, J. (2017). Mutations in the Human Argininosuccinate Synthetase (*ASS1*) Gene, Impact on Patients, Common Changes, and Structural Considerations: HUMAN MUTATION. Hum. Mutat. *38*, 471–484.

Ding, Q., Strong, A., Patel, K.M., Ng, S.-L., Gosis, B.S., Regan, S.N., Cowan, C.A., Rader, D.J., and Musunuru, K. (2014). Permanent Alteration of PCSK9 With In Vivo CRISPR-Cas9 Genome Editing. Circ. Res. *115*, 488–492.

Fagiuoli, S., Daina, E., D'Antiga, L., Colledan, M., and Remuzzi, G. (2013). Monogenic diseases that can be cured by liver transplantation. J. Hepatol. *59*, 595–612.

Fayek, S.A., Quintini, C., Chavin, K.D., and Marsh, C.L. (2016). The Current State of Liver Transplantation in the United States: *Perspective From American Society of Transplant Surgeons (ASTS) Scientific Studies Committee and Endorsed by ASTS Council*. Am. J. Transplant. *16*, 3093–3104.

Ferrari, F.K., Samulski, T., Shenk, T., and Samulski, R.J. (1996). Second-strand synthesis is a rate-limiting step for efficient transduction by recombinant adeno-associated virus vectors. J. Virol. *70*, 3227–3234.

Finn, J.D., Smith, A.R., Patel, M.C., Shaw, L., Youniss, M.R., van Heteren, J., Dirstine, T., Ciullo, C., Lescarbeau, R., Seitzer, J., et al. (2018). A Single Administration of CRISPR/Cas9 Lipid Nanoparticles Achieves Robust and Persistent In Vivo Genome Editing. Cell Rep. *22*, 2227–2235.

Fu, Y., Foden, J.A., Khayter, C., Maeder, M.L., Reyon, D., Joung, J.K., and Sander, J.D. (2013). High-frequency off-target mutagenesis induced by CRISPR-Cas nucleases in human cells. Nat. Biotechnol. *31*, 822–826.

Fu, Y., Sander, J.D., Reyon, D., Cascio, V.M., and Joung, J.K. (2014). Improving CRISPR-Cas nuclease specificity using truncated guide RNAs. Nat. Biotechnol. *32*, 279–284.

Gao, G.-P., Alvira, M.R., Wang, L., Calcedo, R., Johnston, J., and Wilson, J.M. (2002). Novel adeno-associated viruses from rhesus monkeys as vectors for human gene therapy. Proc. Natl. Acad. Sci. *99*, 11854–11859.

Gaudelli, N.M., Komor, A.C., Rees, H.A., Packer, M.S., Badran, A.H., Bryson, D.I., and Liu, D.R. (2017). Programmable base editing of A•T to G•C in genomic DNA without DNA cleavage. Nature *551*, 464–471.

George, L.A., Sullivan, S.K., Giermasz, A., Rasko, J.E.J., Samelson-Jones, B.J., Ducore, J., Cuker, A., Sullivan, L.M., Majumdar, S., Teitel, J., et al. (2017). Hemophilia B Gene Therapy with a High-Specific-Activity Factor IX Variant. N. Engl. J. Med. *377*, 2215–2227.

George, L.A., Ragni, M.V., Rasko, J.E.J., Raffini, L.J., Samelson-Jones, B.J., Ozelo, M., Hazbon, M., Runowski, A.R., Wellman, J.A., Wachtel, K., et al. (2020). Long-Term Follow-Up of the First in Human Intravascular Delivery of AAV for Gene Transfer: AAV2-hFIX16 for Severe Hemophilia B. Mol. Ther. S1525001620302914.

Gonçalves, G.A.R., and Paiva, R. de M.A. (2017). Gene therapy: advances, challenges and perspectives. Einstein São Paulo *15*, 369–375.

Grote, A., Hiller, K., Scheer, M., Munch, R., Nortemann, B., Hempel, D.C., and Jahn, D. (2005). JCat: a novel tool to adapt codon usage of a target gene to its potential expression host. Nucleic Acids Res. *33*, W526–W531.

Harthan, A.A. (2018). An Introduction to Pharmacotherapy for Inborn Errors of Metabolism. J. Pediatr. Pharmacol. Ther. *23*, 432–446.

Heibel, S.K., McGuire, P.J., Haskins, N., Majumdar, H.D., Rayavarapu, S., Nagaraju, K., Hathout, Y., Brown, K., Tuchman, M., and Caldovic, L. (2019). AMP-activated protein kinase signaling regulated expression of urea cycle enzymes in response to changes in dietary protein intake. J. Inherit. Metab. Dis. *42*, 1088–1096.

Herzog, R.W. (2010). Gene Therapy for SCID-X1: Round 2. Mol. Ther. *18*, 1891.

Herzog, R., Cao, O., and Srivastava, A. (2010). Two Decades of Clinical Gene Therapy - Success Is Finally Mounting.

Heyer, W.-D., Ehmsen, K.T., and Liu, J. (2010). Regulation of Homologous Recombination in Eukaryotes. Annu. Rev. Genet. *44*, 113–139.

Horava, S.D., and Peppas, N.A. (2017). Recent advances in hemophilia B therapy. Drug Deliv. Transl. Res. *7*, 359–371.

Hsu, P.D., Scott, D.A., Weinstein, J.A., Ran, F.A., Konermann, S., Agarwala, V., Li, Y., Fine, E.J., Wu, X., Shalem, O., et al. (2013). DNA targeting specificity of RNA-guided Cas9 nucleases. Nat. Biotechnol. *31*, 827–832.

Hsu, P.D., Lander, E.S., and Zhang, F. (2014). Development and Applications of CRISPR-Cas9 for Genome Engineering. Cell *157*, 1262–1278.

Ibraheim, R., Song, C.-Q., Mir, A., Amrani, N., Xue, W., and Sontheimer, E.J. (2018). All-in-one adeno-associated virus delivery and genome editing by Neisseria meningitidis Cas9 in vivo. Genome Biol. *19*, 137.

Jinek, M., Chylinski, K., Fonfara, I., Hauer, M., Doudna, J.A., and Charpentier, E. (2012). A Programmable Dual-RNA-Guided DNA Endonuclease in Adaptive Bacterial Immunity. Science *337*, 816–821.

Kadakol, A., Ghosh, S.S., Sappal, B.S., Sharma, G., Chowdhury, J.R., and Chowdhury, N.R. (2000). Genetic lesions of bilirubin uridine-diphosphoglucuronate glucuronosyltransferase (UGT1A1) causing Crigler-Najjar and Gilbert syndromes: Correlation of genotype to phenotype. Hum. Mutat. *16*, 297–306.

Kao, C.-Y., Yang, S.-J., Tao, M.-H., Jeng, Y.-M., Yu, I.-S., and Lin, S.-W. (2013). Incorporation of the factor IX Padua mutation into FIX-Triple improves clotting activity in vitro and in vivo. Thromb. Haemost. *110*, 244–256.

Karthikeyan, G., Jagadeesh, S., Seshadri, S., and Häberle, J. (2013). Citrullinemia type 1: Genetic diagnosis and prenatal diagnosis in subsequent pregnancy. Indian Pediatr. *50*, 965–966.

Kay, M.A. (2011). State-of-the-art gene-based therapies: the road ahead. Nat. Rev. Genet. *12*, 316–328.

Kay, M.A., and Woo, S.L.C. (1994). Gene Therapy for Metabolic Diseases. ILAR News *36*, 7.

Kim, J.H., Lee, S.-R., Li, L.-H., Park, H.-J., Park, J.-H., Lee, K.Y., Kim, M.-K., Shin, B.A., and Choi, S.-Y. (2011). High Cleavage Efficiency of a 2A Peptide Derived from Porcine Teschovirus-1 in Human Cell Lines, Zebrafish and Mice. PLoS ONE *6*, e18556.

Kleinstiver, B.P., Prew, M.S., Tsai, S.Q., Nguyen, N.T., Topkar, V.V., Zheng, Z., and Joung, J.K. (2015). Broadening the targeting range of Staphylococcus aureus CRISPR-Cas9 by modifying PAM recognition. Nat. Biotechnol. *33*, 1293–1298.

Kleinstiver, B.P., Pattanayak, V., Prew, M.S., Tsai, S.Q., Nguyen, N.T., Zheng, Z., and Joung, J.K. (2016). High-fidelity CRISPR–Cas9 nucleases with no detectable genome-wide off-target effects. Nature *529*, 490–495.

Kok, C.Y., Cunningham, S.C., Carpenter, K.H., Dane, A.P., Siew, S.M., Logan, G.J., Kuchel, P.W., and Alexander, I.E. (2013). Adeno-associated Virus-mediated Rescue of Neonatal Lethality in Argininosuccinate Synthetase-deficient Mice. Mol. Ther. *21*, 1823–1831.

Komor, A.C., Kim, Y.B., Packer, M.S., Zuris, J.A., and Liu, D.R. (2016). Programmable editing of a target base in genomic DNA without double-stranded DNA cleavage. Nature *533*, 420–424.

Lee, K., Conboy, M., Park, H.M., Jiang, F., Kim, H.J., Dewitt, M.A., Mackley, V.A., Chang, K., Rao, A., Skinner, C., et al. (2017). Nanoparticle delivery of Cas9 ribonucleoprotein and donor DNA in vivo induces homology-directed DNA repair. Nat. Biomed. Eng. *1*, 889–901.

Li, F., Hung, S.S.C., Mohd Khalid, M.K.N., Wang, J.-H., Chrysostomou, V., Wong, V.H.Y., Singh, V., Wing, K., Tu, L., Bender, J.A., et al. (2019). Utility of Self-Destructing CRISPR/Cas Constructs for Targeted Gene Editing in the Retina. Hum. Gene Ther. *30*, 1349–1360.

Liu, J., Chang, J., Jiang, Y., Meng, X., Sun, T., Mao, L., Xu, Q., and Wang, M. (2019). Fast and Efficient CRISPR/Cas9 Genome Editing In Vivo Enabled by Bioreducible Lipid and Messenger RNA Nanoparticles. Adv. Mater. *31*, 1902575.

Makarova, K.S., Haft, D.H., Barrangou, R., Brouns, S.J.J., Charpentier, E., Horvath, P., Moineau, S., Mojica, F.J.M., Wolf, Y.I., Yakunin, A.F., et al. (2011). Evolution and classification of the CRISPR–Cas systems. Nat. Rev. Microbiol. *9*, 467–477.

Mali, P., Aach, J., Stranges, P.B., Esvelt, K.M., Moosburner, M., Kosuri, S., Yang, L., and Church, G.M. (2013). CAS9 transcriptional activators for target specificity screening and paired nickases for cooperative genome engineering. Nat. Biotechnol. *31*, 833–838.

Manno, C.S., Pierce, G.F., Arruda, V.R., Glader, B., Ragni, M., Rasko, J.J.E., Ozelo, M.C., Hoots, K., Blatt, P., Konkle, B., et al. (2006). Successful transduction of liver in hemophilia by AAV-Factor IX and limitations imposed by the host immune response. Nat. Med. *12*, 342–347.

Mannucci, P.M. (2020). Hemophilia therapy: the future has begun. Haematologica *105*, 545–553.

Mannucci, P.M., and Tuddenham, E.G.D. (2001). The Hemophilias — From Royal Genes to Gene Therapy. N. Engl. J. Med. 7.

Matoori, S., and Leroux, J.-C. (2015). Recent advances in the treatment of hyperammonemia. Adv. Drug Deliv. Rev. *90*, 55–68.

Mingozzi, F., and High, K.A. (2013). Immune responses to AAV vectors: overcoming barriers to successful gene therapy. Blood *122*, 23–36.

Morris, S.M. (2002). R EGULATION OF E NZYMES OF THE UREA CYCLE AND ARGININE METABOLISM. Annu. Rev. Nutr. *22*, 87–105.

Nathwani, A.C., Gray, J.T., McIntosh, J., Ng, C.Y.C., Zhou, J., Spence, Y., Cochrane, M., Gray, E., Tuddenham, E.G.D., and Davidoff, A.M. (2007). Safe and efficient transduction of the liver after peripheral vein infusion of self-complementary AAV

vector results in stable therapeutic expression of human FIX in nonhuman primates. Blood *109*, 1414–1421.

Nathwani, A.C., Tuddenham, E.G.D., Rangarajan, S., Rosales, C., McIntosh, J., Linch, D.C., Chowdary, P., Riddell, A., Pie, A.J., Harrington, C., et al. (2011a). Adenovirus-Associated Virus Vector–Mediated Gene Transfer in Hemophilia B. N. Engl. J. Med. *365*, 2357–2365.

Nathwani, A.C., Rosales, C., McIntosh, J., Rastegarlari, G., Nathwani, D., Raj, D., Nawathe, S., Waddington, S.N., Bronson, R., Jackson, S., et al. (2011b). Long-term Safety and Efficacy Following Systemic Administration of a Self-complementary AAV Vector Encoding Human FIX Pseudotyped With Serotype 5 and 8 Capsid Proteins. Mol. Ther. *19*, 876–885.

Nathwani, A.C., Reiss, U.M., Tuddenham, E.G.D., Rosales, C., Chowdary, P., McIntosh, J., Della Peruta, M., Lheriteau, E., Patel, N., Raj, D., et al. (2014). Long-Term Safety and Efficacy of Factor IX Gene Therapy in Hemophilia B. N. Engl. J. Med. *371*, 1994–2004.

Nathwani, A.C., Davidoff, A.M., and Tuddenham, E.G.D. (2017). Advances in Gene Therapy for Hemophilia. Hum. Gene Ther. *28*, 1004–1012.

Nayerossadat, N., Ali, P., and Maedeh, T. (2012). Viral and nonviral delivery systems for gene delivery. Adv. Biomed. Res. *1*, 27.

Nelson, C.E., Wu, Y., Gemberling, M.P., Oliver, M.L., Waller, M.A., Bohning, J.D., Robinson-Hamm, J.N., Bulaklak, K., Castellanos Rivera, R.M., Collier, J.H., et al. (2019). Long-term evaluation of AAV-CRISPR genome editing for Duchenne muscular dystrophy. Nat. Med. *25*, 427–432.

Nishimasu, H., Ran, F.A., Hsu, P.D., Konermann, S., Shehata, S.I., Dohmae, N., Ishitani, R., Zhang, F., and Nureki, O. (2014). Crystal Structure of Cas9 in Complex with Guide RNA and Target DNA. Cell *156*, 935–949.

Nuzum, C.T., and Snodgrass, P.J. (1971). Urea Cycle Enzyme Adaptation to Dietary Protein in Primates. Science *172*, 1042–1043.

O'Brien, W.E. (1979). Isolation and characterization of argininosuccinate synthetase from human liver. Biochemistry *18*, 5353–5356.

Okaygoun, D., Oliveira, D.D., Soman, S., and Williams, R. (2021). Advances in the management of haemophilia: emerging treatments and their mechanisms. J. Biomed. Sci. *28*, 64.

Oliva, L., Alemany, M., Remesar, X., and Fernández-López, J.-A. (2019). The Food Energy/Protein Ratio Regulates the Rat Urea Cycle but Not Total Nitrogen Losses. Nutrients *11*, 316.

van der Oost, J., Westra, E.R., Jackson, R.N., and Wiedenheft, B. (2014). Unravelling the structural and mechanistic basis of CRISPR–Cas systems. Nat. Rev. Microbiol. *12*, 479–492.

Ou, L., Przybilla, M.J., Ahlat, O., Kim, S., Overn, P., Jarnes, J., O'Sullivan, M.G., and Whitley, C.B. (2020). A Highly Efficacious PS Gene Editing System Corrects Metabolic and Neurological Complications of Mucopolysaccharidosis Type I. Mol. Ther. *28*, 1442–1454.

Patejunas, G., Bradley, A., Beaudet, A.L., and O'Brien, W.E. (1994). Generation of a mouse model for citrullinemia by targeted disruption of the argininosuccinate synthetase gene. Somat. Cell Mol. Genet. *20*, 55–60.

Paulk, N.K., Wursthorn, K., Wang, Z., Finegold, M.J., Kay, M.A., and Grompe, M. (2010). Adeno-associated virus gene repair corrects a mouse model of hereditary tyrosinemia in vivo. Hepatology *51*, 1200–1208.

Perez, C.J., Jaubert, J., Guénet, J.-L., Barnhart, K.F., Ross-Inta, C.M., Quintanilla, V.C., Aubin, I., Brandon, J.L., Otto, N.W., DiGiovanni, J., et al. (2010). Two Hypomorphic Alleles of Mouse Ass1 as a New Animal Model of Citrullinemia Type I and Other Hyperammonemic Syndromes. Am. J. Pathol. *177*, 1958–1968.

Petris, G., Casini, A., Montagna, C., Lorenzin, F., Prandi, D., Romanel, A., Zasso, J., Conti, L., Demichelis, F., and Cereseto, A. (2017a). Hit and go CAS9 delivered through a lentiviral based self-limiting circuit. Nat. Commun. *8*, 1–9.

Petris, G., Casini, A., Montagna, C., Lorenzin, F., Prandi, D., Romanel, A., Zasso, J., Conti, L., Demichelis, F., and Cereseto, A. (2017b). Hit and go CAS9 delivered through a lentiviral based self-limiting circuit. Nat. Commun. *8*, 15334.

Porro, F., Bortolussi, G., Barzel, A., De Caneva, A., Iaconcig, A., Vodret, S., Zentilin, L., Kay, M.A., and Muro, A.F. (2017). Promoterless gene targeting without nucleases rescues lethality of a Crigler-Najjar syndrome mouse model. EMBO Mol. Med. *9*, 1346–1355.

Puumalainen, A.-M., Vapalahti, M., Agrawal, R.S., Kossila, M., Laukkanen, J., Lehtolainen, P., Viita, H., Paljärvi, L., Vanninen, R., and Ylä-Herttuala, S. (1998). *β* -Galactosidase Gene Transfer to Human Malignant Glioma *In Vivo* Using Replication-Deficient Retroviruses and Adenoviruses. Hum. Gene Ther. *9*, 1769–1774.

Quinonez, S.C., and Thoene, J.G. Citrullinemia Type I. 18.

Ramamoorth, M. (2015). Non Viral Vectors in Gene Therapy- An Overview. J. Clin. Diagn. Res.

Ran, F.A., Cong, L., Yan, W.X., Scott, D.A., Gootenberg, J.S., Kriz, A.J., Zetsche, B., Shalem, O., Wu, X., Makarova, K.S., et al. (2015). In vivo genome editing using Staphylococcus aureus Cas9. Nature *520*, 186–191.

Raper, S.E., Chirmule, N., Lee, F.S., Wivel, N.A., Bagg, A., Gao, G., Wilson, J.M., and Batshaw, M.L. (2003). Fatal systemic inflammatory response syndrome in a ornithine transcarbamylase deficient patient following adenoviral gene transfer. Mol. Genet. Metab. *80*, 148–158.

Robles-Rodríguez, O.A., Pérez-Trujillo, J.J., Villanueva-Olivo, A., Villarreal-Martínez, L., Marfil-Rivera, L.J., Rodríguez-Rocha, H., García-García, A., Saucedo-Cárdenas, O., Loera-Arias, M.J., and de Oca-Luna, R.M. (2020). Advances in gene therapy for hemophilia. J. Biosci. *45*, 88.

Ronzitti, G., Bortolussi, G., van Dijk, R., Collaud, F., Charles, S., Leborgne, C., Vidal, P., Martin, S., Gjata, B., Sola, M.S., et al. (2016). A translationally optimized AAV-UGT1A1 vector drives safe and long-lasting correction of Crigler-Najjar syndrome. Mol. Ther. - Methods Clin. Dev. *3*, 16049.

Rouet, P., Smih, F., and Jasin, M. (1994a). Expression of a site-specific endonuclease stimulates homologous recombination in mammalian cells. Proc. Natl. Acad. Sci. *91*, 6064–6068.

Rouet, P., Smih, F., and Jasin, M. (1994b). Introduction of double-strand breaks into the genome of mouse cells by expression of a rare-cutting endonuclease. Mol. Cell. Biol. *14*, 8096–8106.

Ruan, G.-X., Barry, E., Yu, D., Lukason, M., Cheng, S.H., and Scaria, A. (2017). CRISPR/Cas9-Mediated Genome Editing as a Therapeutic Approach for Leber Congenital Amaurosis 10. Mol. Ther. *25*, 331–341.

Rui, Y., Wilson, D.R., and Green, J.J. (2019). Non-Viral Delivery To Enable Genome Editing. Trends Biotechnol. *37*, 281–293.

Ruiz de Galarreta, M., and Lujambio, A. (2017). Therapeutic editing of hepatocyte genome in vivo. J. Hepatol. *67*, 818–828.

Sadelain, M., Papapetrou, E.P., and Bushman, F.D. (2012). Safe harbours for the integration of new DNA in the human genome. Nat. Rev. Cancer *12*, 51–58.

San Filippo, J., Sung, P., and Klein, H. (2008). Mechanism of Eukaryotic Homologous Recombination. Annu. Rev. Biochem. *77*, 229–257.

Schneller, J.L., Lee, C.M., Bao, G., and Venditti, C.P. (2017). Genome editing for inborn errors of metabolism: advancing towards the clinic. BMC Med. *15*, 43.

Semenova, E., Jore, M.M., Datsenko, K.A., Semenova, A., Westra, E.R., Wanner, B., van der Oost, J., Brouns, S.J.J., and Severinov, K. (2011). Interference by clustered regularly interspaced short palindromic repeat (CRISPR) RNA is governed by a seed sequence. Proc. Natl. Acad. Sci. U. S. A. *108*, 10098–10103.

Sharma, R., Anguela, X.M., Doyon, Y., Wechsler, T., DeKelver, R.C., Sproul, S., Paschon, D.E., Miller, J.C., Davidson, R.J., Shivak, D., et al. (2015). In vivo genome editing of the albumin locus as a platform for protein replacement therapy. Blood *126*, 1777–1784.

Shin, J.H., Jung, S., Ramakrishna, S., Kim, H.H., and Lee, J. (2018). In vivo gene correction with targeted sequence substitution through microhomology-mediated end joining. Biochem. Biophys. Res. Commun. *502*, 116–122.

Smih, F., Rouet, P., Romanienko, P.J., and Jasin, M. (1995). Double-strand breaks at the target locus stimulate gene targeting in embryonic stem cells. Nucleic Acids Res. *23*, 5012–5019.

Thomas, C.E., Ehrhardt, A., and Kay, M.A. (2003). Progress and problems with the use of viral vectors for gene therapy. Nat. Rev. Genet. *4*, 346–358.

Tornabene, P., and Trapani, I. (2020). Can Adeno-Associated Viral Vectors Deliver Effectively Large Genes? Hum. Gene Ther. *31*, 47–56.

Trevisan, M., Masi, G., and Palù, G. (2020). Genome editing technologies to treat rare liver diseases. Transl. Gastroenterol. Hepatol. *5*, 23–23.

Tsuji, S., Stevens, C., Bortolussi, G., Zhang, F., Pekrun, K., Baj, G., Alencastro, G. de, Muro, A., and Kay, M. (2020). Improving the efficiency of liver targeting rAAV-mediated homologous recombination using ribonucleotide reductase inhibitors (In Review).

Tycko, J., Myer, V.E., and Hsu, P.D. (2016). Methods for Optimizing CRISPR-Cas9 Genome Editing Specificity. Mol. Cell *63*, 355–370.

Verdera, H.C., Kuranda, K., and Mingozzi, F. (2020). AAV Vector Immunogenicity in Humans: A Long Journey to Successful Gene Transfer. Mol. Ther. *28*, 723–746.

Wang, L., Wang, H., Bell, P., McMenamin, D., and Wilson, J.M. (2012). Hepatic Gene Transfer in Neonatal Mice by Adeno-Associated Virus Serotype 8 Vector. Hum. Gene Ther. *23*, 533–539.

Wang, L., Yang, Y., Breton, C.A., White, J., Zhang, J., Che, Y., Saveliev, A., McMenamin, D., He, Z., Latshaw, C., et al. (2019). CRISPR/Cas9-mediated in vivo gene targeting corrects hemostasis in newborn and adult factor IX–knockout mice. Blood *133*, 2745–2752.

Wang, M., Zuris, J.A., Meng, F., Rees, H., Sun, S., Deng, P., Han, Y., Gao, X., Pouli, D., Wu, Q., et al. (2016). Efficient delivery of genome-editing proteins using bioreducible lipid nanoparticles. Proc. Natl. Acad. Sci. *113*, 2868–2873.

Wilbie, D., Walther, J., and Mastrobattista, E. (2019). Delivery Aspects of CRISPR/Cas for in Vivo Genome Editing. Acc. Chem. Res. *52*, 1555–1564.

Wirth, T., Parker, N., and Ylä-Herttuala, S. (2013). History of gene therapy. Gene *525*, 162–169.

Woo, H.I., Park, H.-D., and Lee, Y.-W. (2014). Molecular genetics of citrullinemia types I and II. Clin. Chim. Acta *431*, 1–8.

Xue, C., and Greene, E.C. (2021). DNA Repair Pathway Choices in CRISPR-Cas9-Mediated Genome Editing. Trends Genet. *37*, 639–656.

Yang, H., Ren, S., Yu, S., Pan, H., Li, T., Ge, S., Zhang, J., and Xia, N. (2020). Methods Favoring Homology-Directed Repair Choice in Response to CRISPR/Cas9 Induced-Double Strand Breaks. Int. J. Mol. Sci. *21*, 6461.

Yang, Y., Wang, L., Bell, P., McMenamin, D., He, Z., White, J., Yu, H., Xu, C., Morizono, H., Musunuru, K., et al. (2016). A dual AAV system enables the Cas9-mediated correction of a metabolic liver disease in newborn mice. Nat. Biotechnol. *34*, 334–338.

Yao, X., Wang, X., Liu, J., Hu, X., Shi, L., Shen, X., Ying, W., Sun, X., Wang, X., Huang, P., et al. (2017). CRISPR/Cas9 – Mediated Precise Targeted Integration In Vivo Using a Double Cut Donor with Short Homology Arms. EBioMedicine *20*, 19–26.

Ye, X., Whiteman, B., Jerebtsova, M., and Batshaw, M.L. (2000). Correction of argininosuccinate synthetase (AS) deficiency in a murine model of citrullinemia with recombinant adenovirus carrying human AS cDNA. Gene Ther. *7*, 1777–1782.

Yin, H., Kanasty, R.L., Eltoukhy, A.A., Vegas, A.J., Dorkin, J.R., and Anderson, D.G. (2014a). Non-viral vectors for gene-based therapy. Nat. Rev. Genet. *15*, 541–555.

Yin, H., Xue, W., Chen, S., Bogorad, R.L., Benedetti, E., Grompe, M., Koteliansky, V., Sharp, P.A., Jacks, T., and Anderson, D.G. (2014b). Genome editing with Cas9 in adult mice corrects a disease mutation and phenotype. Nat. Biotechnol. *32*, 551–553.

Yin, H., Song, C.-Q., Dorkin, J.R., Zhu, L.J., Li, Y., Wu, Q., Park, A., Yang, J., Suresh, S., Bizhanova, A., et al. (2016). Therapeutic genome editing by combined viral and non-viral delivery of CRISPR system components in vivo. Nat. Biotechnol. *34*, 328–333.

Zuo, E., Sun, Y., Wei, W., Yuan, T., Ying, W., Sun, H., Yuan, L., Steinmetz, L.M., Li, Y., and Yang, H. (2019). Cytosine base editor generates substantial off-target single-nucleotide variants in mouse embryos. Science eaav9973.

Zuris, J.A., Thompson, D.B., Shu, Y., Guilinger, J.P., Bessen, J.L., Hu, J.H., Maeder, M.L., Joung, J.K., Chen, Z.-Y., and Liu, D.R. (2015). Cationic lipid-mediated delivery of proteins enables efficient protein-based genome editing in vitro and in vivo. Nat. Biotechnol. *33*, 73–80.